Montana Water Center
Annual Technical Report
FY 2010

Introduction

The Montana University System Water Center is located at Montana State University in Bozeman, was established by the Water Resources Research Act of 1964. Each year, the Center's Director at Montana State University works with the Associate Directors from the University of Montana - Missoula and Montana Tech of the University of Montana – Butte, to coordinate statewide water research and information transfer activities. This is all in keeping with the Center's mission to investigate and resolve Montana's water problems by sponsoring research, fostering education of future water professionals and providing outreach to water professionals, water users and communities.

To help guide its water research and information transfer programs, the Montana Water Center seeks advice from an advisory council to help set research priorities. During the 2010 research year, the Montana Water Research Advisory Council members were:

Gretchen Rupp, Director and Steve Guettermann, Assistant Director for Outreach, Montana Water Center

Marvin Miller, Montana Tech of the University of Montana and MWC Associate Director

Don Potts, University of Montana and MWC Associate Director

Paul Azevedo, Montana Department of Natural Resources and Conservation, Water Management Bureau Chief

Jeff Tiberi, Montana Association of Conservation Districts, Executive Director

J. P. Pomnichowski, Montana State Legislator

Christian Schmidt, Montana Department of Agriculture, Hydrologist

Tyler Trevor, Montana University System, Associate Commissioner

Mike Volesky, Montana Governor's Office, Natural Resources Policy Advisor

Larry Dolan, Hydrologist - Montana Department of Natural Resources and Conservation

John Kilpatrick, Director - Montana Water Science Center; U.S. Geological Survey

Jim Darling, Fisheries Division - Montana Fish, Wildlife & Parks

Bonnie Lovelace, Water Protection Bureau Chief . Montana Department of Environmental Quality

Dan Clark, Local Government Center, Director

Research Program Introduction

Through its USGS funding, the Montana Water Center partially funded four new water research projects in 2010 and continued funding for three other projects for faculty at three of Montana's state university campuses. The Montana Water Center requires that each faculty research project directly involve students in the field and/or with data analysis and presentations.

This USGS funding also provided research fellowships to five students involved with water resource studies. Here is a brief synopsis of the researchers' and students' work, with the three second year faculty research projects listed first.

Dr. Wyatt Cross and Dr. Brian McGlynn of Montana State University's Department of Land Resources and Environmental Sciences received $16,740. Their project, "Tracking Human-Derived Nitrogen through Stream Food Webs in a Rapidly Developing Mountain Watershed," continued with data gathering and analysis.

Dr. Elizabeth Meredith of Montana Tech of the University of Montana finished work on "Quantification of Coal-Aquifer Baseflow in Montana Rivers Using Carbon Isotopes." Dr. Meredith received $14,500.

Dr. Gary Icopini and his team, also of Montana Tech of the University of Montana, were awarded $12,210 for their work "Organic Wastewater Chemicals in Ground Water and Blacktail Creek, Summit Valley, Montana." This work complements other studies designed to determine groundwater quality in Montana.

Dr. Bwalya Malama, Assistant Professor at Montana Tech of the University of Montana, received $13,217 for his one year study of "Characterization of shallow subsurface hydraulic heterogeneity in the Silver Bow Creek – Butte area through field and laboratory experiments."

The University of Montana's Dr. Marco Maneta improved upon understanding climate change impacts on a local level with his study titled "Ecohydrologic model development for the assessment of climate change impacts on water resources in the Bitterroot Valley." Maneta received $11,710.

Dr. Lucy Marshall, Assistant Professor of Watershed Analysis at Montana State University, received $13,200 for her one-year study titled "Addressing computational paradigms in modeling the impacts of climate variability on watershed yield."

And for his research to better understand stream restoration dynamics, Dr. Geoff Poole of Montana State University was funded $8,328 for his work titled "Assessing hydrologic response to channel reconfiguration: Science to inform the restoration process, Silver Bow Creek, Montana."

Student Fellowships

University of Montana student Adam Clark received a $1,000 award to support his work on "Potential meltwater contributions from the glaciers in Glacier National Park, Montana." Adam is a graduate student in Geosciences.

Elena Evans, also a master's student in Geosciences at the University of Montana, received a $1,000 fellowship to further her work on "Fine sediment infiltration and sediment routing in the Clark Fork River."

Mariah Mayfield is a graduate student in fisheries biology at Montana State University. Her research focused on the fisheries restoration potential of the Clark Fork River superfund site. She received a $1,000 fellowship.

Kien Lim is an undergraduate student at Montana State University majoring in Biotechnology Microbial Systems. Lim received a $1,000 award and worked on his research titled “Rapid detection of pathogens in water using a combination of molecular techniques."

Andrea Stanley, a graduate student at the University of Montana in Geosciences, also received a $1,000 award. Her work is titled: “Distinguishing anthropogenic influences on a changing flow regime of the Upper Smith River, Meagher County, Montana."

Tracking Human-Derived Nitrogen through Stream Food Webs in a Rapidly Developing Mountain Watershed

Basic Information

Title:	Tracking Human-Derived Nitrogen through Stream Food Webs in a Rapidly Developing Mountain Watershed
Project Number:	2009MT189B
Start Date:	3/1/2009
End Date:	2/28/2011
Funding Source:	104B
Congressional District:	At-Large
Research Category:	Ecological Processes
Focus Category:	Ecology, Nutrients, Acid Deposition
Descriptors:	
Principal Investigators:	Geoffrey Poole, Brian Leonard McGlynn

Publications

1. Piper, L.R., W.F. Cross, and B.L. McGlynn. 2010. Stream isotopic and stoichiometric response to spatially-variable nitrogen loading in a rapidly developing mountain watershed. Joint meeting of the American Society of Limnology and Oceanography and the North American Benthological Society. Santa Fe, New Mexico.
2. Piper, L.R., W.F. Cross, and B.L. Mcglynn. 2010. The role of nutrient uptake by epilithon in controlling concentrations and ratios of dissolved nutrients in a developing mountain watershed. Montana Chapter of the American Water Resources Association Annual Meeting. Helena, Montana. First place in student presentation competition.
3. Piper, L.R., W.F. Cross, and B.L. McGlynn. 2011. The stoichiometry of uptake: dual nutrient uptake kinetics from ambient to saturation. North American Benthological Society Annual Meeting. Providence, Rhode Island.

USGS 104(b) Final Technical Report

Tracking human-derived nitrogen through stream food webs in a rapidly-developing mountain watershed

Leslie Piper, graduate student MSU

Drs. Wyatt F. Cross and Brian McGlynn, faculty in Ecology and LRES, MSU

Abstract

Recent, rapid development in the mountain west of the United States has resulted in dramatic increases in the availability of key nutrients such as nitrogen and phosphorus in these watersheds, primarily due to wastewater loading. These nutrients are in turn incorporated into in-stream food webs, with potentially significant impacts on the structure, function, and overall condition of these ecosystems. The elevated $\delta^{15}N$ signature associated with wastewater-derived nitrogen can be used as a quantitative tracer to follow this nutrient source through the watershed and into the food web. We conducted two synoptic surveys in the West Fork watershed of the Gallatin River in southwestern Montana to quantify the impact of development and associated wastewater loading on stream food webs. Our results show that wastewater-derived nitrogen plays a strong role in the support of both epilithon and macroinvertebrates at more heavily developed sites. During the summer months, this wastewater support appears to have little overall effect on the condition of the in-stream community, likely due to a disconnect between stream reaches and their sub-watersheds during the summer months. Further analysis of data from the winter months, as well as more detailed analysis of collected macroinvertebrates, is

expected to show a stronger relationship between development influence and the condition of stream food webs, with more impacted sub-watersheds draining to more degraded reaches as a result of increased nutrient loading from development.

Introduction

Over the last few decades, global population growth has driven humans into additional and previously untouched systems. The mountain west has been particularly prone to such development, making it one of the fastest growing regions in the United States. Development in these areas ranges from year-round communities to ski resort areas of varying sizes. Such changes in watershed land use are responsible for increases in the availability of nutrients such as nitrogen and phosphorus in these watersheds, often due to wastewater loading from septic systems and sewage treatment plants (Vitousek et al. 1997). While such loads affect terrestrial systems, the impacts are greatly increased as these nutrients are transported downgradient to lakes and streams, making these aquatic systems highly vulnerable to any changes in watershed conditions.

As a result, in-stream food webs can be treated as integrative "mirrors" of the conditions within their contributing sub-watersheds. Different metrics can be used to quantify the extent of human influence on systems and the impact of that influence. First, stable isotope ratios of nitrogen can be treated as a quantitative tracer of human-derived nitrogen. This is possible because wastewater tends to be relatively enriched in ^{15}N over natural sources such as atmospheric deposition and geologic weathering (e.g., deBruyn and Rasmussen 2002, Kaushal et al. 2006, Singer and Battin 2007). When dissolved inorganic nitrogen from wastewater is taken up by algae and bacteria within a stream, the $\delta^{15}N$ signature associated with that nitrogen is

incorporated into this biomass at the base of the food web. Macroinvertebrate consumers feeding on this material in turn integrate that $\delta^{15}N$ signature into their own biomass. By comparing the $\delta^{15}N$ values within the food web at different sites, the relative influence of wastewater-derived nutrients at each site can be estimated.

Elevated nutrient loading can also have significant impacts on the condition of stream ecosystems. Oftentimes, increased nutrient availability can lead to higher growth rates and total standing biomass of in-stream algae and bacteria (hereafter "epilithon") (e.g., Vitousek et al. 1997, Carpenter et al. 1998, Dodds et al. 2002). If a site is experiencing only modest increases in loading, however, there may not be noticeable increases in biomass. In these cases, the elemental composition, or stoichiometry, of the epilithon can be used as a more sensitive indicator of the influences of nutrient loading on food webs (e.g., Singer and Battin 2007). This is particularly noticeable in the algal component, as autotrophs are stoichiometrically flexible – they can take on a wide range of elemental ratios in response to elevated nutrient loading (Sterner and Elser 2002). A large influx of nitrogen to a stream reach, for example, will reduce the dissolved carbon to nitrogen ratio in the water column, which can in turn lead to reduced ratios in the epilithon at that reach.

While numerous studies have quantified these, and other, effects of nutrient enrichment on stream ecosystems (e.g., Peterson et al. 1993, Cross et al. 2006), few have explicitly tracked the relative importance of human-derived nutrients in driving these effects. This research effort attempted to fill this knowledge gap via two main objectives: 1) to quantify spatial and temporal variability of nitrogen isotope values in algae and invertebrates across a rapidly developing watershed to characterize the degree to which human-derived nitrogen is utilized by stream food

webs; and 2) to quantify the community-level consequences of human-derived nitrogen by relating spatial variability in stream community structure to variation in nitrogen subsidies.

Site Description

The West Fork of the Gallatin River drains a 212 km^2 watershed in the Rocky Mountains in southwestern Montana (Figure 1; taken from Gardner and McGlynn 2009). This watershed is home to three ski resorts, four golf courses, and almost 3000 structures, all built since the 1970s. Structures in the upper part of the watershed are on septic systems, with the rest of the watershed serviced by a sewage treatment plant. Nutrient loading from this wastewater infrastructure has resulted in an almost 10-fold increase in dissolved nitrate concentrations at the watershed outlet over the last 40 years.

The majority of this development, including the Big Sky Resort, is located along the middle tributary. Scattered structures are located on the southern tributary, while the northern tributary is practically pristine. This gradient of development influence results in substantial and predictable variation in dissolved nutrient concentrations (Gardner and McGlynn 2009), making the West Fork watershed an ideal site for testing some key hypotheses about the effects of nutrient loading on in-stream food webs and ecosystem processes.

Methods

Spatial variation in the stoichiometric and isotopic ratios of various stream food web components were assessed via two synoptic surveys – one conducted in August to September of 2009 (hereafter “summer”) and the other in February to March 2010 (hereafter “winter”). We

visited 31 stream sites across the watershed, covering full ranges in stream order, elevation, and development influence, during each survey.

A sample of stream water was collected in a 1 L high-density polyethylene (HDPE) bottle from the thalweg at each site. Samples were chilled and transported to the laboratory, where they were filtered with 0.45 μm polyethersulfone membranes within 24 hours of collection. Filtered samples were then stored frozen until analysis. Water samples were analyzed for all major species of nitrogen (nitrate [NO3-], nitrite [NO2-], ammonium [NH4+], and dissolved organic nitrogen [DON]), phosphorus (soluble reactive phosphorus [SRP] and dissolved organic phosphorus [DOP]), and carbon (dissolved inorganic carbon [DIC] and dissolved organic carbon [DOC]), as well as other major ions.

Four replicate epilithon samples were also collected at each site during each survey. Each sample was collected by selecting a rock at random and scrubbing the surface into a clean bucket of stream water. This slurry was then transported to the laboratory. A subsample of each slurry was filtered onto a GF/F glass microfiber filter and dried for ash-free dry mass (AFDM) analysis. AFDM measurements are used as a proxy for total epilithic biomass. Another subsample was filtered onto a second GF/F filter and stored at -27°C until they could be analyzed for chlorophyll *a*, which is used as an estimate of the metabolically active algal biomass at a site. The remaining slurry was then concentrated via centrifugation. The concentrated epilithon was frozen at -27°C, freeze-dried, homogenized with a mortar-pestle, and weighed for subsequent analysis for C, N, and P content, as well as carbon and nitrogen isotopic ratios. Scrubbed rocks were also taken back to the laboratory for surface area measurements to enable areal estimates of AFDM and chlorophyll *a* levels at each site.

Representative samples of macroinvertebrate consumers were also collected at each site during each survey. Invertebrates were collected from the surfaces of rocks using forceps and placed into a 250 mL HDPE bottle of stream water. The bottle was chilled and transported to the laboratory, where they were stored in the refrigerator overnight to allow for gut clearance. The invertebrates were separated by taxonomic group and placed into individual cryovials, frozen at 27°C, freeze-dried, homogenized with a mortar-pestle, and weighed for subsequent analysis for C, N, and P content, as well as isotopic ratios.

Results

Objective 1

Figures 2 and 3 show the $\delta^{15}N$ values associated with dissolved NO_3 for the summer and winter, respectively. As we expected, increases in development influence resulted in overall increases in $\delta^{15}N$, due to the higher $\delta^{15}N$ signature associated with wastewater. While these increases are significant in both cases, the relationship is both stronger and more positive in the winter.

The predictive power of development influence increases if we look at $\delta^{15}N$ values within the food web. Figures 4 and 5 show the relationships between development influence and the $\delta^{15}N$ values associated with the epilithon and with macroinvertebrate consumers, respectively, during the summer synoptic survey. These same figures will be constructed using data from the winter synoptic survey once the sample analyses are complete.

Objective 2

As our strongest predictive relationship was that between development influence and the $\delta^{15}N$ of epilithon, we used these isotopic signatures as the independent variable in assessments of the community-level consequences of human-derived nitrogen. Figures 6 and 7 show the relationships between epilithon $\delta^{15}N$ and areal estimates of AFDM and chlorophyll *a*, respectively, during the summer synoptic survey. These relationships were both statistically insignificant, although sites with high epilithon $\delta^{15}N$ values did tend to have higher areal AFDM and chlorophyll *a* levels. These same figures will be constructed using data from the winter synoptic survey once the sample analyses are complete.

Figures 8 and 9 show the relationships between epilithon $\delta^{15}N$ and molar C:N and C:P ratios, respectively, in the epilithon during the summer synoptic survey. There were no statistically significant relationships between these variables during the summer months. These same figures will be constructed using data from the winter synoptic survey once the sample analyses are complete.

Discussion

Objective 1

The first objective of this study was to quantify the variability of $\delta^{15}N$ values within the food web to characterize the degree to which human-derived nitrogen is used by stream food webs. To do this, we first looked at the relationship between the number of structures in the contributing subwatershed (used as a proxy for wastewater loading) and the $\delta^{15}N$ values associated with dissolved nitrate at each site. As dissolved nitrogen is assumed to be the primary carrier of high $\delta^{15}N$ nitrogen into the food web through algal and bacterial uptake, this was a key step to see if we might even expect to see increased $\delta^{15}N$ values at more impacted sites. In both

surveys, there was a significant positive relationship between development influence and the $\delta^{15}N$ of nitrate, but this relationship was noticeably weaker during the summer. This weaker correlation agrees with Gardner and McGlynn's (2009) findings that nitrate concentrations in this system were disconnected from development influence during the summer months. McNamara (2010) suggests that this lack of relationship is due to increased rates of nutrient uptake within streams during the summer growing season – in this case, the measured concentrations are what is left over following uptake, and may not be representative of initial loading levels. We still saw a significant relationship between development influence and $\delta^{15}N$ in the dissolved pool during the summer because biotic uptake should be relatively constant across different isotopic values, so the remaining nitrate should still retain its original $\delta^{15}N$ signature. Nevertheless, the strength of this relationship was much greater in the winter, reflecting the stronger link between development influence and dissolved nutrients during the dormant winter season.

Next, we looked at the incorporation of these development-driven $\delta^{15}N$ values into the food web during the summer months, beginning with the epilithon. Even with this initial step into the food web, we saw a dramatic increase in the strength of this positive relationship over that of the dissolved pool. We believe that this improved relationship was due to the longer temporal window represented by the epilithic assemblage. Measurements obtained within the dissolved pool only represent stream conditions at that precise point in time. The epilithon, on the other hand, constantly takes up nutrients from the water column, and so integrates stream conditions over the turnover time of the assemblage (a matter of days to weeks). As a result, short-term fluctuations that may have complicated our analysis of the dissolved pool were averaged out, making this relationship stronger and hence more reliable. We expect the strength

of this relationship to be even greater during the winter months, reflecting the improved relationship in the dissolved pool.

We also looked at the further progression of $\delta^{15}N$ values up the food web into macroinvertebrate consumers. While this relationship was still strongly positive and significant, we did not see the further increase in strength that we expected over the epilithic relationship, as invertebrates integrate the $\delta^{15}N$ values of their food over time scales of one to four months (e.g., Hamilton et al. 2004). This lack of an improved relationship may be due to the lumping of all taxa found at each site into a single group. Different taxa have different feeding strategies, and therefore may have different isotopic relationships to their food sources. Separating these points out by consumer taxa may further improve the strength of this relationship. As for the epilithon, we also expect this relationship to be stronger during the winter.

The average $\delta^{15}N$ values of the epilithon and macroinvertebrates were also entered into a very simple two-component mixing model to estimate the percent support of these food web components by wastewater at each site. In this model, natural sources of nitrogen such as atmospheric deposition and geologic weathering were assumed to have a $\delta^{15}N$ of 0‰. Wastewater-derived nitrogen was assumed to have a $\delta^{15}N$ of 12‰ (Kendall and McDonnell 1998). Each biotic $\delta^{15}N$ value was entered into the following equation:

$$\partial 15N \text{ sample} = [(W*12.0 ‰) + ([1-W]*0.0‰])*100$$

The value of W corresponded to the percent support of that particular sample by wastewater-derived nitrogen. These values are plotted as a second y-axis on Figures 4 and 5. While there is certainly some variation in the $\delta^{15}N$ values of these end-members that must be incorporated in

further analyses, this simple approach provides some evidence that an increase in the number of structures in the contributing subwatershed leads to increased importance of wastewater-derived nitrogen (and presumably other nutrients as well) in the support of in-stream food webs.

Objective 2

Since we have shown that there is indeed significant and predictable variability in the degree of wastewater support of food webs across the West Fork watershed, the second objective of the study was to quantify the community-level consequences of such human-derived nitrogen. For all figures relating to this objective, we use the $\delta^{15}N$ values associated with the epilithon as the independent variable, as this metric showed the strongest relationship to development influence in our previous analyses. During the summer months, however, there were no significant relationships between epilithon $\delta^{15}N$ values and any of the community responses (AFDM, chlorophyll *a*, and C:N and C:P ratios of the epilithon during the summer months) we examined. This lack of relationship may again be due to the disconnect between development influence and in-stream nutrient availability during the growing season. Even though the $\delta^{15}N$ values may suggest high influence of wastewater nutrients at a site, that doesn't necessarily mean that there are high levels of nutrients available at that site – it just means that wastewater is responsible for a large portion of the initial nutrient loading relative to natural sources. High uptake, both in the terrestrial system and at upstream sites, may reduce the nutrient availability at that site to levels that do not support significant in-stream growth, regardless of the original source of those nutrients. Similarly, we would not see shifts in the elemental make-up of the epilithon without significant shifts in loading levels. As with the isotopic data, we expect to see stronger relationships between these community responses and development influence during the

winter months, when uptake is much lower and stream reaches are more closely linked to their sub-watersheds in terms of nutrient dynamics.

Next steps

Even though sampling has been completed for this project, there is significant work left to be done in terms of data analysis, particularly regarding the epilithon and invertebrate samples collected during the winter synoptic survey. As stream reaches tend to be more influenced by development influence within their sub-watersheds during the dormant winter season, we expect that the results of these remaining analyses will help answer some questions remaining after our summer survey.

Significant analysis also remains to be done with the invertebrate samples. In particular, we plan to separate out the invertebrates collected at each site by taxa, rather than grouping them all together, and rerun these analyses, to see if there are differences in the responses of various taxa to nutrient loading from wastewater, in terms of both presence/absence and stoichiometric ratios within their tissues. We expect more sensitive taxa such as *Ephemeroptera* and *Trichoptera* to be more strongly affected by development influence than more tolerant taxa, and so we should see different relationship patterns across groups.

The results presented here, as well as the anticipated results of our remaining analyses, will result in a significant contribution of this research effort to the current body of scientific knowledge on the impacts of anthropogenic nutrient loading on stream ecosystems.

Figures

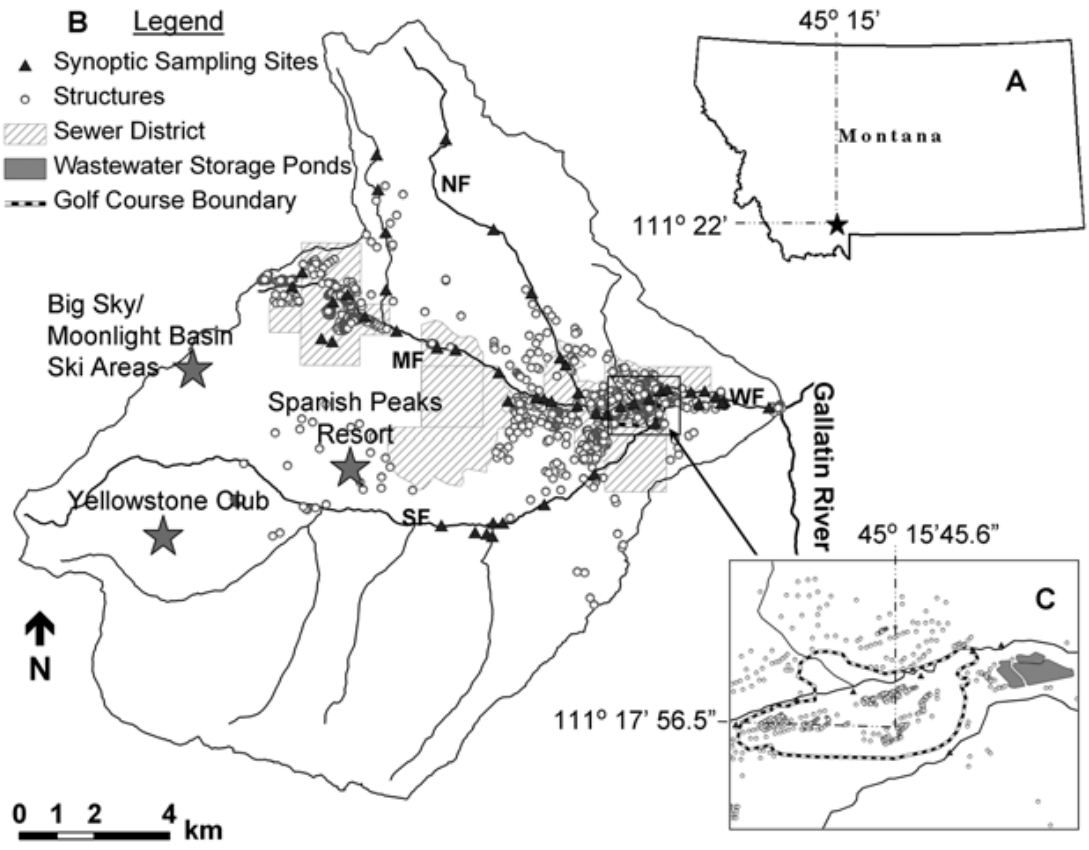

Figure 1: Site map of the West Fork watershed of the Gallatin River.

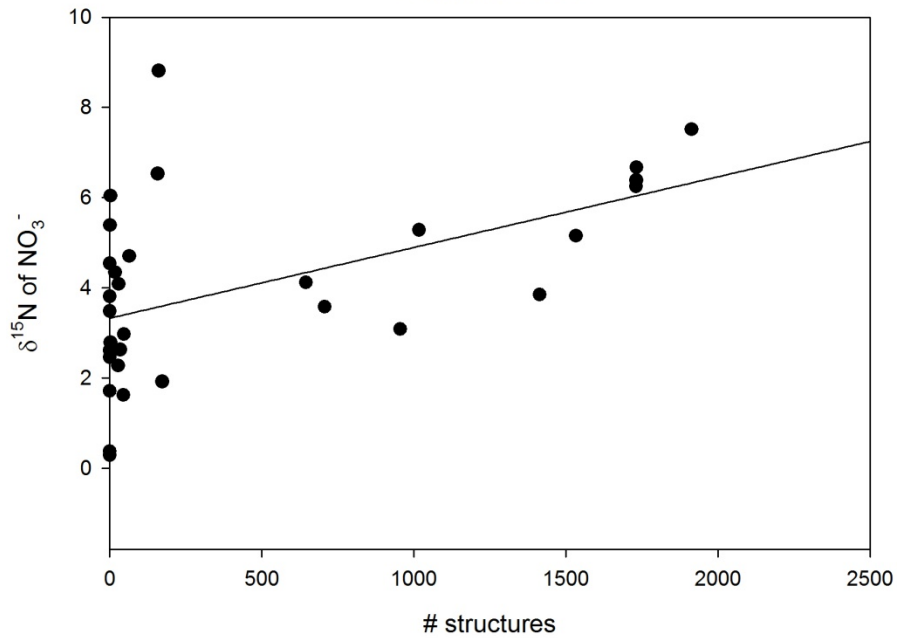

Figure 2: $\delta^{15}N$ values associated with dissolved nitrate in stream water versus number of structures in the contributing sub-watershed during the summer ($r^2 = 0.27$, $p = 0.003$).

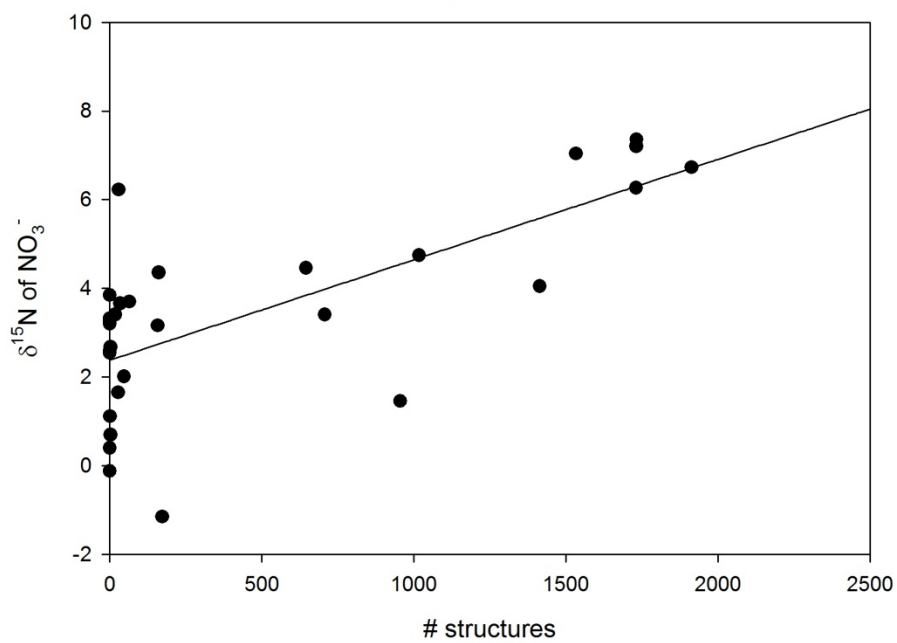

Figure 3: $\delta^{15}N$ values associated with dissolved nitrate in stream water versus number of structures in the contributing sub-watershed during the winter ($r^2 = 0.49$, $p < 0.001$).

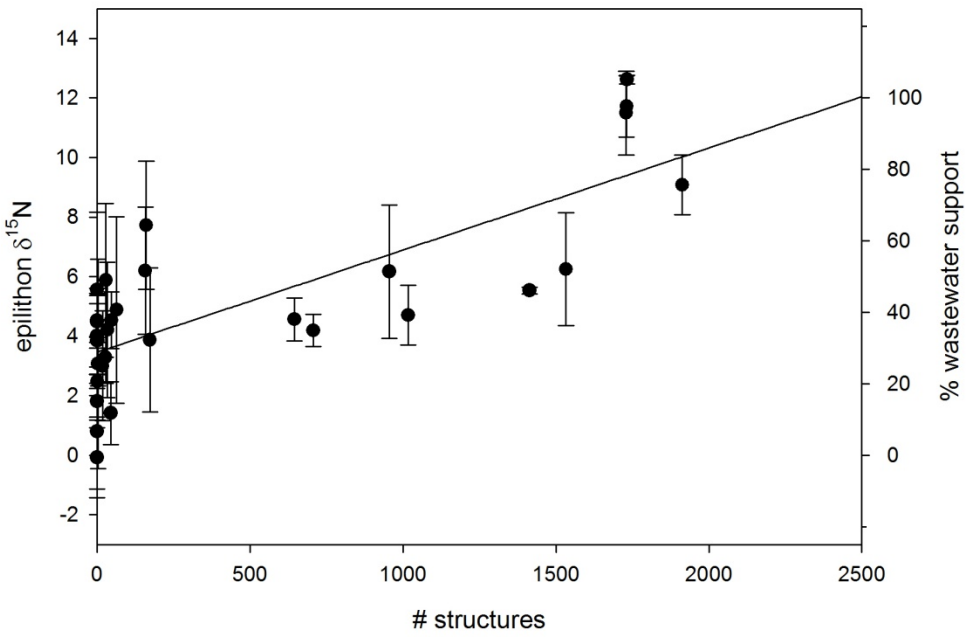

Figure 4: $\delta^{15}N$ values associated with epilithon versus number of structures in the contributing sub-watershed during the winter ($r^2 = 0.60$, $p < 0.001$). Estimated percent support of the epilithon (based on the $\delta^{15}N$ values) is shown on the second y-axis.

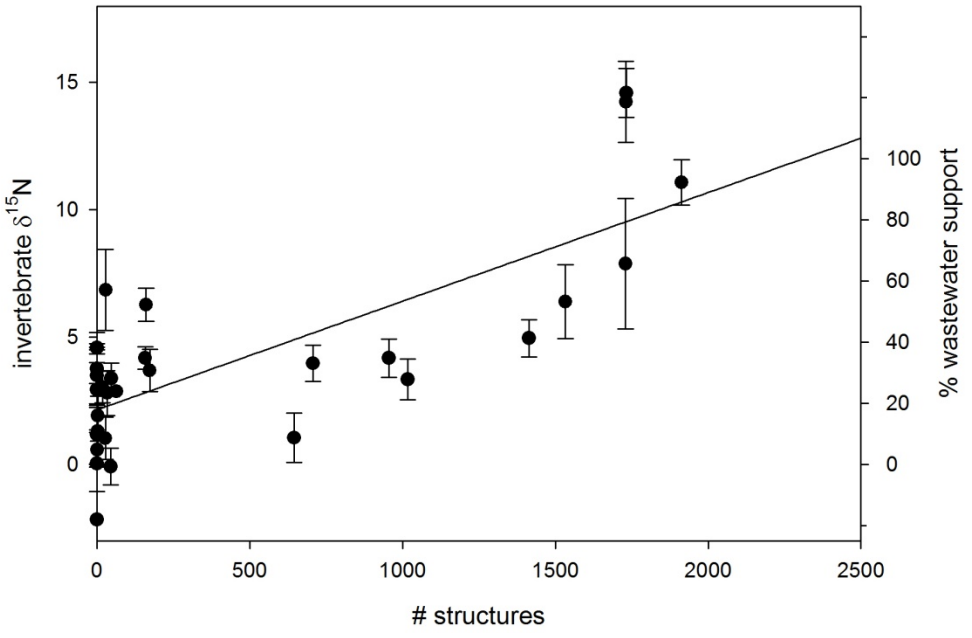

Figure 5: $\delta^{15}N$ values associated with macroinvertebrate consumers versus number of structures in the contributing sub-watershed during the winter ($r^2 = 0.57$, $p < 0.001$). Estimated percent support of the macroinvertebrates (based on the $\delta^{15}N$ values) is shown on the second y-axis.

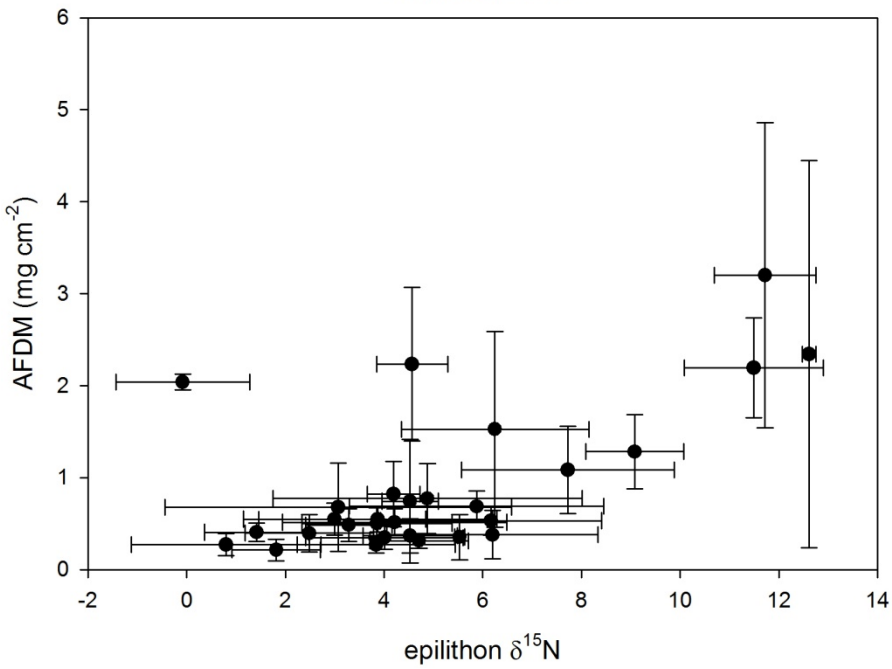

Figure 6: Areal standing in-stream biomass (represented as ash-free dry mass (AFDM)) versus $\delta^{15}N$ values of epilithon during the summer ($p = 0.68$).

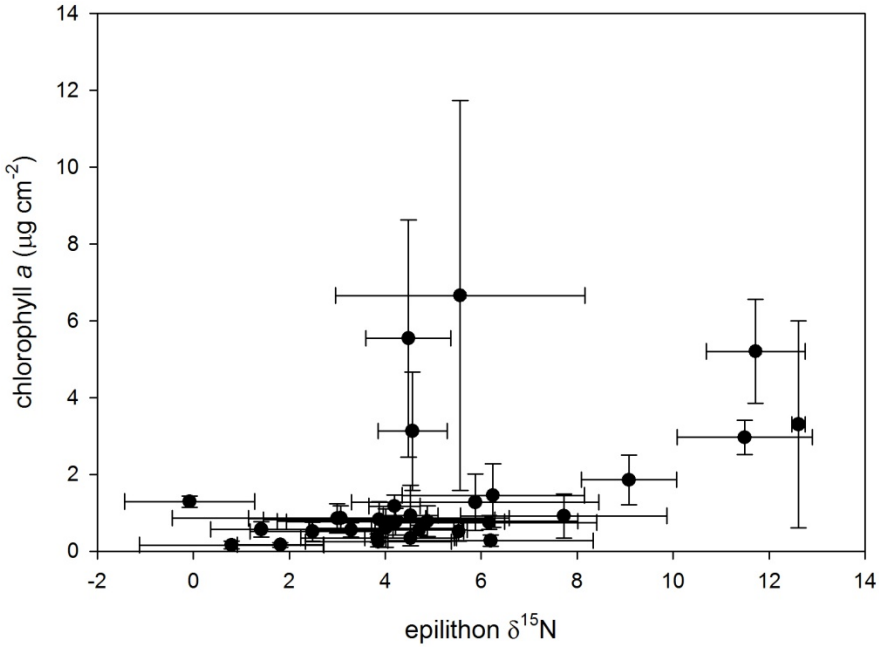

Figure 7: Areal active biomass of primary producers (represented as chlorophyll *a*) versus $\delta^{15}N$ values of epilithon during the summer ($p = 0.86$).

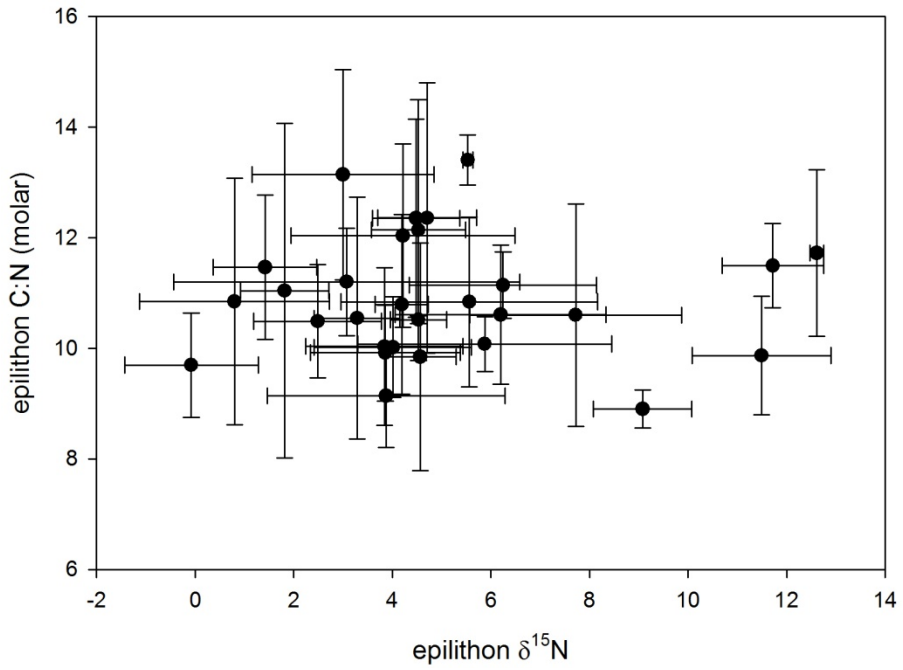

Figure 8: Molar C:N ratio of epilithon versus $\delta^{15}N$ values of epilithon during the summer (p = 0.78).

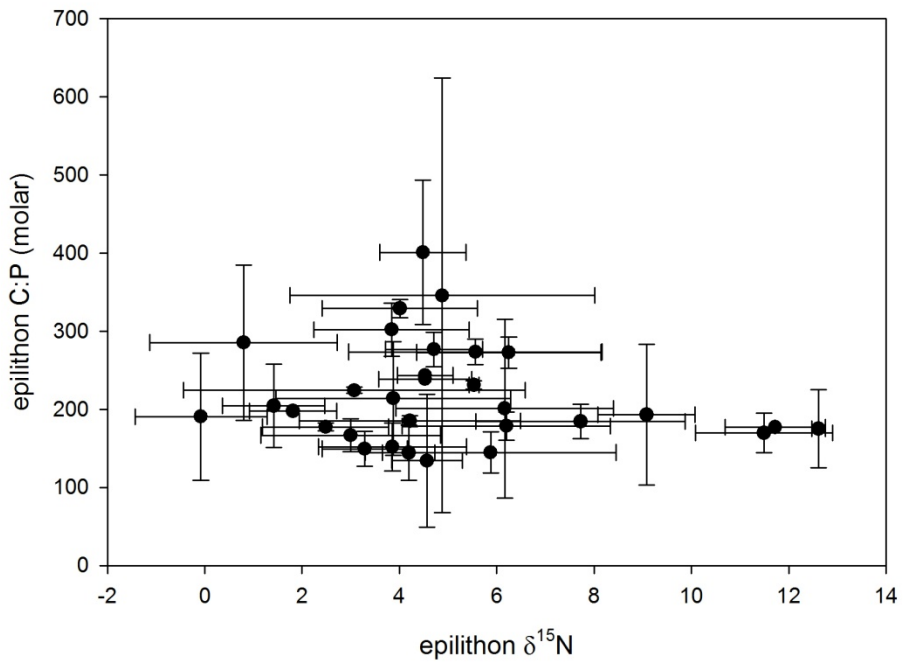

Figure 9: Molar C:P ratio of epilithon versus $\delta^{15}N$ values of epilithon during the summer (p = 0.35).

References

Carpenter, S.R., N.F. Caraco, D.L. Correll, R.W. Howarth, A.N. Sharpley, and V.H. Smith. 1998. Nonpoint pollution of surface waters with phosphorus and nitrogen. *Ecological Applications*, **8**: 559-568.

Cross, W.F., J.B. Wallace, A.D. Rosemond, and S.L. Eggert. 2006. Whole-system nutrient enrichment increases secondary production in a detritus-based ecosystem. *Ecology*, **87**: 1556-1565.

deBruyn, A.M.H. and J.B. Rasmussen. 2002. Quantifying assimilation of sewage-derived organic matter by riverine benthos. *Ecological Applications*, **12**: 511-520.

Dodds, W.K., V.H. Smith, and K. Lohman. 2002. Nitrogen and phosphorus relationships to benthic algal biomass in temperate streams. *Canadian Journal of Fisheries and Aquatic Sciences*, **59**: 865-874.

Gardner, K.K. and B.L. McGlynn. 2009. Seasonality in spatial variability and influence of land use/land cover and watershed characteristics on stream water nitrate concentrations in a developing watershed in the Rocky Mountain West. *Water Resources Research*, **45**.

Hansen, A.J., R. Rasker, B. Maxwell, J.J. Rotella, J.D. Johnson, A.W. Parmenter, U. Langner, W.B. Cohen, R.L. Lawrence, and M.P.V. Kraska. 2002. Ecological causes and consequences of demographic change in the new west. *BioScience*, **52**: 151-162.

Kaushal, S.S., W.M. Lewis, Jr., and J.H. McCutchan, Jr. 2006. Land use change and nitrogen enrichment of a Rocky Mountain watershed. *Ecological Applications*, **16**: 299-312.

Kendall, C. and J.J. McDonnell. 1998. *Isotope Tracers in Catchment Hydrology*, Elsevier, New York.

McNamara, R. 2010. Stream nitrogen uptake kinetics from ambient to saturation across

development gradients, stream network position, and seasons. MS Thesis. Dept. of Land Resources and Environmental Sciences, Montana State University – Bozeman.

Peterson, B.J., L. Deegan, J. Helfrich, J.E. Hobbie, M. Hullar, B. Moller, T.E. Ford, A. Hershey, A. Hiltner, G. Kipphut, M.A. Lock, D.M. Fiebig, V. McKinley, M.C. Miller, J.R. Vestal, R. Ventullo, and G. Volk. 1993. Biological responses of a tundra river to fertilization. *Ecology*, **74**: 653-672.

Singer, G.A. and T.J. Battin. 2007. Anthropogenic subsidies alter stream consumer-resource stoichiometry, biodiversity, and food chains. *Ecological Applications*, **17**: 376-389.

Sterner, R.W. and J.J. Elser. 2002. *Ecological Stoichiometry*. Princeton University Press, Princeton, New Jersey.

Vitousek, P.M., J.D. Aber, R.W. Howarth, G.E. Likens, P.A. Matson, D.W. Schindler, W.H. Schlesinger, and D.G. Tilman. 1997. Human alteration of the global nitrogen cycle: sources and consequences. *Ecological Applications*, **7**: 737-750.

Organic Wastewater Chemicals in Ground Water and Blacktail Creek, Summit Valley, Montana

Basic Information

Title:	Organic Wastewater Chemicals in Ground Water and Blacktail Creek, Summit Valley, Montana
Project Number:	2009MT190B
Start Date:	3/1/2009
End Date:	2/28/2011
Funding Source:	104B
Congressional District:	At-Large
Research Category:	Water Quality
Focus Category:	Groundwater, Water Quality, Water Supply
Descriptors:	
Principal Investigators:	Gary Icopini, Stephen Parker

Publications

There are no publications.

Organic Wastewater Chemicals in Ground Water and Blacktail Creek, Summit Valley, Montana

By

Gary A. Icopini[1], Jacqueline Timmer[1,2], and Steven Parker[2]

Abstract

Organic wastewater chemicals (OWCs) originate from human or animal wastewater discharges (treated or untreated) to the environment. OWCs encompass a wide variety of chemicals and include pharmaceuticals, hormones, fire retardants, industrial chemicals, personal care products, and pesticides. Many of these chemicals have been shown to interfere with the endocrine system of both animals and humans at very low concentrations. Surface waters receiving treated wastewater effluent have received the most attention by researchers studying OWC occurrences and effects on the environment. Relatively few studies have examined the occurrence or fate of OWCs in ground waters.

A previous study has documented elevated nitrate concentrations that have been attributed to septic system discharges in the groundwaters and surface waters of the Summit Valley near Butte, Montana. Because the factors that control nitrate sources, mobility and persistence in the subsurface are similar to those that influence OWCs, it is likely that the ground waters of the Summit Valley will also contain elevated OWC concentrations. In this study enzyme-linked immunosorbent assays were used to quantify the concentrations of sulfamethoxazole, sulfamethazine, progesterone, and 17-estradiol in 13 groundwater and 2 surface-water samples from the Summit Valley. At least one OWC was detected in all samples collected. Sulfamethoxazole and progesterone were detected in all samples; however, the progesterone detections were likely result of interferences with DOC. Approximately 40 percent of the samples had detectable concentrations of 17β-estradiol. Sulfamethazine was not detected in any samples. One treated sample was collected from a reverse osmosis unit and the results indicated that reverse osmosis may be a cost-effective method for removal of OWC contamination.

[1]Montana Bureau of Mines and Geology, Montana Tech, Butte, MT 59701; 406-496-4841; 406-496-4451(fax)

[2]Dept. of Chem. & Geochem., Montana Tech, Butte, MT 59701; 406-496-4185(office); 406-496-4135(fax)

Grant Obligations and Deliverables

Results from this project were presented at the American Water Resources Association Montana Section 2010 Conference in Helena Montana (citation below). The results were presented by Jacqueline Timmer. Ms. Timmer is currently working toward her Master's of Science degree in Geochemistry from Montana Tech. The funding from this grant was used to support her graduate research. She has chosen the "publishable paper" option instead of a standard thesis option and plans to publish the results from this work in a journal. As result of this collaboration Parker and Icopini have recently submitted a preproposal for additional funding to investigate the fate of OWCs in Silverbow Creek.

Timmer, J., and G.A. Icopini, 2010, Screening for Organic Wastewater Chemicals in the Groundwater of Summit Valley, Montana, in Proceeding of the American Water Resources Association Montana Section 2010 Conference, Helena Montana, p. 43.

Introduction

The purpose of this research was to assess OWC contamination of groundwater and surface water in selected areas of the southern part of the Summit Valley near Butte, Montana. A recent study of the groundwater in of the Summit Valley near Butte Montana has identified areas with elevated nitrate concentrations, which have been attributed to septic systems associated with unsewered residential development (LaFave, 2008). In addition to the elevated nitrate concentrations observed in groundwaters, elevated nitrate concentrations were also observed in Blacktail Creek, which runs through unsewered areas in Summit Valley. Ground-water wells were sampled in both fractured-rock and valley-fill aquifers, and both aquifers were found to be equally likely to contain elevated nitrate concentrations (LaFave, 2008). The valley-fill deposits in the Summit Valley consist principally of decomposing granite having a sandy texture, which is highly transmissive and contains little organic matter (LaFave, 2008). Similarly, the fractured-rock aquifers are very transmissive (where fractured) and also contain little organic matter. These aquifer characteristics create conditions that contribute to the enhanced mobility, persistence and distribution of nitrate in the subsurface (LaFave, 2008). These same aquifer characteristics are also likely to enhance OWC mobility and persistence in the aquifer. In addition, the presence of elevated nitrate due to septic system discharges strongly suggests that OWC contamination will be encountered as well, since many OWCs appear to be more persistent than nitrate in subsurface environments (Miller and Meek, 2006; Icopini, 2008).

Although this study was located in the Summit Valley, there are other locations in Montana that are likely to be equally susceptible to OWC contamination. Essentially, any aquifer that has an immediate hydraulic connection with the surface, receives human or animal waste discharges, and has little organic matter will be susceptible to this type of contamination. Recently, a national reconnaissance was conducted of OWC contamination in groundwaters that were deemed to be at risk of being contaminated with OWCs (i.e., down gradient of a landfill, unsewered residential development, or animal feedlot). Ground-water samples were collected from 47 sites across the nation and 81 percent were found to contain at least one of the 65 OWCs that the study monitored (Barnes et al., 2008).

Miller and Meek (2006) sampled 35 water supply wells in the Helena Valley of Montana for 28 different OWCs. OWCs were found in 91 percent of the wells sampled. Sulfamethoxazole (78 percent of wells), atrazine, carbamazepine, dilantin, and diclofenac were the most frequently detected OWCs. Individual septic systems were deemed the most likely source for the OWC contaminants observed by Miller and Meek (2006); however, no correlation was observed between inorganic chemical indicators (including nitrate) and OWC occurrences. Batt et al. (2006) documented plumes of sulfamethazine and sulfadimethoxine emanating from a large-scale commercial feedlot operation. Both sulfamethazine and sulfadimethoxine are antibiotics that have been approved for use in cattle feed (USDA 2007).

There are numerous possible adverse impacts to both humans and wildlife from the release of OWCs to the environment. It has been proposed that the release of human and agricultural antibiotics to the environment may be promoting the emergence of antibiotic-resistant bacteria (Levy, 1997; Boxall et al., 2003; Kumar et al., 2005). There is even more compelling evidence that OWCs, especially estrogenic substances, are having adverse impacts on aquatic life. Researchers studying wild fathead minnows

exposed to feedlot effluent observed significant alterations to reproductive biology including decreased testosterone synthesis, altered head morphology, smaller testis size in males, and decreased estrogen:androgen ratio in females (Orlando et al. 2004). Researchers in Colorado observed that 83 percent of white suckers were female downstream of the wastewater treatment plant (WWTP) outfall from the city of Boulder, CO compared to only 45 percent female white suckers upstream of the WWTP (Woodling et al., 2006). In a Canadian experiment, a lake was doped with 5-6 ng/L of 17α-ethynylestradiol (EE2; synthetic hormone), which caused the feminization of fathead minnows and led to population collapse after two years of EE2 addition to the lake (Kidd et al., 2007). While arguments can be made that low levels (ng/L) of other OWCs may not be a health concern, these low levels of estrogens and other hormones have been demonstrated to have a negative impact on the health of other animals and are likely to have a negative impact on human health.

OWC concentrations for this project were determined using enzyme-linked immunosorbent assays (ELISA). ELISA utilizes antibodies that have been shown to respond to a specific molecule (the antigen). In one type of ELISA assay the antibodies have photoactive functional groups attached to a surface of the molecule which allows colorimetric visualization of the antibody. When the antigen binds with the antibodies, the result is either an increase or decrease in light absorbance at a specific wavelength. This is then used to quantify the amount of antibody (the OWC in this case) that is binding to the antigen. A second type of ELISA assay will be used to detect sulfamethazine (antibiotic) and 17β-estradiol (natural hormone). This assay uses the magnetic particle format, which is very sensitive due to the large surface area of the particles and does not require pre-concentration of the sample. Sulfamethoxazole (antibiotic) and progesterone (steroid hormone) will be quantified using the microtiter plate format. Due to the limited surface area of the plate's wells, a pre-concentration step is needed to detect compounds. The pre-concentration step is often the greatest source of error in these analyses. There are currently no standard methods for the pre-concentration step used in conjunction with ELISA OWC analysis. Limited method development was conducted to identify the best pre-concentration procedure for these analytes.

This report presents data from thirteen domestic wells and two surface-water sites that were sampled for OWCs. These data are compared with inorganic parameters and dissolved organic carbon (DOC) in an effort to evaluate the source of the OWCs. In addition, one sample that had been treated through a reverse osmosis unit was also sampled to provide a preliminary assessment of the ability of reverse osmosis to serve as treatment technology for OWC contamination.

Methods

Site Selection and Sampling

The study location was the Summit Valley south of Butte Montana (Figure 1). The selection of wells used in this study was primarily based on a previous study (LaFave, 2008), which evaluated nitrate concentrations in the area. Although the previous study sampled wells throughout Summit Valley, sample collection for this project was primarily in the south-eastern part of the valley. The south-eastern portion of the valley is under the most intense development pressure and also contains one of the oldest unsewered residential developments in the area. The nitrate concentrations in

domestic wells from this area ranged from below 2 mg/L nitrate to above 10 mg/L nitrate (drinking-water standard), with most having concentrations between 2 and 10 mg/L. Thirteen wells were sampled for this project (Table 1). Samples were arbitrarily numbered from 1 to 15; samples numbered 1 – 13 were groundwater samples and samples numbered 14 and 15 were surface-water samples from Blacktail Creek. All, but one of the wells sampled were sampled as part of the previous study. Eight samples were collected from wells that had previous nitrate concentrations between 2 and 10 mg/L. Two samples were collected from wells with previous nitrate concentrations that exceeded 10 mg/L. Since elevated nitrate concentrations do not always co-occur with OWCs (Miller and Meek, 2006; Icopini, 2008), three wells in unsewered residential areas that did not contain elevated nitrate concentrations were also sampled to further evaluate the susceptibility of these aquifers to OWC contamination. Wells installed in both bedrock and valley-fill aquifers were sampled for this study (Table 1).

In addition to the ground-water samples, two surface-water samples from Blacktail Creek were also collected (Figure 1). One sample was collected from an area that was upstream from the most heavily developed areas. The other sample was collected at the current boundary between sewered and unsewered developments. All samples, except sample number 13, were collected between September 13th and September 17th 2010, which was during baseflow conditions for Blacktail Creek. Sample number 13 was collected on May 10th 2010 for the method evaluation.

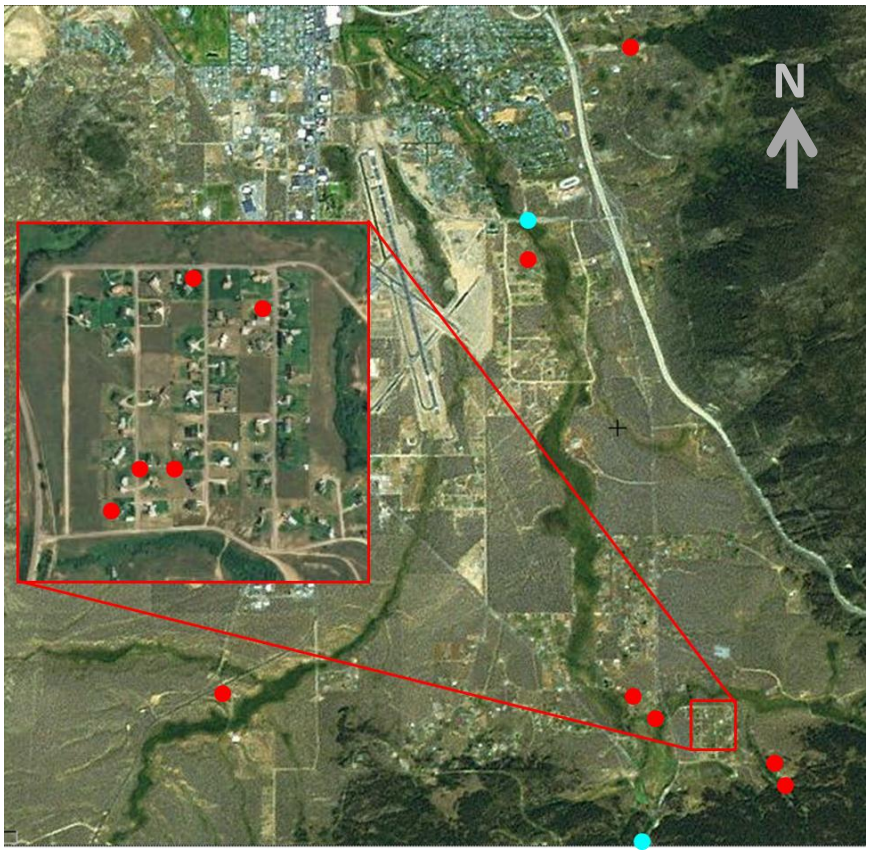

Figure 1. This aerial photo shows the sampling locations for groundwater sites (red dots) and surface-water sites (blue dots).

Table 1. Summary of the site characteristics for each sampling site.

Site Number	GWIC Number	Well Depth (Feet)	Depth Water Enters (Feet)	Nitrate* (mg/L as N)	Aquifer Type
1	137147	180	80	3.94	Boulder Batholith
2	120297	54	48	< 0.5	Sand and Gravel
3	179158	100	80	20.4	Boulder Batholith
4	145960	100	80	2.72	Boulder Batholith
5	49421	71	66	8.58	Sand and Gravel
6	49551	340	300	8.67	Boulder Batholith
7	165216	180	160	7.48	Boulder Batholith
8	891015	140	80	17.6	Boulder Batholith
9	49537	87	77	< 0.25	Boulder Batholith
10	150276	160	140	7.26	Boulder Batholith
11	49260	134	120	0.651	Sand and Gravel
12	179162	80	60	4.05	Boulder Batholith
13	255446	NA	NA	2.54**	Sand and Gravel
14	191284			< 0.5	Surface Water - Upstream
15	191286			1.17	Surface Water - Downstream

* Data from LaFave, 2008.
** Data from this study.

Well samples were collected from individual water-supply wells with permanently installed pumps and distribution systems. Samples were collected using established MBMG sampling protocols for the collection of inorganic water-quality samples using a hose on an existing tap. These protocols include purging the well until water-quality parameters (temperature, pH, specific conductance, dissolved oxygen, and reduction potential) stabilize. At least three well volumes were purged from all wells. Personal protective equipment, consisting of nitrile gloves and face masks was worn during the collection of OWC samples and while handling equipment using clean hands/dirty hands technique. After purging the well and collection of the filtered (0.45 µm), water-quality samples (cation, anion, trace metals, ammonium, and alkalinity), all of the hoses were removed and the tap was first rinsed with HPLC grade methanol then HPLC grade water. The OWC samples were collected straight from a permanently installed tap while wearing nitrile gloves and face mask to prevent sample contamination. Unfiltered OWC samples were collected in pre-cleaned, amber glass bottles (VWR

15900-142) preserved with H_2SO_4. After collection the samples were maintained on ice until delivery to the MBMG Laboratory. Triplicate samples were taken at one groundwater site (well) and at one surface-water (Blacktail Creek) site. In addition to triplicate field samples, blanks were collected and submitted to the laboratory for QA/QC.

Field measurements including pH, dissolved oxygen, water temperature, specific conductivity (SC) and reduction-oxidation (redox) potential were obtained throughout the well purging process and at the time of sample collection using a Hanna Multiparameter (HI9828) water-quality meter. Alkalinity was measured in the field using a Hach Digital Titrator (Model AL-DT). Sulfide was measured in the field using a CHEMetrics field spectrophotometer (V-2000) and CHEMetrics kit K-9503. Instrumentation was calibrated daily prior to sampling.

Laboratory Analyses

A comprehensive geochemical analysis was performed on all the samples collected in an effort to identify inorganic or organic indicators of OWC contamination. The concentrations of major cations, major anions, trace metals, and dissolved organic carbon, were determined for each sample. Major cation concentrations were determined using an inductively coupled plasma-atomic emission spectrometer (ICP-AES; EPA Method 200.7) while trace metal concentrations were determined using an ICP mass spectrometer (ICP-MS: EPA Method 200.8). The anion concentrations were determined using a Metrohm ion chromatograph (IC; EPA Method 300.0). Nitrate/nitrate as N and total nitrogen concentrations of H_2SO_4 preserved samples were determined using a HACH TNTPlus^{TM} 880 spectrophotometer. Dissolved organic carbon (DOC) was performed on filtered samples using a GE Innovox total organic carbon analyzer (EPA Methods 415.1/415.2.

OWCs for this project were analyzed using enzyme-linked immunosorbent assays (ELISA) in two formats (Table 2). Sulfamethoxazole (antibiotic) and progesterone (steroid hormone) were quantified using the microtiter plate format, which is not sensitive enough to determine concentrations in the ng/L concentration range; a pre-concentration step was necessary for sulfamethoxazole and progesterone. A second type of ELISA assay was used to detect sulfamethazine (antibiotic) and 17β-estradiol (natural hormone). This assay uses the magnetic particle format, which is very sensitive due to the large surface area of the particles and does not require pre-concentration of the sample.

Table 2. Organic wastewater chemical name, use, ELISA format, and detection limit.

OWC	OWC use	ELISA Form	Detection Limit (ng/L)
Sulfamethoxazole	antibiotic	microtiter plate	0.1
Progesterone	steroid hormone	microtiter plate	0.06
17β-estradiol	natural hormone	magnetic particle	1.0
Sulfamethazine	antibiotic	magnetic particle	50

The OWCs chosen for this project were selected because they have been shown to be mobile in the subsurface and for their potential human health risk. Sulfamethoxazole and sulfamethazine were chosen because they are widely used and appear to be persistent in subsurface environments (Miller and Meek, 2006; Batt et al., 2008). The hormones for this study were selected based on their abundance and potency. 17β-estradiol is the most common and most potent natural estrogen (Norris, 2006). Progesterone, a hormone involved in the female menstrual cycle and pregnancy, is the major naturally occurring human progestogen.

Once received by the laboratory, the OWC samples were split. Approximately 10 mL was taken from the OWC sample for magnetic-particle analysis (sulfamethazine and 17β-estradiol), 500 mL was filtered through solid phase extraction (SPE) cartridges and frozen to be concentrated, and the remaining sample was stored for use as a backup, if needed. After extracting the sample with the SPE cartridge, the cartridge can be wrapped in foil and frozen for up to 2 months. The magnetic-particle analysis was completed within 2 weeks of sample collection.

Two methods were evaluated to concentrate the samples prior to ELISA microtiter plate analysis; EPA Method 1694: Pharmaceuticals and Personal Care Products in Water, Soil, sediment, and Biosolids by HPLC/MS/MS (U.S. EPA, 2007) and Procedure for Extraction and Analysis of Water Samples for Endocrine Disrupting Compounds by Enzyme Linked Immuno Assay (developed by MBMG personnel based on Hilton and Thomas, 2003). These methods are similar in that they both require extraction and concentration of the water sample prior to analysis; however, there are differences in the methods. The major difference in the methods is the manner in which the extracts will be analyzed; the EPA method uses high-performance liquid chromatography with tandem mass spectrometric detection (HPLC-MS/MS), while the MBMG method utilizes ELISA. The extraction portions of the methods are similar; however, there are several differences. While the solid phase extraction (SPE) cartridges used in either method is the same, the manner in which they are conditioned differs slightly. The EPA method uses 20 ml of methanol, 6 ml of reagent water and 6 ml of reagent water at pH 2.0 ± 0.5, whereas the MBMG method uses only 6 ml of methanol, 6 ml reagent water and 6 ml of pH 3 water. In both methods, samples are similarly loaded onto the cartridges. The biggest difference in the extraction portion of the two methods comes in the elution and concentration of the analytes. EPA Method 1694 uses 12 ml of methanol for the elution. The extracts are then concentrated to near dryness under a stream of nitrogen in a 50 ± 5 °C water bath. The method was modified this point in the method. Since extracts were being analyzed by ELISA, they cannot contain more than 10% methanol. Therefore, extracts were brought up to a volume of 4 mL with reagent water, rather than methanol as directed in the method. The MBMG method requires 6 mL of methylene chloride to elute the analytes. The concentration of the extract takes place in water bath at room temperature under a stream on nitrogen. The extracts are taken to dryness, 200 μL of methanol is added and vortexed and 1800 μL of reagent water is added. From this point, both extracts were analyzed the same using ELISA.

To assess the different extraction procedures, 5 standards were made with known concentrations of sulfamethoxazole and progesterone. Concentrations of the OWCs ranged from 0 – 200 ng/L. In addition to the standards, two unknown samples were spiked at the same five concentrations. These standards and spiked samples were extracted, eluted and concentrated using both the EPA and MBMG methods.

The extracts were then analyzed (in triplicate) for sulfamethoxazole using the 96 well-plate ELISA assay. In this type of ELISA assay the antibodies have photoactive functional groups attached to a surface of the molecule, which allows colorimetric visualization of the antibody. When the antigen binds with the antibodies the result is either an increase or decrease in light absorbance at a specific wavelength which is then used to quantify the amount of antibody (the OWC in this case) that is binding to the antigen.

Results and Discussion

Method Development

The assessment of the different extraction methods was complicated by numerous analytical issues. Initial analyses indicated a contamination source, particularly for the blank and low concentration standards and spikes (up to 3 ng/L in the blanks). The blank standards and unspiked samples from this first attempt were re-analyzed, which resulted in similarly high concentrations. The initial hypothesis for these high concentrations was impure deionized water (DI).

All previous ELISA analyses had been performed using DI water obtained from a different source. To rule this out, several DI water samples were taken from various sources, including the previous source and the source currently being used. In addition to the DI samples, HPLC-grade water was also analyzed. These water samples were extracted, eluted, concentrated using a modified version of the EPA method. These extracts were then analyzed by ELISA. Due to limited supplies, a full calibration was not performed with this analysis. Instead, a standard zero, supplied by the manufacturer and included in the kit, was used to assess concentrations observed in the DI water samples. Concentrations of all the water samples were significantly higher than the zero- standard.

The results of the DI water evaluation lead to questions of possible contamination during the extraction procedure. To test this possible contaminant source, un-extracted samples were analyzed along with sample extracts. Results of this test were inconclusive; although it appeared that the high concentrations were present in both the extracts and the un-extracted samples.

At this point it was necessary to start evaluating each individual step in the analysis procedure. The procedure involves the addition and removal of two solutions prior to color development and measurement. In between solution additions, a wash is required to remove the previous solution. A commercial microplate washer (Stat Fax 2600) was used to wash the microtiter plates. Because the sipper tubes that dispense the wash and remove liquid from the wells were not cleaned between wells, it was suspected that there may have been carry over between wells. An analysis of control samples, blanks and standards was performed using a manual wash procedure (pipetter) to assess this potential source of contamination. The analysis of the samples analyzed using the manual wash procedure resulted in the control samples were well within the acceptable range, the blanks were non-detect, and the standard results were within 97% of the expected value. A confirmation analyses was performed with several samples, which included blanks. The results were acceptable; the blanks were below the reporting limit and the sample triplicates were within 3% relative percent difference. All subsequent samples were analyzed using the manual wash procedure.

The ELISA kits purchased for the comparison of extraction methods were used prior to identification of the contamination source. Additional kits purchased by the

MBMG were also used in an effort to identify the contamination source. As a result, the planned extensive method comparison was not successfully completed. However, the detailed evaluation of the ELISA procedure created greater confidence in the method prior to analysis of the environmental samples. Even though the detailed comparison was not successful, the analyses that were conducted allowed for the determination of the best extraction method. While both extraction methods provided useable results, it was observed that the methylene chloride (used as the eluent for the MBMG method) reacted with the microtiter plate causing reduced light transmission and negatively affecting concentration determinations. Typically methylene chloride is eliminated from the sample by evaporation to near dryness after which the sample was resolubilized in methanol for analysis. Evaporation to complete dryness increases the risk of sample loss to the atmosphere and the method was sensitive to the amount of residual methylene chloride. The EPA method uses methanol as the eluent, which doesn't react with microtiter plates and the use of this method eliminates the source potential measurement errors. As a result of these observations, the EPA Method 1694 was determined to be the best method and the environmental samples were analyzed using the modified version of EPA Method 1694.

Environmental Results

Detectable OWC concentrations were observed in all of the groundwater and surface-water samples (Figure 2). Sulfamethoxazole was detected in all samples and had the highest concentrations of all the OWCs analyzed. Although 100 percent detection is a higher occurrence rate than expected, Miller and Meek (2006) detected sulfamethoxazole in 78 percent of the wells they sampled in the Helena Valley, Montana, which is a similar setting. The source of sulfamethoxazole in the Helena Valley was assumed to be from septic systems or possibly livestock in some areas. In the Summit Valley (this study), there are few livestock and all the wells sampled for this study were at low risk of contamination from livestock sources. The most likely source for groundwater OWC contamination is septic systems.

Sulfamethoxazole concentrations were also positively correlated with nitrate concentrations (R^2 of 0.67; Figure 3). Nitrate concentrations above 2 mg/L are considered elevated above background (LaFave, 2008) and ten of the wells sampled had elevated nitrate concentrations. Previous isotope analyses suggest that elevated nitrate concentrations in these groundwaters can be attributed to human and animal waste; the most likely source in this area being sewage from septic systems (LaFave, 2008). Sulfamethoxazole was not correlated with DOC (R^2 of 0.00; Figure 3). Elevated DOC is commonly associated with wastewater discharges, but unlike nitrate there are also likely to be naturally occurring sources in the aquifer. The lack of a correlation between DOC and sulfamethoxazole indicates that DOC may not be a good indicator of OWC contamination in this aquifer.

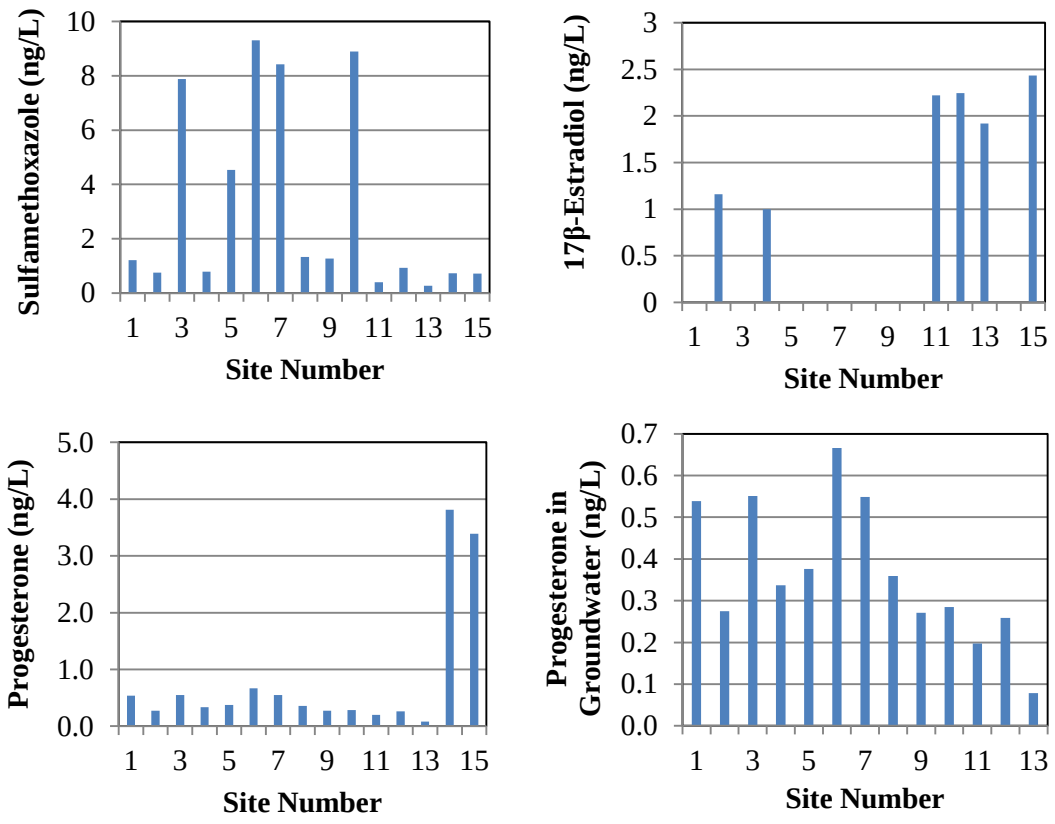

Figure 2. Concentrations of sulfamethoxazole, 17-estradiol, and progesterone in the 15 samples collected for this study.

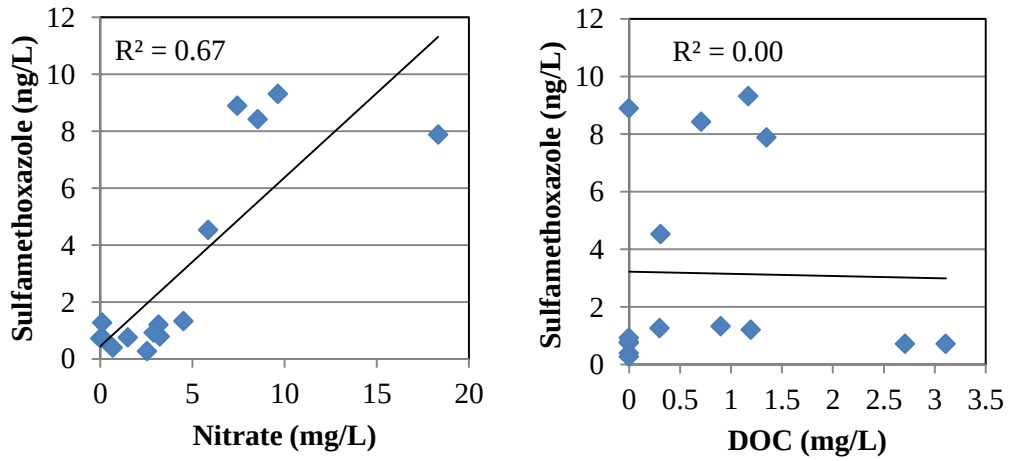

Figure 3. Plots of the correlations between sulfamethoxazole and both nitrate and DOC.

Progesterone was also detected in all of the groundwater and surface-water samples (Figure 2), with highest concentrations observed in the two stream samples (sample numbers 14 and 15). The apparent prevalence of progesterone was unexpected and is not supported by the prevalence of progesterone (four percent) in the groundwater of the Helena Valley (Miller and Meek, 2006) or the prevalence in Gallatin Valley (Montana) where no progesterone was detected in the groundwater or surface water (Icopini et al., 2008). The Helena and Gallatin Valley concentrations were determined using high-performance liquid chromatography with tandem mass spectrometric (HPLC-MS/MS). ELISA is dependent on complexation with target compounds and the transmission of light through a sample. If there are compounds in the sample that interfere with the complexation reaction or light transmission, the method can produce false positives. The HPLC-MS/MS method detects the compound directly and is not susceptible the same potential interferences as the ELISA method. The prevalence of detectable progesterone in these samples that is not supported by data from other areas suggests that these may be false positives.

The progesterone concentrations are also not strongly correlated with the nitrate concentrations (R^2 of 0.08), but progesterone concentrations were strongly correlated with DOC concentrations (R^2 of 0.84; Figure 4). The highest progesterone concentrations were observed in the Blacktail Creek samples (3.387 and 3.814 ng/L), which also had the highest DOC concentrations (2.71 and 3.11 mg/L). These correlations were similar when the creek data were removed from consideration with slightly a lower correlation between progesterone and DOC (R^2 of 0.72) and a higher correlation between progesterone and nitrate (R^2 of 0.44). The strong correlation between progesterone and DOC in the absence of a similar correlation between sulfamethoxazole and DOC suggests most or all of these detections are false positives arising from the interaction between DOC and some aspect of the ELISA method. False positives with ELISA analysis of hormones has been observed by others (Farré et al., 2006). The presence of a possible interference in these samples is strengthened by the fact that the highest progesterone concentration in the stream was detected in the sample collected upstream from the most heavily developed area. However, the slight correlation between progesterone and nitrate in the groundwater samples indicates that there may be progesterone in some of these samples. Given the likelihood of an interference with the method, the presence of progesterone in these waters should be considered inconclusive at best and more data is needed to fully evaluate the presence of progesterone in this aquifer.

17β-estradiol was observed in in five well samples and the down-stream creek sample (Figure 2). The frequency of 17β-estradiol occurrences was also higher than expected. Approximately 4 percent of the Helena Valley groundwater samples had detectable 17β-estradiol concentrations (Miller and Meek, 2006) and none of the stream or groundwater samples in the Gallatin Valley had detectable 17β-estradiol concentrations (Icopini et al., 2008). There were insufficient data for a meaningful calculation of the correlation coefficients with 17β-estradiol. However, the absence of detectable 17β-estradiol in the up-stream creek sample and the presence of detectable 17β-estradiol in the down-stream creek sample indicate that DOC did not significantly interfere with the ELISA 17β-estradiol analysis.

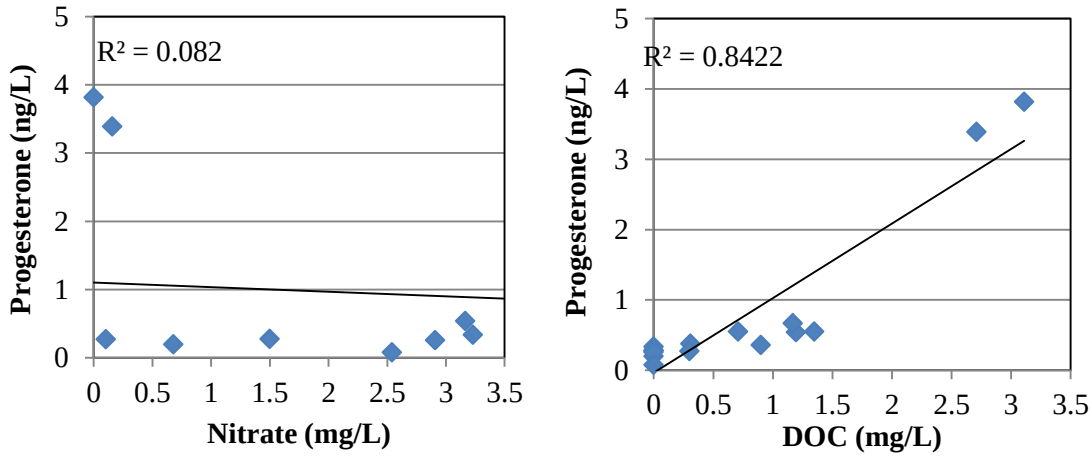

Figure 4. Plots of the correlations between progesterone and both nitrate and DOC.

Sulfamethazine was not detected in any samples. Sulfamethazine was not included in the analyte lists for the Helena Valley or the Gallatin Valley studies (Miller and Meek, 2006; Icopini et al., 2008, so there is no reference to evaluate the absence of sulfamethazine in these waters.

A comparison of the depth water enters the well (Table 1) and the occurrence of OWCs (Figure 2) indicates that depth water enters a well had little influence on the whether or not OWCs were detected in the well. Theoretically, wells with deeper intakes should be less susceptible to OWC contamination, because the source is near the surface and the OWCs will have to travel further to get into the well. This increased travel time to the well intake will also increase the potential for microbial degradation or adsorption of the OWCs onto aquifer material. Elevated nitrate concentrations were also observed to be largely independent of the depth water enters the well in this area. Additionally, the occurrence of OWCs did not appear to be influenced by aquifer type (alluvial or bedrock; Table 1 and Figure 2).

Reverse Osmosis Treatment

One of the well owners allowed the sampling of treated water, which was processed through a point of use (under the sink) reverse osmosis system (RO). This particular owner had a history of poor water quality (sample number 3; Table 1) and had the highest nitrate concentration (18.33 mg/L) of all the samples collected for this project. This well also had detectable concentrations of both sulfamethoxazole and progesterone. The RO system was effective at removing OWCs with a 94 percent reduction of sulfamethoxazole concentrations and a 61 percent reduction of progesterone concentrations in the treated water (Figure 5). The RO system was also effective at removing inorganic constituent with a 78 reduction of nitrate and a 98 reduction of sulfate in the treated water. Although the assessment of treatment systems was outside the scope of this study, this preliminary data may be value for future studies. The analysis of the RO treated water indicates that this relatively inexpensive treatment system (less than $500) can effectively remove some OWC and inorganic contaminants.

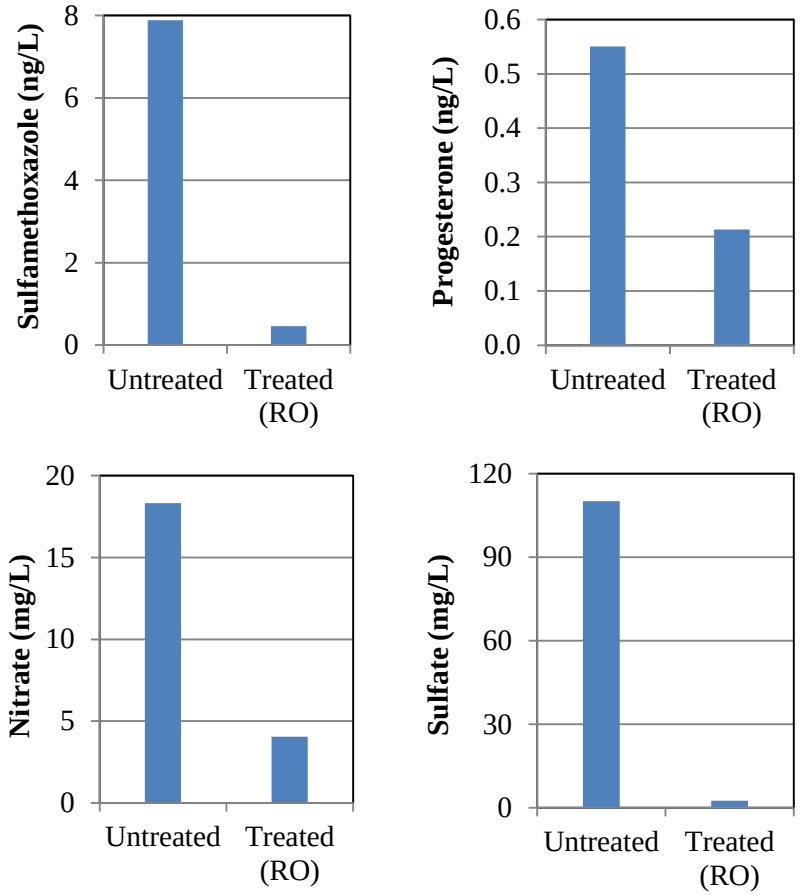

Figure 5. A comparison of sulfamethoxazole, progesterone, nitrate and sulfate concentrations in untreated water from site number 3 with water from site number 3 treated through a reverse osmosis unit (RO).

Conclusions

Organic wastewater chemicals were detected in all groundwater and surface-water samples collected for this project. Sulfamethoxazole was detected in all samples. Based on previous studies sulfamethoxazole appears to persist in the environment, which likely explains the prevalence of sulfamethoxazole in this area. Sulfamethoxazole concentrations were positively correlated with nitrate concentrations. The correlation between sulfamethoxazole and nitrate indicates that these compounds may have a similar source, which is most likely to be septic systems discharging wastewater to the aquifer. Progesterone was also detected in all groundwater and surface-water samples collected for this project. However, progesterone was strongly correlated with DOC and poorly correlated with nitrate. The detected progesterone concentrations most likely represent false positives resulting from interference of some aspect of the ELISA method by DOC and the progesterone data should treated as suspect until confirmation analyses can be conducted to support these data. 17β-estradiol was detected in 40 % of the samples and the 17β-estradiol did not appear to be affected by the presence of DOC. Sulfamethazine was not detected in any of the samples. The occurrence of OWCs did not appear to be influenced by the depth water enters the well or the aquifer composition. The results of

this study indicate that OWC contamination is widespread in the Summit Valley. However, more research with an expanded analyte list is needed to confirm these results and fully evaluate the presence of OWCs in these waters.

Although only one treated sample was collected, relatively inexpensive reverse osmosis systems appear to effectively remove OWCs and inorganic contaminants. This is a potentially cost-effective approach to dealing with OWC contamination. More research is needed to fully evaluate reverse osmosis as a treatment technology for a wider range of OWC contaminants.

References

Barnes, K.K., D.W. Kolpin, E.T. Furlong, S.D. Zaugg, M.T. Meyer, and L.B. Barber, 2008, A national reconnaissance of pharmaceuticals and other organic wastewater contaminants in the United States – I) Groundwater, *Science of the Total Environment*, 402: 192-200.

Batt, A.L., D.D. Snow, and D.L. Aga, 2006, Occurrence of sulfonamide antimicrobials in private water wells in Washington County, Idaho, USA, *Chemosphere*, 64: 1963–1971.

Boxall, A.B.A., Kolpin, D.W., Sorensen, B.H., Tolls, J., 2003. Are veterinary medicines causing environmental risks?, *Environmental Science & Technology* 37, 265A–304A.

Farré, M., Brix, R., Kuster, M., Rubio, F., Goda, Y., López de Alda, M.J., and Barceló, D., 2006, Evaluation of commercial immunoassays for the detectionof estrogens in water by comparison with high-performance liquid chromatography tandem mass spectrometry HPLC–MS/MS (QqQ) *Anal. Bioanal. Chem.* 385: 1001-1011.

Hilton, M.J., and Thomas, K.V., 2003, Determination of selected human pharmaceutical compounds in effluent and surface water samples by high-performance liquid chromatography-electrospray tandem mass spectrometry, *J. Chromatogr. A* 1015**:** 129–141.

Icopini, G.A., 2008, Screening for Pharmaceuticals and Endocrine Disrupting Chemicals in Montana Ground Water, Technical Report submitted to U.S. Department of Agriculture, Natural Resources Conservation Service, 48 pp.

Kidd, K.A., Blanchfield, P.J., Mills, K.H., Palace, V.P., Evans, R.E., Lazorchak, J.M., and Flick, R.W., 2007, Collapse of a fish population after exposure to a synthetic estrogen, *Proceedings of the National Academy of Sciences*, Vol. 104(21), p. 8897-8901.

Kumar, K., Gupta, S.C., Chander, Y., and Singh, A.K., 2005, Antibiotic use in agriculture and its impact on the terrestrial environment, *Advances in Agronomy*, 87:1–54.

LaFave, J.I., 2008, Nitrate in the ground water and surface water of the Summit Valley near Butte, Montana, Montana Bureau of Mines and Geology: Ground-Water Open-File Report 22, 35 p.

Levy, S.B., 1997, Antibiotic resistance: an ecological imbalance, In Antibiotic Resistance: Origins, Evolution, Selection and Spread. Wiley, West Sussex, England, pp 1-14.

Miller, K.J. and Meek, J., 2006, Helena Valley Ground Water: Pharmaceuticals, Personal Care Products, Endocrine Disruptors (PPCPs), and Microbial Indicators of Fecal

Contamination, Montana Bureau of Mines and Geology Open-File Report 532, 19p.

Norris, D.O., 2006, Xenoestrogen actions on reproduction: implications for health of wildlife and humans, in Proceedings of the 2007 AWRA Summer Specialty Conference on Emerging Contaminants of Concern in the Environment, Vail, CO.

Orlando, E.F., Kolok, A.S., Binzcik, G.A., Gates, J.L., Horton, M.K., Lambright, C.S., Gra, L.E., Jr., Soto, A.M., and Guillette, Jr., L.J., 2004. Endocrine-disrupting effects of cattle feedlot effluent on an aquatic sentinel species, the fathead minnow. Env. Health Persp. 1 March.

USDA, 2007. Antimicrobial Resistance Issues in Animal Agriculture. C10.1299. Fort Collins, CO: USDA:APHIS:VS, Centers for Epidemiology and Animal Health; 1993c. http://www.aphis.usda.gov/vs/ceah/cei/taf/emerginganimalhealthissues_files/antiresist2007update.pdf.

U.S. EPA, 2007, Method 1694: Pharmaceuticals and Personal Care Products in Water, Soil,Sediment, and Biosolids by HPLC/MS/MS, U.S. Environmental Protection Agency, EPA-821-R-08-002, 77 pp.

Woodling, J.D., Lopez, E.M., Maldonado, T.A., Norris, D.O., and Vajda, A.M., 2006, Intersex and other reproductive disruption of fish in wastewater effluent dominated Colorado streams, *Comparative Biochemistry and Physiology Part C: Toxicology & Pharmacology* Vol. 144(1), p. 10-15.

Quantification of Coal-Aquifer Baseflow in Montana Rivers Using Carbon Isotopes

Basic Information

Title:	Quantification of Coal-Aquifer Baseflow in Montana Rivers Using Carbon Isotopes
Project Number:	2009MT191B
Start Date:	3/1/2009
End Date:	2/28/2011
Funding Source:	104B
Congressional District:	At-Large
Research Category:	Ground-water Flow and Transport
Focus Category:	Hydrogeochemistry, Methods, Water Quantity
Descriptors:	
Principal Investigators:	Elizabeth Meredith

Publications

There are no publications.

Title

Identification and quantification of baseflow using carbon isotopes

Authors

Elizabeth Meredith[a]*

Shawn Kuzara[a]

Affiliations

[a] Montana Bureau of Mines and Geology
Montana Tech of the University of Montana
1300 N 27th Street
Billings, Montana 59101 USA
*corresponding author: emeredith@mtech.edu, 406-657-2929 phone, 406-657-2633 fax.

Abstract

Six locations along Otter Creek in southeastern Montana and a nearby monitoring well completed in the Knobloch coal were sampled and analyzed for carbon isotope ratios. Between where it becomes a perennial stream near the town of Otter to where it meets the Tongue River near the town of Ashland, Otter Creek crosses the Knobloch coal outcrop. The carbon isotope ratio of the creek becomes progressively more similar to that of the Knobloch coal aquifer in samples collected down-gradient from the town of Otter. The isotope ratio of the stream changes from -10.5 to -8.9$^{o}/_{oo}$, reflecting the influence of the Knobloch coal aquifer baseflow contribution which has a carbon isotope value of +3.9$^{o}/_{oo}$. The dissolved inorganic carbon concentrations of the ground water and surface water are similar (approximately 90 mg/L), which allowed the use of the simplified, first-order, two-end-member mixing equation. Using carbon isotope ratios, calculations of the fraction of water contributed by the Knobloch coal aquifer indicate that approximately 11% of the surface water in Otter Creek at its mouth near Ashland was originally Knobloch coal aquifer ground water.

Acknowledgements

Funding for this project came from a grant through the U.S. Geological Survey Water Resources Research 104b program. Sample collection was aided by Simon Bierbach and Clay Schwartz. The authors would like to thank Dr. Carol Frost for productive discussions regarding this study.

Introduction

Baseflow

The ground-water contribution to surface water is notoriously hard to measure. Traditionally, baseflow has been quantified by measuring surface-water flow rates along a section of river and accounting for gains and losses. Any gains not accounted for through surface-water inputs are assumed to be ground-

water baseflow (Kalbus et al. 2006). However, as stream valleys widen or narrow, surface water can be forced in and out of the river channel masking the actual contribution from ground-water sources. Additionally, alluvial and bedrock ground water sources cannot be distinguished using this method. Ground-water modeling is another method that is being used more commonly to define the water budget of streams and alluvial valleys, but modeling requires a high density of monitoring wells, water-level data, and in-stream flow measurements (Kasper et al. 2010; Kuzara et al. 2011). The infrastructure and time required to create an accurate model are often prohibitive. Baseflow, none-the-less, is an important element in the water budget equation. Ground-water contributions play an important role in regulating the temperature of surface water and, in areas dominated by small streams, can be important for keeping surface water open for wildlife in the winter (Kalbus et al. 2006).

Site location

Otter Creek is a small, perennial, meandering stream in southeastern Montana. It becomes a perennial stream just north of the town of Otter and meets the Tongue River at the town of Ashland approximately 48 kilometers (30 miles) to the north (Figure 1). Along the 48 kilometer valley, the elevation drops by 224 meters (736 feet) resulting in a relatively low gradient of 4.7 meters/kilometer (24.5 feet/mile). The flow rate of Otter Creek, as measured using a Swoffer brand fiber optic flow meter, on December 1, 2010 at sample site OC-2 was 23.5 liters/second (0.83 cubic feet per second). In this rural area, residents primarily raise cattle and grow hay grasses in the alluvial valley. The valley floor is generally less than 0.8 kilometers (½ mile) wide, but at its widest points can exceed 1.3 kilometers (0.8 miles). The edges of the valley are flanked by steeply rising hills of the Ashland Ranger District of the US Forest Service. Several ephemeral streams feed into Otter Creek from the Forest including: Home Creek, 10 Mile Creek, 15 Mile Creek, and Taylor Creek (Figure 1). These tributary streams carry surface water during periods of high run-off in the spring and early summer.

Otter Creek crosses the Tertiary Fort Union Formation, which is composed of layered sandstone, shale, and coal (Figure 2)(Cannon, 1985). The Fort Union Formation is the target of most of the coal and coalbed methane development in eastern Montana (Meredith et al. 2011). The largest named subunit that the creek crosses is the Knobloch coal, a subbituminous coal that ranges in thickness from 5 to 24 meters (17 to 78 feet) thick (Cannon, 1985). The Knobloch coal is split into two subunits in the southern end of the study area: the Upper Knobloch and Lower Knobloch. The coal is combined into one unit in the northern end of the study area near US Highway 212 (Figure 1). The Fort Union Formation is generally flat-lying and coal is exposed through down-cutting by Otter Creek.

Otter Creek crosses several small coal seams (Figure 2) along its length; it crosses the Upper Knobloch coal approximately 5 kilometers up-stream from sample site OC-3 and crosses the Lower Knobloch coal approximately 3 kilometers down-stream from sample site OC-4 (Figure 1).

Ground-water extraction

Coal seams are the primary bedrock aquifers in semi-arid southeastern Montana and support a stable livestock industry. Development of coal-related energy in southeastern Montana places large demands on the ground-water resources. Coalbed methane development to the south and west of the study area

withdraws large amounts of ground water from coal aquifers as a part of the methane extraction process; however, no coalbed methane development is currently taking place in the Knobloch coal. Coal mining, such as that taking place in Colstrip, Montana approximately 64 kilometers (40 miles) to the northwest of the study site, requires dewatering coal for production. Both coal mining and coalbed methane production has been shown to drawdown the water table for several miles away from the dewatering source (Meredith et al. 2011; Van Voast and Reiten, 1988). An open-pit coal mine is proposed for the study area, which could impact domestic and stock water wells and could potentially impact the surface flows in Otter Creek depending upon the amount of baseflow the Knobloch coal aquifer provides to the stream.

Isotope mixing model

Isotopes of carbon have been shown to be effective tracers of ground water/surface water interaction (Campbell et al. 2008; McLaughlin et al. 2011; Sharma and Frost, 2008; Frost et al. 2010). Ground water attains its isotopic signature through its interaction with the aquifer material along its flow path and through the activities of microbes; the isotopic signature of surface water is gained through its interaction with soils, the atmosphere, and the surrounding geology. In many situations, the ground water of interest will have a measurably different isotopic signature than the surface water with which it is interacting (Brinck and Frost, 2007).

When two isotopically distinct waters interact, the resulting isotope ratio will fall between the two end-member isotope ratios in proportion to the concentrations (Faure, 1998). Stable carbon isotopes are measured in the dissolved inorganic carbon (DIC) component of the water and are expressed as per mil deviation from the carbon standard, the Pee Dee Belemnite ($\delta^{13}C$). The carbon isotope ratio of the mixed water is related to the ground-water and surface-water isotope ratios and can be expressed in the following relationship:

$$\delta^{13}C_{mix} = \delta^{13}C_{GW} f_{GW} \frac{[DIC]_{GW}}{[DIC]_{mix}} + \delta^{13}C_{SW}(1 - f_{GW}) \frac{[DIC]_{SW}}{[DIC]_{mix}} \qquad \text{Eq. 1}$$

Where $\delta^{13}C_{mix}$ is the carbon isotope ratio of the mixed surface and ground water, $\delta 13C_{GW}$ is the carbon isotope ratio of the ground-water end-member, and $\delta^{13}C_{SW}$ is the carbon isotope ratio of the surface water end-member. The symbols $[DIC]_{GW}$, $[DIC]_{SW}$, and $[DIC]_{mix}$ refer to the DIC concentrations of the ground water, surface water and mixed water, respectively. The fraction of the mixed water that was contributed by the ground-water end-member is represented by the term f_{GW}.

If the DIC concentration of the ground water and surface water are similar, Equation 1 can be simplified to a first-order mixing model:

$$\delta^{13}C_{mix} = \delta^{13}C_{GW} f_{GW} + \delta^{13}C_{SW}(1 - f_{GW}) \qquad \text{Eq. 2}$$

In situations where the isotope ratios and concentrations of the two end-members and the mixture can be measured, these equations (1 and 2) can be rearranged to solve for the fraction of water that was contributed by ground water (f_{GW}).

Methods

The ground-water sample was collected after first purging the well of three casing volumes of water. Surface-water samples were sampled at access points at culverts and bridges. If the stream was open, the collected sample was a homogenized, depth- and width-integrated sample. If the stream was frozen at the sample collection point, a hole was drilled through the ice over the stream thalweg and a depth-integrated sample was collected. Parameters of temperature, specific conductance, pH, and water level were collected in the field.

Samples for major and minor constituent analysis and DIC were filtered, preserved and stored in accordance with the standard laboratory procedures of the Montana Bureau of Mines and Geology Analytical Laboratory. Analytical error of DIC measurement is approximately 10%. Samples for carbon isotope analysis were filtered through 0.45 micron filters, stored with no head space and sent overnight to the University of Arizona. The analytical precision of the carbon isotope measurements varied between 0.030 and 0.034.

Otter Creek was sampled at six locations along the entire perennial reach (Figure 1). The Knobloch coal aquifer was sampled at well WO-2 near the Otter Creek sample site OC-3, between the outcrops of the Upper Knobloch and Lower Knobloch. Well WO-2 is completed in the Lower Knobloch coal, which is the thicker and more transmissive subunit (Figure 2). Site location information and all major and minor constituent analyses are available on the Montana Bureau of Mines and Geology on-line database (GWIC: http://mbmggwic.mtech.edu/). Sample information is accessed by the GWIC ID number listed on Table 1.

Surface water samples were collected after: 1. the first freezing temperatures shut down transpiration in plants that may have intercepted ground-water baseflow to the stream and 2. the tributary streams no longer had free-flowing surface water. This ensured that the maximum contribution of baseflow to the stream would be measured without dilution from other sources. Sample sites OC-1 and OC-2 were open when sampled, sample sites OC-3 to OC-6 were frozen and were sampled through the ice.

Results and Discussion

The isotope ratio of the surface-water samples move progressively toward the isotope ratio of the ground water from the Knobloch coal aquifer as the stream crosses the Knobloch coal outcrop (Table 1). The carbon isotope ratio becomes progressively more positive from OC-1 (-10.5$^{o}/_{oo}$) to OC-6 (-8.9$^{o}/_{oo}$). Contribution from the Knobloch coal aquifer, with a carbon isotope ratio of +3.9$^{o}/_{oo}$, would drive this change.

The DIC concentration of the Knobloch aquifer is very similar to the DIC concentration of the surface water (the concentrations are within the measurement error of 10%). Therefore equation 2 can be used

to calculate the fraction of ground water contributed at each sample location. Sample OC-1 (-10.5$^{o}/_{oo}$) is used as the $\delta^{13}C_{SW}$ term, +3.9 $^{o}/_{oo}$ (the Knobloch coal aquifer carbon isotope value) for the $\delta^{13}C_{GW}$ term, and each individual surface water sample site for the $\delta^{13}C_{mix}$ term (Table 2). While the sample collected at OC-1 does not necessarily represent a complete absence of a Knobloch coal aquifer ground-water contribution, it will be used in this situation to represent one end-member of the mixing equation. The following calculated fractions represent the Knobloch ground-water contribution in addition to any amount already present at sample site OC-1 and are therefore minimum percentages (Table 2).

This isotope tracing method indicates a contribution of ground-water baseflow to Otter Creek from the Knobloch coal aquifer. Calculations indicate progressively more ground water present in the surface water as the creek crossed the Knobloch coal outcrop. By the time Otter Creek reaches the Tongue River at Ashland, Montana, approximately 11% of the surface water present was from the Knobloch coal aquifer.

Conclusions

Carbon isotopes are effective tracers of ground water/surface water interaction. Carbon isotopes proved especially useful because the DIC concentration of the coal aquifer water and the surface water were similar and the two isotope ratios were very dissimilar. These characteristics made detecting changes to the isotope ratio of the surface water likely if a ground-water contribution existed. Several factors can influence the DIC concentration and carbon isotope ratio of surface water, such as interaction with the atmosphere, with soil air and soil water, and fractionation from plants and animals. These complications were limited in this study by sampling after the creek was frozen (at 4 of the 6 sites), which limits the creek's interaction with the atmosphere. Additionally, by December in Montana plant and animal respiration is very low and the shallow soil water is frozen. Calculations of isotope mixing indicate that approximately 11% of the surface water in Otter Creek at its mouth near Ashland, Montana was originally ground water from the Knobloch coal. Disruption of the Knobloch coal aquifer by coal mining could potentially reduce the in-stream flows of Otter Creek.

Future work should include confirming these results with additional parameters such as measuring flow rates along Otter Creek just prior to freezing to monitor for gains and losses. Additionally, sampling at other times of the year when the tributary streams are flowing would allow the identification of coal aquifer ground-water contributions to the smaller watersheds. The utility of carbon isotopes in identifying the presence of methane and the isolation of reservoirs has been shown by several groups (Frost et al. 2010; Sharma and Frost, 2008; McLaughlin et al. 2011) and therefore it would be beneficial for Wyoming and Montana to require the coalbed methane industry to submit ground water samples for carbon isotope analysis from all new coalbed methane wells. Carbon isotope analyses of DIC are relatively inexpensive (ranging from $11 to $30) and a large, basin-wide dataset would provide the basis for additional studies, such as flow path and geochemical evolution identification (Brinck et al. 2008).

References

Brinck, E.L., J.I. Drever, and C.D. Frost. 2008. The geochemical evolution of water coproduced with coalbed natural gas in the Powder River Basin, Wyoming. *Environmental Geosciences* 15, no. 4: 153-171.

Brinck, E.L., and C.D. Frost. 2007. Detecting infiltration and impacts of introduced water using strontium isotopes. *Ground Water* 45, no. 5: 554-568.

Campbell, C.E., B.N. Pierson, and C.D. Frost. 2008. Strontium isotopes as indicators of aquifer communication in an area of coal-bed natural gas production, Powder River Basin, Wyoming and Montana. *Rocky Mountain Geology* 43, no. 2: 171-197.

Cannon, M.R. 1985. Effects of potential surface coal mining on dissolved solids in Otter Creek and in the Otter Creek alluvial aquifer, Southeastern Montana. *U.S. Geological Survey Water Resources Investigation* 85-4206, 52 p.

Drever, J.I., and C.L. Smith. 1978. Cyclic wetting and drying of the soil zone as an influence on the chemistry of groundwater in arid terrains. *American Journal of Science* 278: 1448-1454.

Faure, G. 1998. *Principles and Applications of Geochemistry*. Upper Saddle River, New Jersey: Prentice Hall.

Frost, C.D., E.L. Brinck, J. Mailloux, S. Sharma, C.E. Campbell, S.A. Carter, and B.N. Pearson. 2010. Innovative approaches for tracing water co-produced with coalbed natural gas: applications of strontium and carbon isotopes of produced water in the Powder River Basin, Wyoming and Montana (invited). In K.J. Reddy (ed.) *Coalbed Methane: Energy and Environment*, Nova Science Publishers, New York (in press).

Kalbus, E., F. Reinstorf, and M. Schirmer. 2006. Measuring methods for groundwater - surface water interactions: a review. *Hydrology and Earth System Sciences* 10, no. 6: 873-887.

Kasper, J. W., J.M. Denver, T.E. McKenna, and W.J. Ullman. 2010. Simulated impacts of artificial groundwater recharge and discharge on the source area and source volume of an Atlantic Coastal Plain stream, Delaware, USA. *Hydrogeology Journal* 18, no. 8: 1855-1866.

Kuzara, S., E. Meredith, and P. Gunderson. 2011. Aquifers and streams in the Stillwater and Rosebud watersheds. *Montana Bureau of Mines and Geology Open-File Report*, *in press*.

McLaughlin, J.F., C.D. Frost, and S. Sharma. 2011. Geochemical analysis of Atlantic Rim water, Carbon County, Wyoming: New applications for characterizing coalbed natural gas reservoirs. *AAPG Bulletin* 95, no. 2: 191-217.

Meredith, E., S. Kuzara, J. Wheaton, S. Bierbach, K. Chandler, T. Donato, J. Gunderson, and C. Schwartz. 2011. 2010 Annual Coalbed Methane Regional Groundwater Monitoring Report: Powder River Basin, Montana. *Montana Bureau of Mines and Geology Open-File Report* 600, 130p.

Sharma S., and C. D. Frost. 2008. Tracing Coal Bed Natural Gas Co-Produced Water Using Stable Isotopes of Carbon . *Ground Water* 46: 329-334.

Van Voast, W.A., and J.C. Reiten. 1988. Hydrogeologic responses twenty years of surface coal mining in southern Montana. *Montana Bureau of Mines and Geology Memoir* 62, 30 p.

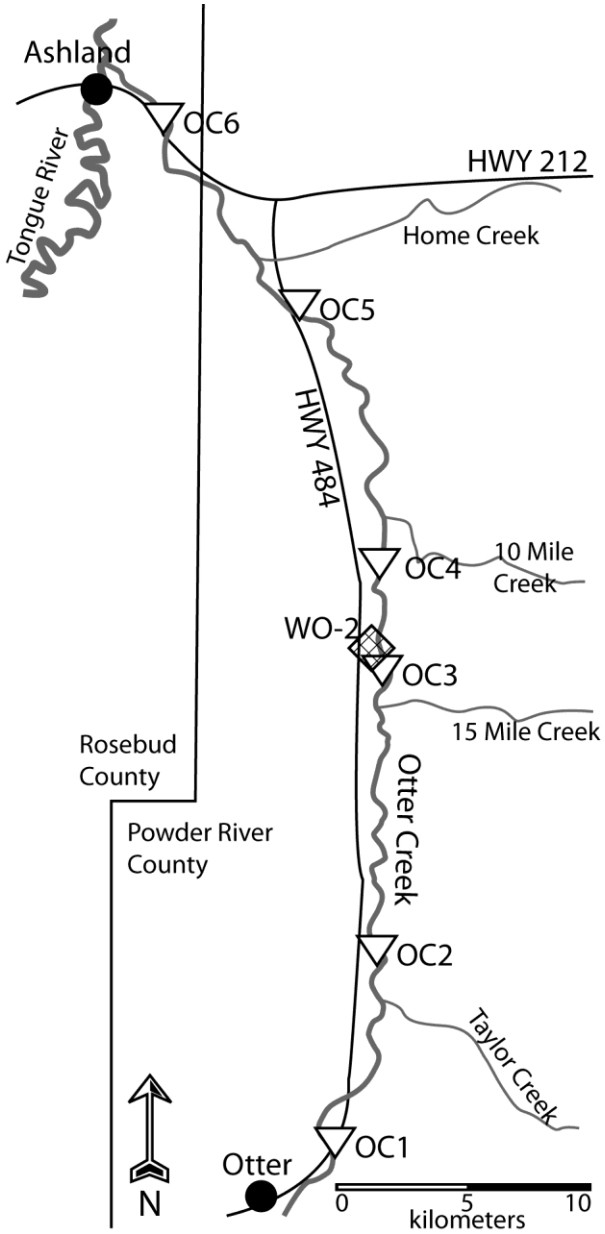

Figure 1. Locations of stream sample sites (triangles) and the Lower Knobloch coal monitoring well WO-2 (diamond) along Otter Creek.

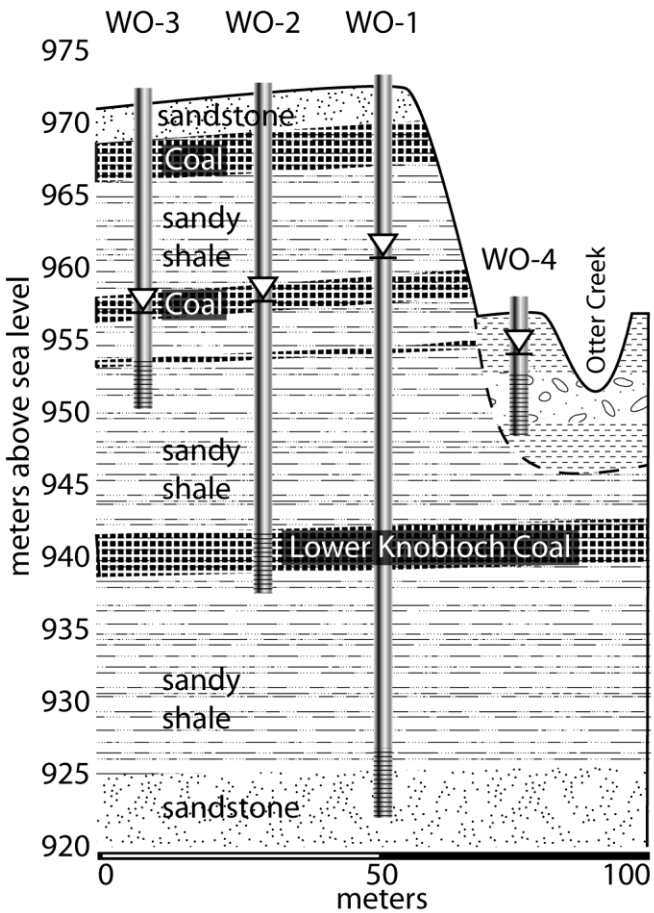

Figure 2. Stratigraphy of the Otter Creek monitoring well site near 15 Mile Creek and the surface water sampling site OC-3. Well WO-2, completed in the Lower Knobloch coal, was sampled February 16, 2011. The potentiometric surface of the monitored aquifers is represented by white triangles.

Table 1. Otter Creek and Knobloch coal carbon isotope ratios and major ion chemistry

	Sample Date	GWIC ID*	Sample Name	δ13C (UofA)	DIC mg/L (Mtech)	Water Chemistry (Mtech)
Otter Creek surface water samples	12/1/2010	259296	OC1 @ Bear Creek	-10.5	96.2	Na SO_4
	12/1/2010	7910	OC2 @ Taylor	-10.1	107	Mg Na SO_4
	12/1/2010	259300	OC3 @ 15 Mile	-9.8	109	Mg Na SO_4
	12/1/2010	259302	OC4 @ 10 Mile	-9.4	108	Mg Na SO_4
	12/1/2010	259304	OC5 @ Br s of Willow	-9.1	70.3	Mg Na SO_4
	12/1/2010	259306	OC6 @ Ashland	-8.9	106	Na SO_4
Lower Knobloch ground water sample	2/16/2011	7781	WO-2	3.9	87.4	Na HCO_3

*To access location information and analytical chemistry analyses enter the GWIC ID into the Ground Water Information Center online database:http://mbmggwic.mtech.edu/

Table 2. Calculated fraction of surface water contributed by Knobloch coal aquifer ground water

Sample Name	Carbon f_{GW} (%)
OC1 @ Bear Creek	0.00
OC2 @ Taylor	2.64
OC3 @ 15 Mile	4.79
OC4 @ 10 Mile	7.78
OC5 @ Br s of Willow	9.86
OC6 @ Ashland	11.53

Appendix A

Preliminary Study

A preliminary study was done to assess the viability of the proposed strontium and carbon isotope tracing method and to identify promising field sites. Three streams that cross the Knobloch coal outcrop were sampled in March, 2010 above and below the outcrop: Otter Creek (O.C.), Rosebud Creek (R.C.), and the Tongue River (T.R.). Additionally, three wells completed in the Knobloch coal were sampled in November, 2009 (Table A1). Surface-water samples in Table A1 are listed with the up-gradient sample first followed by the down-gradient sample.

The strontium isotope ratios of the down-gradient samples were lighter than the up-gradient samples with the exception of the Tongue River, which had similar strontium isotope ratios for both up-gradient (0.70949) and down-gradient (0.70951). The fact that the down-gradient isotope ratio is heavier may just reflect the natural variability (the values may not be statistically different) or the fact that it is difficult to get a homogeneous sample that accurately reflects the whole system from a large stream such as the Tongue River. The carbon isotope ratio got heavier down-gradient in Otter Creek and lighter in Rosebud Creek and the Tongue River. The direction one would expect the ratio to change depends upon the carbon isotope ratio of the ground-water input. The three sampled wells did not make this clear.

The three wells sampled in November 2009 illustrate the isotopic variability of the Knobloch coal. The carbon isotope ratio ranged from -1 to -13.9 $^{o}/_{oo}$. The strontium isotope ratio had a narrower range of 0.70825 to 0.70847. This variability in the coal aquifer water was not expected based upon the results from previous studies in Wyoming (Campbell et al. 2008; McLaughlin et al. 2010), which found similar carbon and strontium isotope values in ground-water samples collected over large areas of a single coal aquifer. The variability of the Knobloch coal ground water indicated that the final study site required a ground-water sample location near the coal outcrop/surface water interface. The three wells sampled for the preliminary study were several miles from the nearest stream so another well had to be identified.

Well WO-2 was chosen because it is completed in the Lower Knobloch and is in the alluvial valley of Otter Creek between where the Upper Knobloch outcrops and where the Lower Knobloch outcrops. No similar wells were available for the Tongue River or for Rosebud Creek, limiting the final study to Otter Creek. In addition to the availability of a ground-water sample site, Otter Creek is a good location for an isotope study such as this one because there are few tributaries, especially in winter when most tributaries are dry, and its small size makes collecting a homogeneous sample relatively straight forward. The final study design, therefore, included strontium and carbon isotope samples of the well WO-2 and six locations along Otter Creek from above the coal outcrop to where the creek meets the Tongue River at Ashland, Montana.

Table A1. Sample results for preliminary and final studies

	Date	GWIC ID	Sample	d13C (UofA)	DIC (Mtech)	Water Chemistry (Mtech)	Sr Isotope ratio (UNC)	%STD error	[Sr]	dO (U.Wyo)	dH (U.Wyo)
									UNC/MTECH		
River Samples	3/11/2010	7910	O.C. @ Taylor	-8.6	no reading	Mg Na SO4	0.709638	0.0008	1.97/1.893	-139.1	-20.8
	3/11/2010	259302	O.C. @ 10 mile	-8.4	no reading	Mg Na SO4	0.709576	0.0008	1.86/0.713	-143.4	-21.2
	3/10/2010	223687	R.C. @ Taylor	-8.8	no reading	Mg HCO3	0.710365	0.0008	0.731/0.713	-146.0	-22.2
	3/10/2010	191129	R.C. @ N.C.	-8.9	no reading	Ca Mg HCO3	0.710184	0.0007	0.799/0.769	-146.2	-21.8
	3/10/2010	242240	T.R. @ Birney	-6.3	no reading	Ca Mg HCO3	0.709490	0.0008	0.599/0.569	-137.3	-20.7
	3/10/2010	242239	T.R. @ B.D.	-6.4	no reading	Ca Mg HCO3	0.709517	0.0008	0.546/0.548	-135.9	-20.4
									/MTECH		
Knobloch Coal Samples	11/4/2009	203697	CBM02-8KC	-13.2	208	Na HCO3	0.708382	0.0009	/0.249	n/a	n/a
	11/3/2009	251797	GC09-KC	-13.9	139	Na SO4	0.708473	0.0007	/7.631	n/a	n/a
	11/3/2009	207099	WL-2	-1.0	289	Na HCO3	0.708258	0.0008	/0.356	n/a	n/a
	2/16/2011	7781	WO-2	3.9	87.4	Na HCO3	pending		/0.121	n/a	n/a
									UNC/MTECH		
Otter Creek Samples	12/1/2010	259296	OC1 @ Bear Creek	-10.5	96.2	Na SO4	0.709347	0.000014	2.2655/2.035	n/a	n/a
	12/1/2010	7910	OC2 @ Taylor	-10.1	107	Mg Na SO4	0.709610	0.000011	2.492/2.240	n/a	n/a
	12/1/2010	259300	OC3 @ 15 Mile	-9.8	109	Mg Na SO4	0.709603	0.000013	2.3527/2.108	n/a	n/a
	12/1/2010	259302	OC4 @ 10 Mile	-9.4	108	Mg Na SO4	0.709588	0.000011	2.5431/2.260	n/a	n/a
	12/1/2010	259304	OC5 @ Br S of Willow	-9.1	70.3	Mg Na SO4	0.709418	0.000011	2.4809/2.223	n/a	n/a
	12/1/2010	259306	OC6 @ Ashland	-8.9	106	Na SO4	0.709300	0.000010	2.3189/2.084	n/a	n/a

Strontium concentrations were measured by both University of North Carolina (UNC) by isotope dilution on a thermal ionization mass spectrometer and by Montana Tech Analytical Chemistry Laboratory by ICP-MS.

Appendix B

Strontium Isotope Study

Strontium isotopes were measured on each surface water sample and the four ground-water samples (see Table A1). Strontium has two common stable isotopes: ^{87}Sr and ^{86}Sr. The isotope ^{87}Sr is the stable, radiogenic daughter product of ^{87}Rb (87-rubidium). The ratio between ^{87}Sr and ^{86}Sr will vary depending upon the original Rb content of aquifer host rock. The strontium isotope mixing relationship between ground water and surface water is similar to Equation 1:

$$\frac{^{87}Sr}{^{86}Sr}_{mix} = \frac{^{87}Sr}{^{86}Sr}_{GW} f_{GW} \frac{[Sr]_{GW}}{[Sr]_{mix}} + \frac{^{87}Sr}{^{86}Sr}_{SW} (1 - f_{GW}) \frac{[Sr]_{SW}}{[Sr]_{mix}} \qquad \text{Eq. B1}$$

Where $^{87}Sr/^{86}Sr_{mix}$ is the strontium isotope ratio of the mixed surface and ground water, $^{87}Sr/^{86}Sr_{GW}$ is the strontium isotope ratio of the ground-water end-member, and $^{87}Sr/^{86}Sr_{SW}$ is the strontium isotope ratio of the surface water end-member. The symbols $[Sr]_{GW}$, $[Sr]_{SW}$, and $[Sr]_{mix}$ refer to the strontium concentrations of the ground water, surface water and mixed water, respectively. The fraction of the mixed water that was contributed by the ground-water end-member is represented by the term f_{GW}.

In the final study along Otter Creek, the strontium isotope ratio becomes lighter from OC-2 (0.70961) to OC-6 (0.70930). Baseflow from the Knobloch coal, with a strontium isotope ratio of *0.7083**, would drive this lowering of the strontium isotope ratio. (**Based on results from three sampled wells completed in the Knobloch coal – the actual result is pending analysis by the University of North Carolina.)*

The strontium concentration of the Knobloch coal aquifer (0.12 mg/L) is lower than the Otter Creek surface water (approximately 2.5 mg/L). Sample OC-2 is used as the surface water end-member because sample OC-1 does not appear to represent unaltered surface water. Sample OC-1 may have been affected by disturbing the mud when wading to sample the stream. This was not an issue at OC-2 which had a gravel bottom and at OC-3 to OC-6, which were sampled through the ice. The measured strontium concentrations of the surface water samples are not progressively lower as the creek crosses the Knobloch outcrop, as would be expected if the change in concentration were caused by the addition of Knobloch coal ground water to the surface water. However, with the exception of OC-4, the samples collected down stream from OC-2 have a lower strontium concentration than OC-2 (as measured by

Montana Bureau of Mines and Geology Analytical Laboratory). The strontium isotope ratio and concentration allowed the calculation of the f_{GW} term as presented in Table B1.

Table B1. Calculated fraction of surface water contributed by Knobloch coal aquifer ground water

Sample Name	Strontium f_{GW} (%)
OC1 @ Bear Creek	
OC2 @ Taylor	0.00
OC3 @ 15 Mile	6.23
OC4 @ 10 Mile	-0.94
OC5 @ Br s of Willow	0.83
OC6 @ Ashland	7.40

The strontium isotope calculations were complicated by the varying concentration of strontium in the surface water. This may be due to the surface water interaction with the soil and alluvium of the valley. Soils in this arid area have soluble salts dominated by calcium carbonate (calcite) and calcium sulfate (gypsum) (Drever and Smith, 1978; Brinck et al. 2008). Strontium is chemically similar to calcium and can replace calcium in these minerals. Surface water interaction with the soil soluble salts may be causing this variation in strontium concentrations unrelated to the ground-water contribution.

While the strontium isotope ratio appears to be a good indication of the presence of Knobloch coal aquifer ground water, the measured concentrations of strontium were not consistent enough to make quantifying its influence possible.

Characterization of shallow subsurface hydraulic heterogeneity in the Silver Bow Creek - Butte, Montana area through field and laboratory experiments

Basic Information

Title:	Characterization of shallow subsurface hydraulic heterogeneity in the Silver Bow Creek - Butte, Montana area through field and laboratory experiments
Project Number:	2010MT213B
Start Date:	3/1/2010
End Date:	2/28/2011
Funding Source:	104B
Congressional District:	At-Large
Research Category:	Ground-water Flow and Transport
Focus Category:	Groundwater, Hydrology, Models
Descriptors:	None
Principal Investigators:	Bwalya Malama

Publications

There are no publications.

Characterisation of the shallow subsurface in the Butte–Silver Bow and Dillon areas in southwest Montana using pneumatic slug tests

Final Report

Prepared by: Bwalya Malama, Ph.D.
Formerly of the Department of Geological Engineering,
Montana Tech of the University of Montana

Submitted to: The Montana Water Center
Montana University System
and
the U.S. Geological Survey

February 8, 2011

Summary

Results of pneumatic slug tests conducted in an unconfined aquifer at various sites in the Butte–Silver Bow area in southwestern Montana are presented. The results vary from monotonic decay to oscillatory, and seem to indicate that the water table does have a significant effect on slug test response. The analyses of the data were performed with the AQTESOLV implementation of the KGS unconfined aquifer model (Hyder et al., 1994) which does to account for wellbore inertial effects and water table kinematics. Estimates of hydraulic conductivity at the site near Miles Crossing were comparable to those obtained by others from similar tests (Haley, 2010) and with pumping tests. However, there was greater variability and uncertainty in the estimated values of specific storage, as one would expect from slug test data.

A model is presented where the linearized kinematic condition is use as the boundary condition at water table. The model accounts well-bore inertial effects but neglects the effect of well-bore skin. A qualitative comparison of predicted model behavior and observed field test responses suggests that slug test data may be useful in estimating, not only hydraulic conductivity, but also unconfined aquifer specific storage. This is a new development since all model published hitherto in the hydrogeology literature for analyzing unconfined aquifer slug test data neglect water table entirely. Future work would involve reanalyses of the data with the new model.

Contents

1 Introduction **4**

2 Materials and Methods **5**
2.1 Pneumatic slug testing kit 5
2.2 Description of field sites and test wells 5
2.3 Field tests 8

3 Field test results **9**
3.1 Miles Crossing Wells 9
3.2 Clark Fork River Sites 9
3.3 Dillon Site 16

4 Preliminary analysis with KGS model **17**

5 Proposed new model **18**
5.1 Mathematical Formulation 23
5.2 Solution 24

6 Discussion and Conclusion **25**

1 Introduction

Slug tests are widely used in aquifer characterization since they can be performed quickly, and require less equipment and labor than other methods such as pumping and injection tests. Additionally, they do not produce water, which may be contaminated and require costly disposal. They can be conducted by immersing or removing a slug mass into or from a well (Cooper et al., 1967), by instantaneous injection of water using a high-pressure pump (Bredehoeft and Papadopulos, 1980), or by instantaneous application or removal of pressurized gas to the water column in a well (Butler Jr., 1998). All three approaches involve the near-instantaneous raising or lowering of hydraulic head in a source well and observing its recovery, for single well tests, or observing the response in another well, for multi-well tests.

Mathematical solutions to the slug test flow problem for both confined and unconfined aquifers are available in the hydrogeology literature (e.g., (Butler Jr., 1998)). The solution of Hyder et al. (1994), referred to hereafter as the KGS solution, was developed to analyze slug tests in confined and unconfined aquifers, incorporating wellbore skin and storage effects. However, it does not account for wellbore inertial effects that are manifested by oscillatory head responses in the source well. Other models for unconfined aquifers, such as those of Springer and Gelhar (1991) (referred to as SG) and Zlotnik and McGuire (1998) (referred to as ZM), account for inertial effects but not for the presence of a filter pack around the source wellbore or for formation storage. Hence, there is a need for a unified solution that accounts for inertial, skin (or filter-pack) and storage effects for analyzing slug tests performed in unconfined aquifers. For confined aquifers, the solution of Butler Jr. and Zhan (2004) serves this purpose.

In modeling flow to a pumping well in unconfined aquifers, it is common to model the water table as a moving boundary and use a linearized form of the kinematic condition as the boundary condition at the water table (Neuman, 1972; Moench, 1997). However, when modeling stug tests in such aquifers, owing to the rapidity of the dissipation and relatively small magnitude of the initial slug, it is common to impose a Dirichlet-type (constant head) boundary condition at the water table (Bouwer and Rice, 1976; Hyder et al., 1994). The effect of a moving water table condition on slug test response has never been investigated, nor has the potential for using slug tests to estimate specific yield.

In this work we present the results of slug test experiments conducted during the summer of 2010 in the Butte-Silver Bow and Dillon areas of southwestern Montana. Additionally, a model that addresses the deficiencies of available unconfined aquifer slug test models is presented. The proposed model uses the linearized kinematic condition of Neuman (1972) as the water-table boundary condition. Inertial effects are treated using the simplified momentum balance equation of Butler Jr. and Zhan (2004); that

is, nonlinear dissipative processes associated with fittings and flow path constrictions inside the well, as discussed in McElwee and Zenner (1998); Zenner (2009), are neglected. The KGS model cannot be used close to the water table, due to the constant head assumption at the water table. The use of the linearized kinematic condition obviates this limitation for wells with negligible skin effects, and leads to a solution that can be used to analyze data collected anywhere along a well emplaced in a water table aquifer.

2 Materials and Methods

2.1 Pneumatic slug testing kit

The major components of the slug test kit are:

1. A manifold with a pressure gage, a compressed gas valve and a release valve,
2. an inflatable packer and straddle packer separated by a perforated PVC tube of variable (1–3 ft) length,
3. 1.5 inch PVC tubing connecting the manifold to the packer system,
4. an *In-situ inc. level troll 700* pressure transducer, and
5. an inert gas pressure regulator.

To run the field experiments, one needs a supply of compressed gas for presurising the water column in the test interval. A schematic of the slug test kit is shown in Figure 2.

2.2 Description of field sites and test wells

The tests were conducted at sites near Miles Crossing, the Clark Fork River (CFR) Coalition ranch and the Governor's Ranch, near Warmsprings, northwest of Butte, Montana. Additional tests were conducted near Dillon, in a well at Anderson Lane, courtesy of the Montana Bureau of Mines and Geology. Field tests reported herein were conducted during the summer of 2010.

The site near Miles Crossing lies on the northern bank of the Silver-Bow Creek, and comprises 5 wells that are emplaced in a thin gravel aquifer undelain with Tertiary clayey material. The wells were installed in the summer of 2009. The tests were conducted in 2-inch schedule 40 PVC wells that are screened over a 5 ft interval in a formation with a saturated thickness of about 8 ft. The wells at CFR Coalition ranch are also emplaced in an unconfined alluvial aquifer with a saturated thickness of about 20 ft. The wells are 2 inches in diameter and have a 10 ft screen. At the Miles Crossing

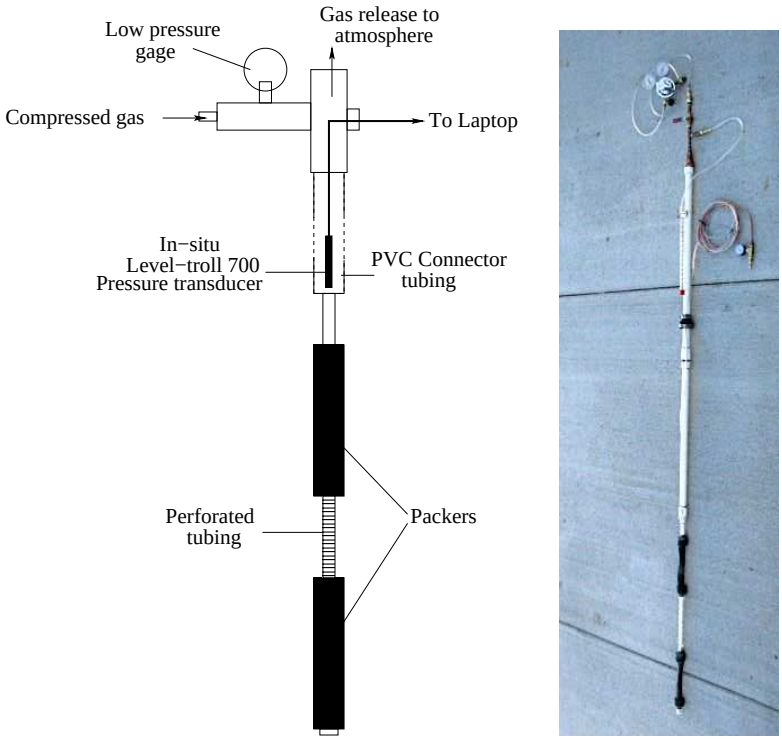

(a) (b)

Figure 1: (a) A schematic of the slug test kit used in the field tests described herein, and (b) the assembled rudimentary slug test kit constructed to be used in a student Undergraduate Research Project (URP) conduct preliminary tests (Photo after Haley (2010)).

(a) (b)

Figure 2: Student (a) assembling slug test kit in the field and (b) inflating the packers to isolate a test interval in preparation for a test at the Miles Crossing site as part of the Undergraduate Research Project (URP) (Photos after Haley (2010)).

site, pneumatic slug tests were conducted in each of the five wells, whereas such tests were only conducted in two wells at the CFR Coalition site. A schematic of the layout of the test wells at the Miles Crossing site. Well completion and location details can be found in Gammons and McGivern (2010)

Tests were also conducted in wells CFR-4 and CFR-5 at the CFR coalition ranch. Wells CFR-4 and CFR-5 are 2 inch diameter wells and are well suited for packer insertion. On the day of testing, the depth to static water level in wells CFR4 and CFR-5 were 1.55 and 2.50 ft, respectively, and these did not change significantly over the course of the experiment. The well have been completed to a an average depth of 10 ft below ground surface. The tests were conducted across the entire screened interval which was packed off with the packer system.

Additional tests were conducted in seven 2 inch diameter wells at the Governor's Ranch site. Three of the wells (ML-1, ML-2 and ML-3), completed on 11/06/09, are located on the western bank of the Clark Fork River, and the other four (WST-1, WST-2, WST-3 and WST-4), completed on 10/30/09, are on the eastern bank (Gordon et al., 2010). Most of these wells were installed to a depth of 10 ft below ground surface, except well WST-2, which was installed to a depth of 20 ft below ground surface. Additional details of well completion, location and elavation, can be found in Gordon et al. (2010). The tests were conducted across the entire 5 ft screened interval in each of these wells. Tests were also conducted in a pre-existing 6

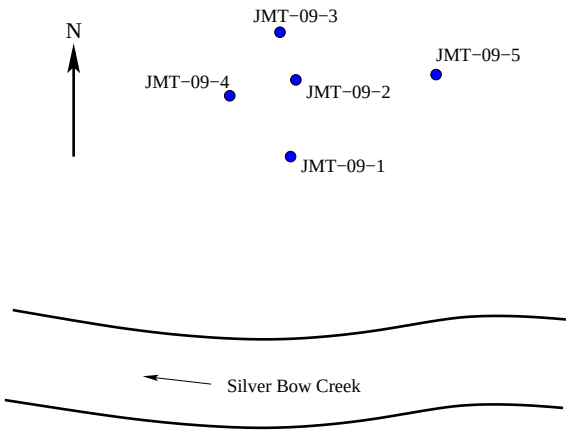

Figure 3: A schematic of the well layout at the Miles Crossing site, showing the relative positions of the well.

inch diameter well CFR-2 on the eastern bank of the Clark Fork River near the Governor's Ranch. The well was open to the atmosphere during testing, since it was to big for insertion of the packers. This well was completed to a depth of about 60 ft (with 10 ft screen??).

Tests were conducted in an unconfined aquifer at the Anderson lane site near Dillon, Montana. The well was completed to an approximate depth of 60 ft with a 10-foot screened interval. The formation is mainly gravel with sands. The site is on the western bank of the Beaverhead river. The well is used for ground water monitoring and characterization by the Montana Bureau of Mines and Geology.

2.3 Field tests

Pneumatic slug tests with varying initial displacements were concudted across the entire screened section of all the wells tested. Additional tests were carried out in smaller packed-off intervals in wells at the Miles Crossing site. The objective was to study the influence of the water table, and to determine whether models using a constant head Dirichlet condition at water table are adequate.

The tests were run by inserting the packer assembly over the appropriate test interval and inflating them to isolate the interval. The air column above the water in the PVC tubing was then presurized and allowed to stabilize. After a sufficient (1-2 minute) rest period, the release valve was openned and response of the water column over time recorded with the pressure transducer. The tests in each test interval were repeated three times, with differring nominal initial displacements of 2, 4 and 8 inches. Due to pressure gage malfunction, the actual initial water level displacements during the tests had to be deduced from pressure transducer data. The *In-situ inc.*

level troll 700 pressure transducer was set to record data on a linear time scale at a frequency of four data points per second. The high rate of data acquisition was used to ensure sufficient data points were recorded at very early-time following slug initiation.

Owing to the small thickness of the aquifer formation (comparable to actual length of the packer assembly), one packer was used to isolate the lower 1, 2, and 3 ft interval of each well for three tests in each of the intervals. Additional test were conducted in the upper 2 and 3 ft of the formation by packing off the lower portion of the formation with the straddle packer, and pressuring the water column above. Tests were also first conducted across the entire screened interval in each of the five wells at the site. At the very least, each well was tested at three nominal initial displacements of 2, 4 and 8 inches. Sometimes, the tests were repeated for a nominal value smaller than 2 inches or higher than 8 inches, depending on observed behavior.

3 Field test results

3.1 Miles Crossing Wells

The data collected in the wells also shown in Figures 4–8. The actual initial displacement showed some variability from these nominal values. This is reflected in the greater variability of responses at very early-time. Despite the great variability in very early-time responses, it is clear that the results show anomalous aquifer behavior with responses that are neither monotonous nor oscillatory in the traditional sense. They seem to indicate that filter packs outside the well casing and/or water table kinematics play a significant role in slug test response as they exhibit a characteristic S-shape in semi-log space, reminiscent of dual-storage media. The two storage mechanisms may be due to the filter pack or gradual water release by the recovery of the water table to its initial state. All the five well at the Miles Crossing site exhibited this behavior.

Additionally, the results seem to indicate a dependence on the value of the initial slug displacement, H_0. In linear systems, no such dependence would be expected, and the normalized plots for different H_0 values should be coincident, within limits of random measurement error. A systematic dependence on H_0 suggests system nonlinearity, associated with flow dynamics in the packer-tubing assembly (McElwee and Zenner, 1998; Zenner, 2008).

3.2 Clark Fork River Sites

The Clark Fork River Sites include the wells on the banks (east and west) of the Clark Fork River near the Governor's ranch, and the those at the Clark Fork River Coalition Ranch. The tests were conducted across the entire screened interval of each well. Different values of the initial displacement,

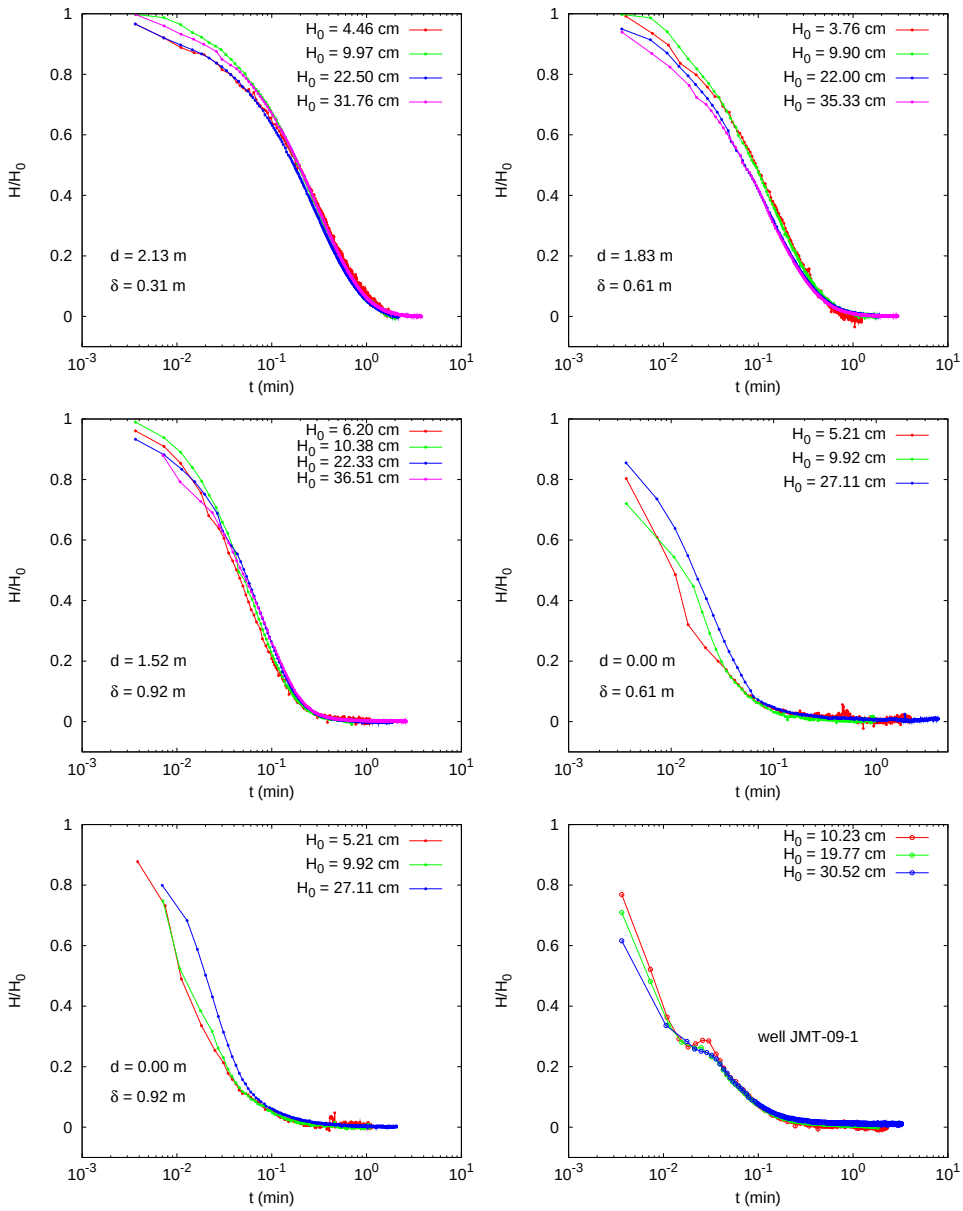

Figure 4: Results of tests conducted in packed off intervals in well JMT-09-1. The plots are normalized change in head versus time in minutes, for different values of the initial displacement, H_0.

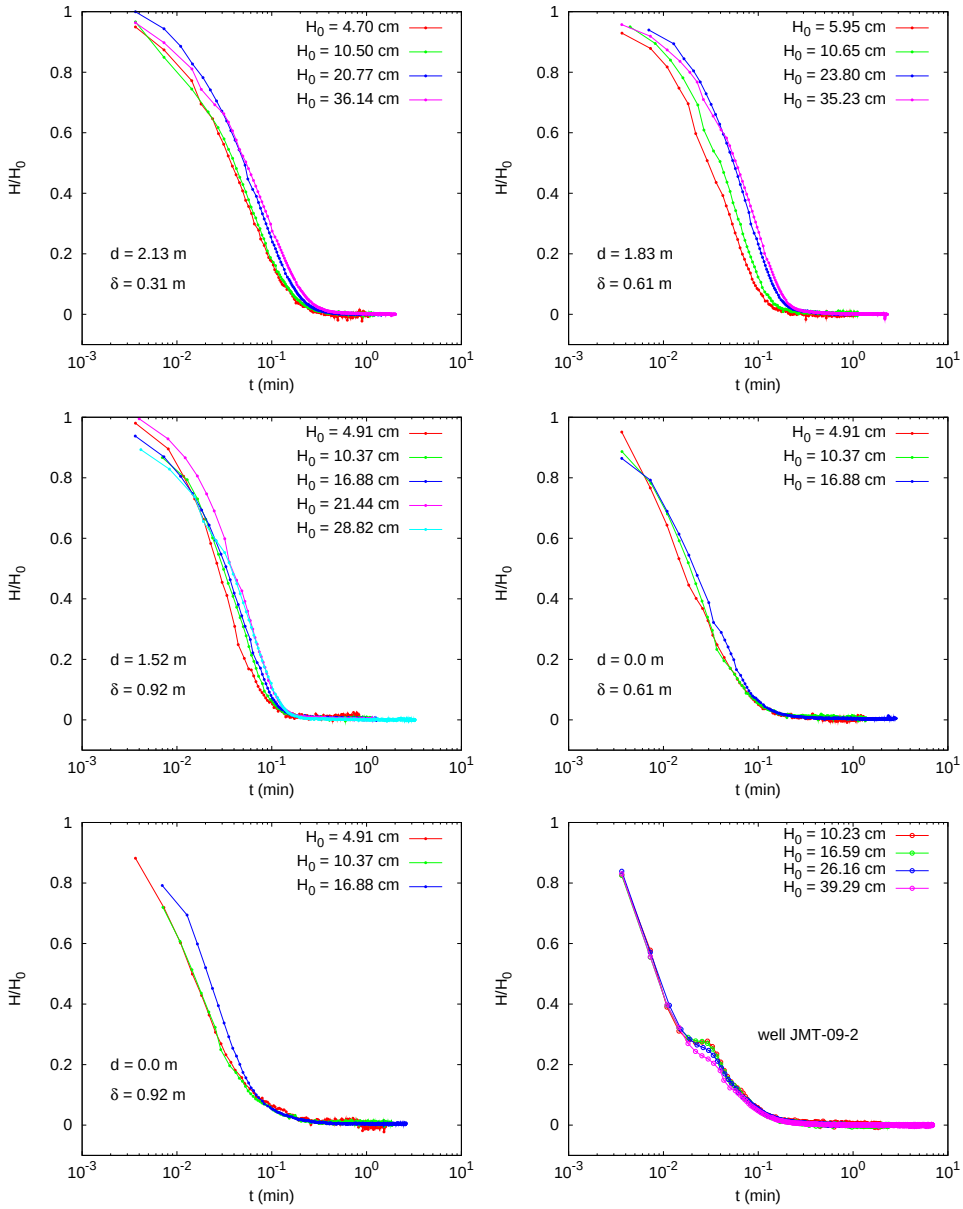

Figure 5: The plots are normalized change in head versus time in minutes, for tests conducted in well JMT-09-2 at the Miles Crossing site.

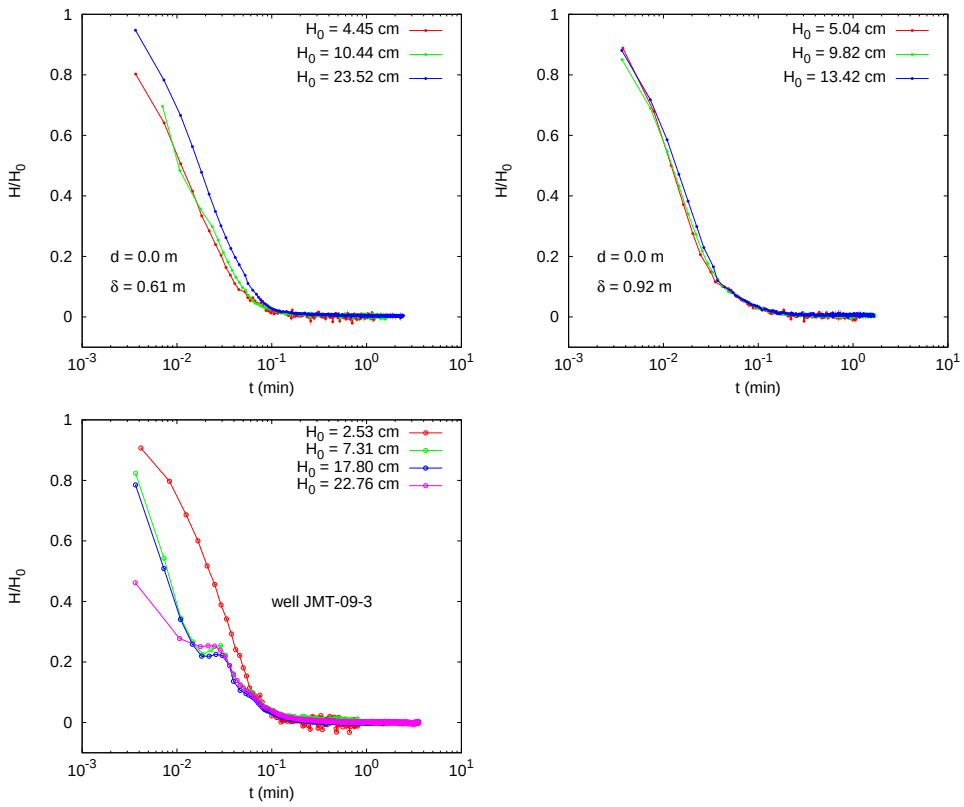

Figure 6: The plots are normalized change in head versus time in minutes, for conducted in well JMT-09-3 at the Miles Crossing site.

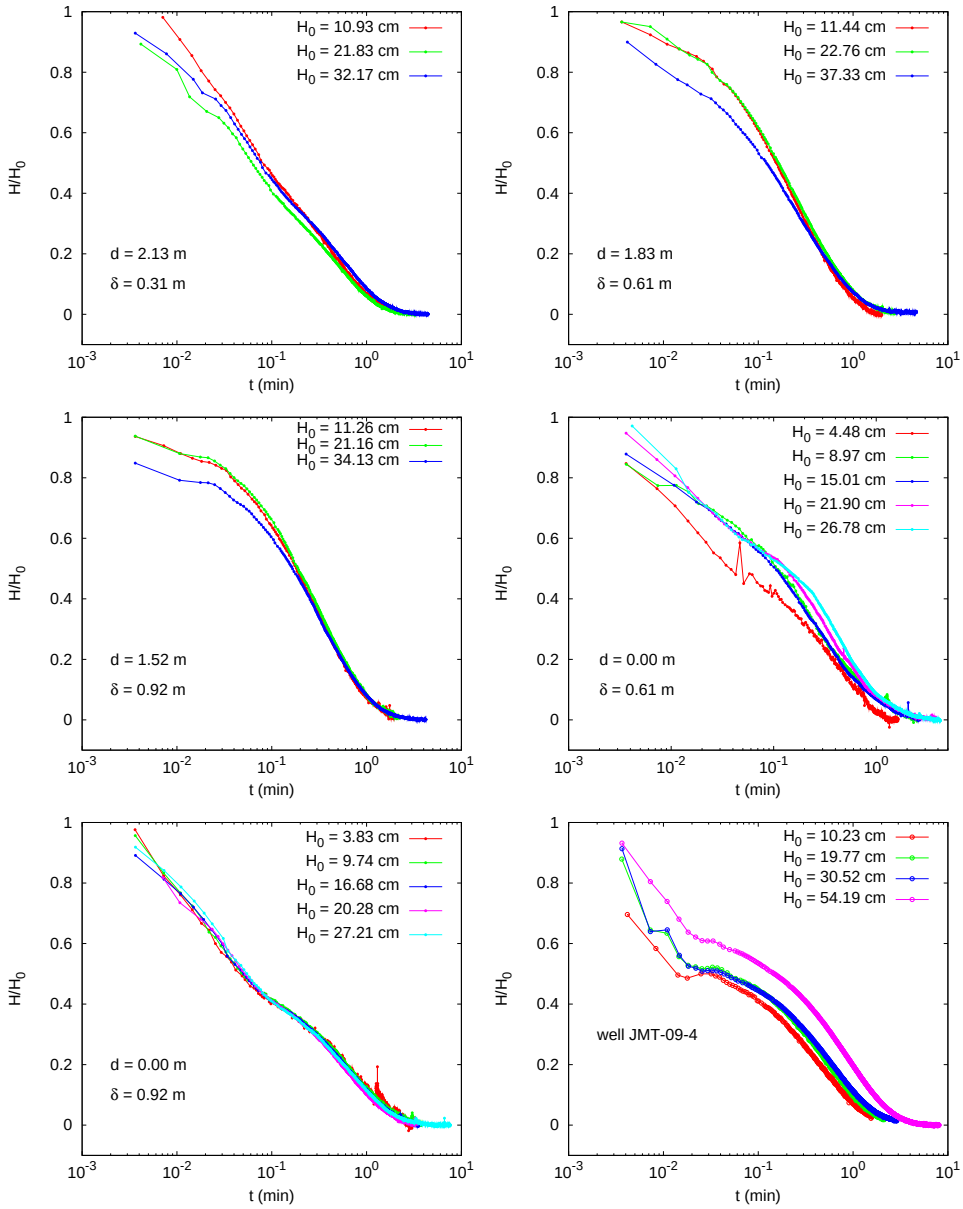

Figure 7: The plots are normalized change in head versus time in minutes, for tests conducted in well JMT-09-4 at the Miles Crossing site.

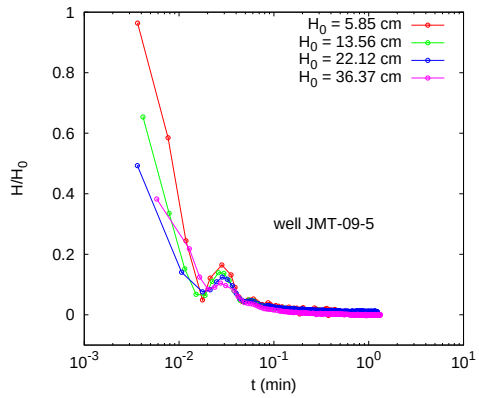

Figure 8: The plots are normalized change in head versus time in minutes, for slug tests conducted in well JMT-09-5 at the Miles Crossing site.

H_0, were used for the tests to investigate repeatability of the results. Some of the test results showed sufficient repeatability, where the variability may be attributable to measurement error. Others showed a systematic dependence of the observed response on H_0.

The results of the tests conducted in the three wells at the site on the western bank of the Clark Fork River near the Governor's ranch, are shown in Figure 9. Of these tests, only those conducted in well ML-1 showed no significant dependence on H_0 over the range of H_0 values used for that well. It should be noted, however, that only three tests were conducted in this well and that the maximum value of H_0 used for this well was significantly smaller than that for the other two wells. Hence, the results obtained for well ML-1 may still be within the system linearity range. Another important observation is that results from well ML-2 seem to show the effects of a filter pack or the water table. Similar results were obtained in the wells at the Miles Crossing site. This effect appears to diminish with increasing values of H_0. It is manifested by a non-monotonic decay of the head perturbation with time, which is most pronounced for small values of H_0.

The responses observed in the four wells on the eastern bank of the Clark Fork River near the Governor's ranch are shown in Figure 10. They show monotonic decay for well WST-1, and quasi-oscillatory responses in the other wells, with the most oscillatory responses being those obtained in well WST-2. It should be noted that of the four wells at this site, well WST-2 was the deepest, having been installed to a depth of 20 ft. Hence, this well has the largest effective water column length. Oscillations are known to increase with the length of the water column in the well bore (Malama et al., Manuscript in review). The wells at this site were also experiencing significant background head changes during the tests, that one

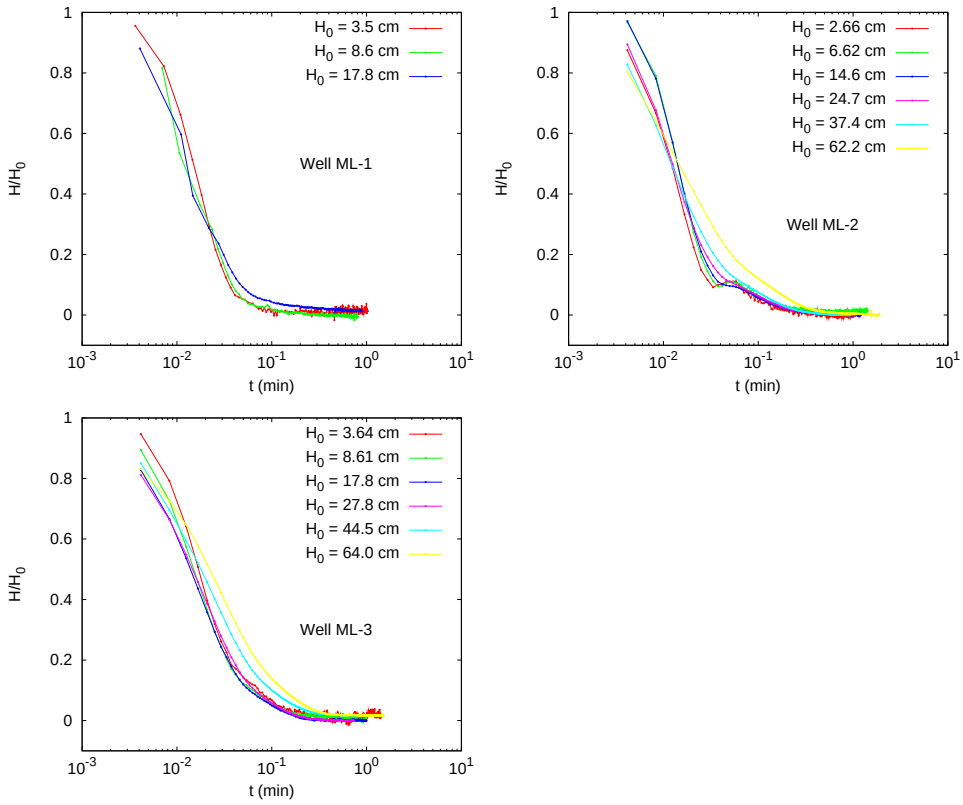

Figure 9: Results of tests conducted in wells on the western bank of the Clark Fork River near the Governor's Ranch. The plots show the normalized responses in each well for different values of H_0.

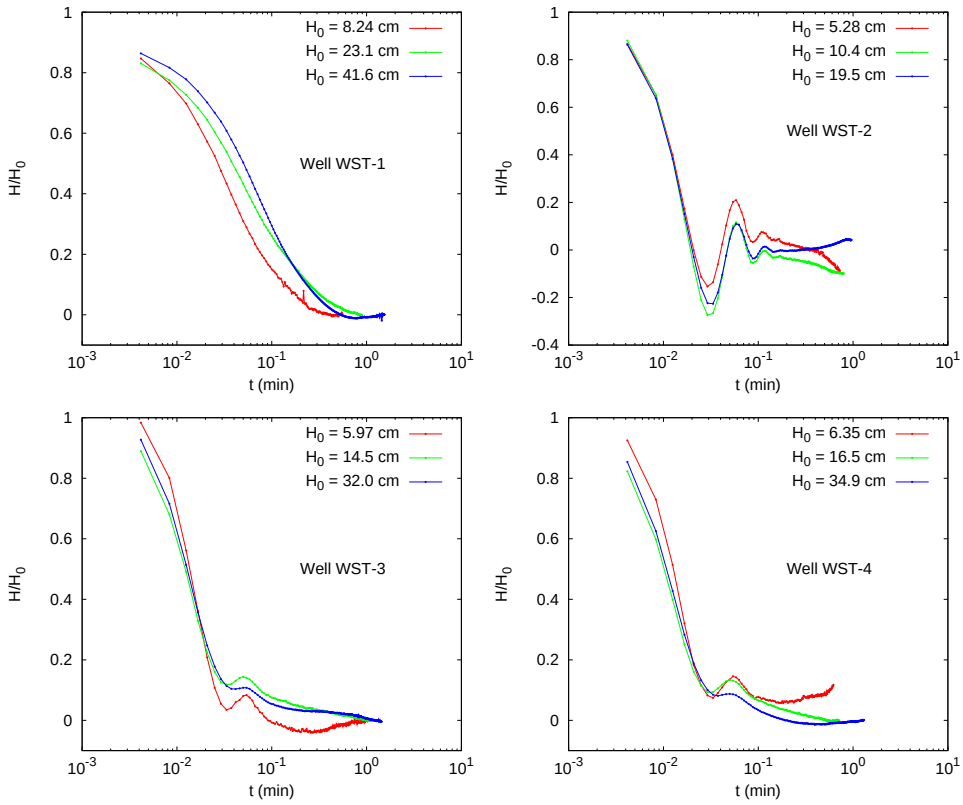

Figure 10: Results of tests conducted in wells on the eastern bank of the Clark Fork River near the Governor's Ranch. The plots show the normalized responses in each well for different values of H_0.

has to filter out before the data can be analyzed with available methods. These changes may be attributable to river fluctuations, evapotranspiration and/or infiltration from ponded water that was present on the surface during the tests. The tests were conducted around the time when the region was experiencing sigificant precipitation (rainfall) events.

Figure 11 shows the data collected in wells CFR-4 and CFR-5 at the Clark Fork River Coalition Ranch. Both data set show evidence of wellbore nonlinearities (dependence of responses on H_0). Responses from well CFR-4 are monotonic, whereas those from CFR-5 show oscillation at small values of H_0. These oscillation decrease with increasing H_0.

3.3 Dillon Site

A series of tests were conducted in a deep (60 ft) well located on a ranch on Anderson Lane near Dillon, Montana. The well is screened over the bottom 10 ft, and is situated in an alluvial (cobbles and sand) unconfined

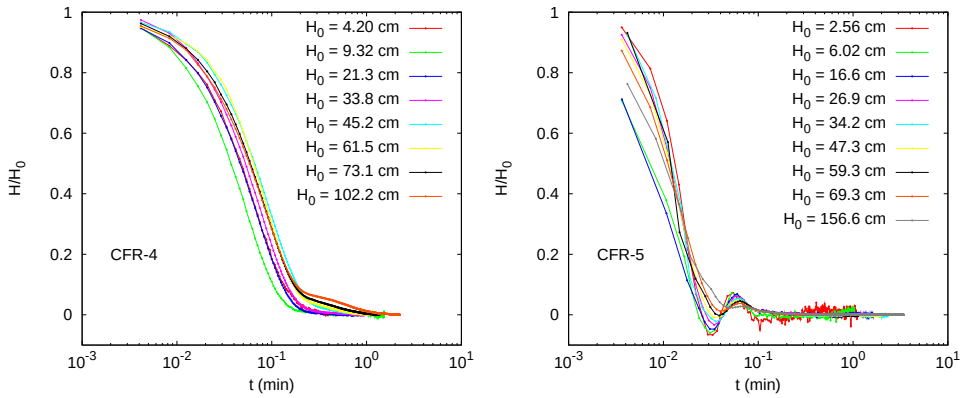

Figure 11: Results of tests conducted in wells CFR-4 and CFR-5 at the Clark Fork River Coalition Ranch. The plots show the normalized responses in each well for different values of H_0.

aquifer. Nine tests were conducted in the well at different values of the initial displacement, H_0. The results are shown in Figure 12, where plots show the responses for (a) small and (b) large initial displacements.

The responses were highly oscillatory owing to the length of the water column in the well bore. The amplitudes of the oscillations, however, decayed to zero with one minute of slug initiation, even for the large values of H_0, indicating a highly conductive (with low storage) formation. The amplitudes of the oscillations also showed strong dependence on the values of H_0. They appear to increase initially with increasing H_0, then begin to decrease as H_0 is increased further. Linear slug test theory suggests that there should be not such dependence when random measurement errors are accounted for.

4 Preliminary analysis with KGS model

The most physically based model available in the literature for estimating hydraulic parameters for unconfined aquifers is that of Hyder et al. (1994). The model assumes that the water table can be treated as a constant head boundary. It neglects water table kinematics as commonly simulated in unconfined aquifer pump test analysis. This model is implemeted in the software package AQTESOLV as the KGS model with skin. It was used to analyze the slug test data and to obtain the hydraulic parameter estimates reported here. The model has the limitation that it cannot be used to estimate specific yield or to analyze oscillatory data.

The KGS model (with skin) was fitted to data collected at the Miles Crossing wellfield, and the results are shown in Figure 13. The model was able to reproduce the inflection observed in the data. Such an inflection is

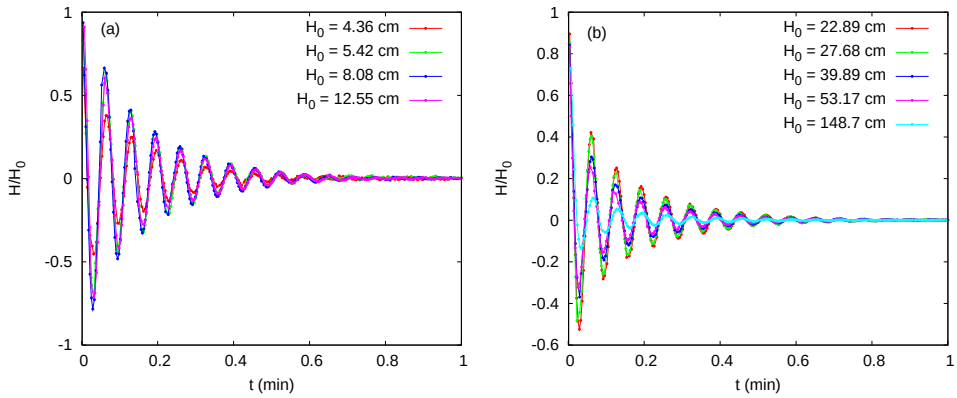

Figure 12: Results of tests conducted in a well at the Anderson Lane site near Dillon, Montana. The plots show the responses for (a) small and (b) large initial displacement, H_0.

typically associated with two storage mechanisms, and for the KGS model, the mechanisms are associated with aquifer and skin specific storage. The estimated values are $S_{\text{s,aquifer}} = 6.35 \times 10^{-4}$ m^{-1} and $S_{\text{s,skin}} = 3.72 \times 10^{-2}$ m^{-1}. However, during the exercise of fitting the model to the data, the value of skin conductivity, K'_r, had the most impact in reproducing the inflection. Estimated values of hydraulic parameters at the Miles Crossing wellfield are summarised in Table 1. These values were obtained from data collected in tests across the entire screened interval of each well. The estimated hydraulic conductivity range from a low of 2.15×10^{-5} m/s (6.1 ft/day) in well-1 to a high of 5.65×10^{-4} m/s (160 ft/day) in well-5.

Parameters estimated from select wells near the Governor's Ranch and at the Clark Fork River Coalition Ranch are reported in Table 2. Sample model fits to the data are shown in Figures 14–16. The estimated values of formation conductivity reported here range from a low value of 1.94×10^{-4} m/s (55 ft/day) at well CFR-4 to a high value of 6.51×10^{-4} m/s (182 ft/day). Estimates of storage parameters are less reliable as they tend to equal the low bounds set in the estimation routine.

5 Proposed new model

Since the KGS model of Hyder et al. (1994) cannot, in principle, be used to estimate specific yield or to model oscillating response, a model is proposed below where we attempt, for the first time in slug test modeling, to incorporate water table kinematics into model derivation.

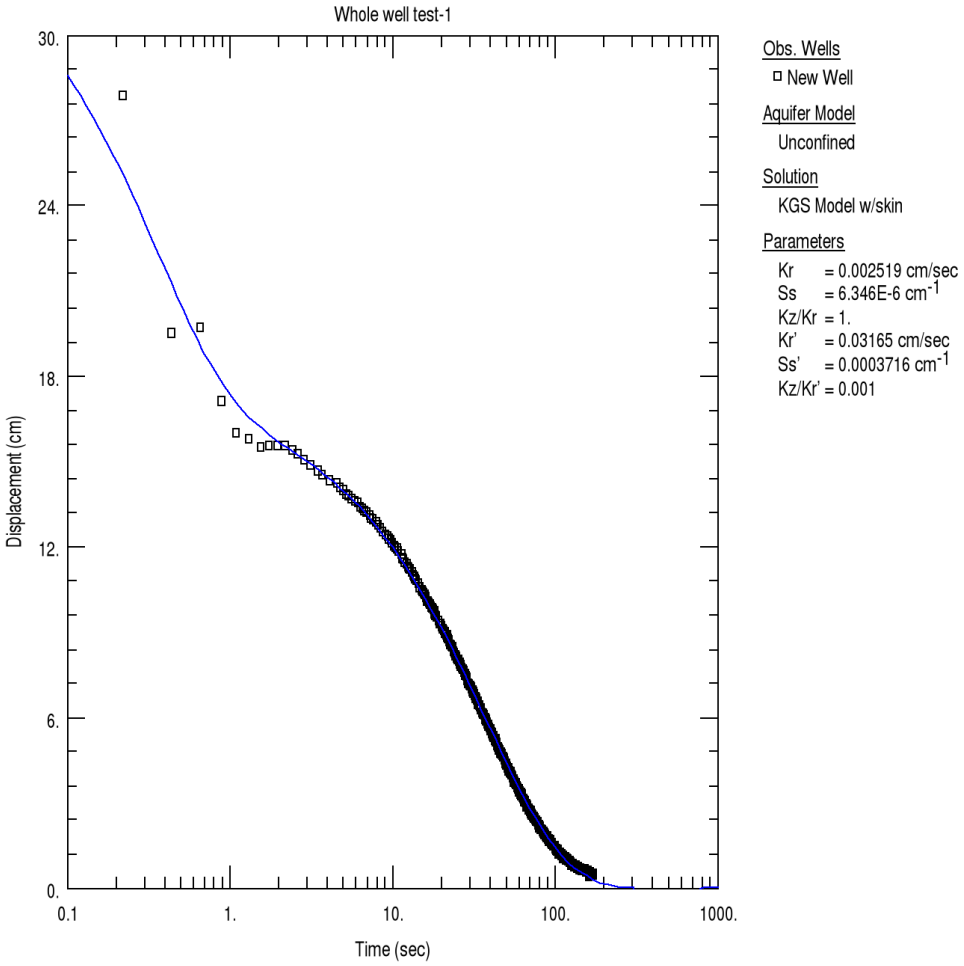

Figure 13: Fit of the KGS model (Hyder et al., 1994) to data collected in well JMT-09-4 at the Miles Crossing site. The test was conducted across the entire screened interval.

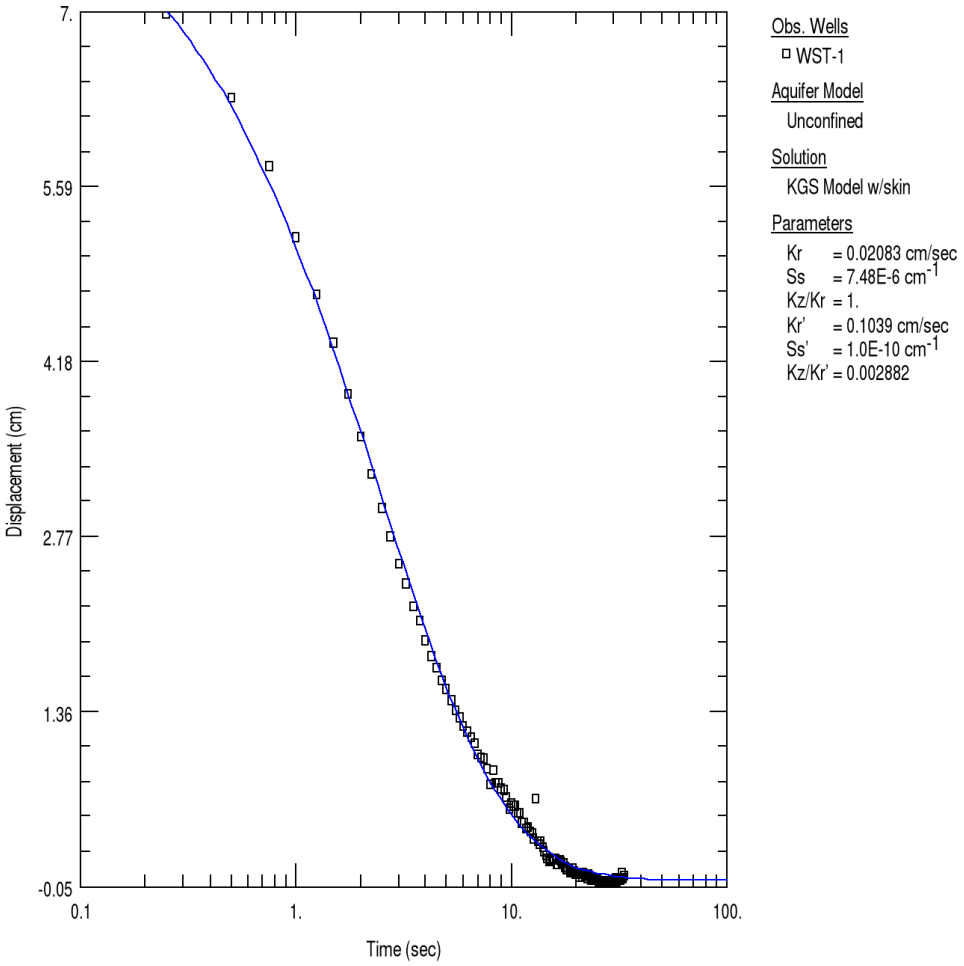

Figure 14: Fit of the KGS model (Hyder et al., 1994) to data collected in well ML-1 at the Governor's Ranch west site.

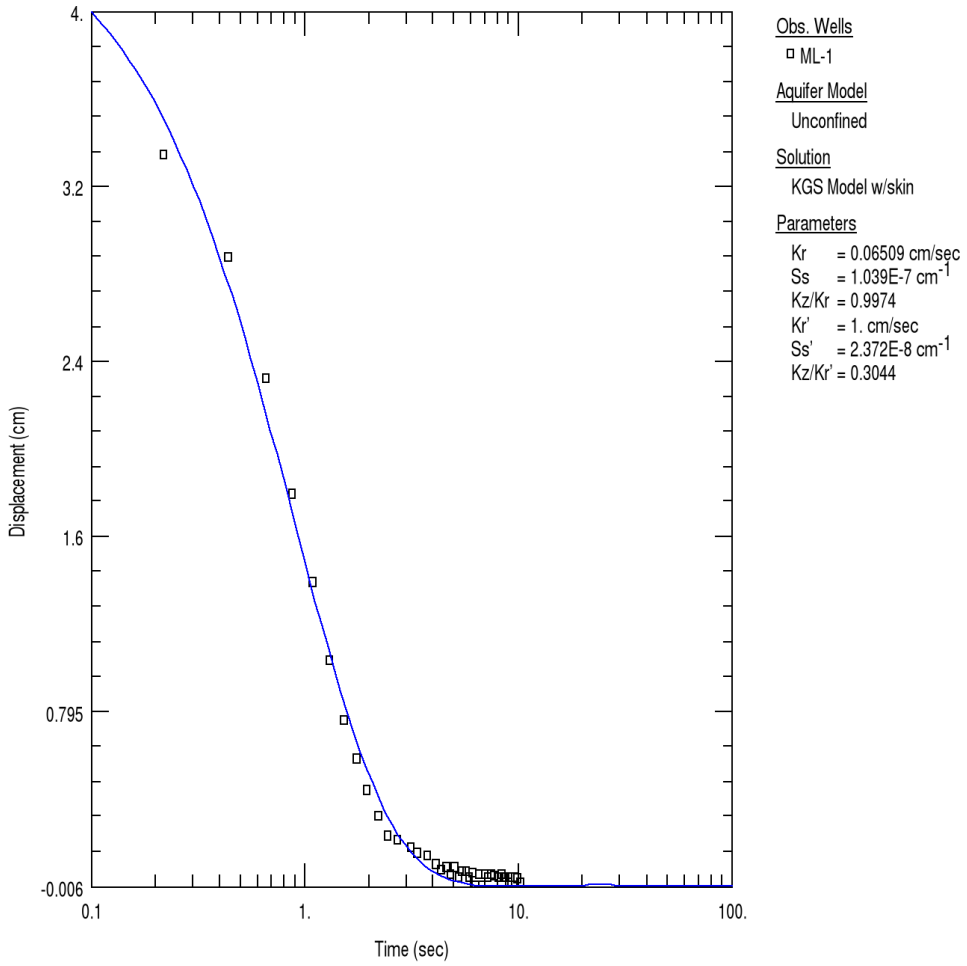

Figure 15: Fit of the KGS model (Hyder et al., 1994) to data collected in well WST-1 at the Governor's Ranch east site.

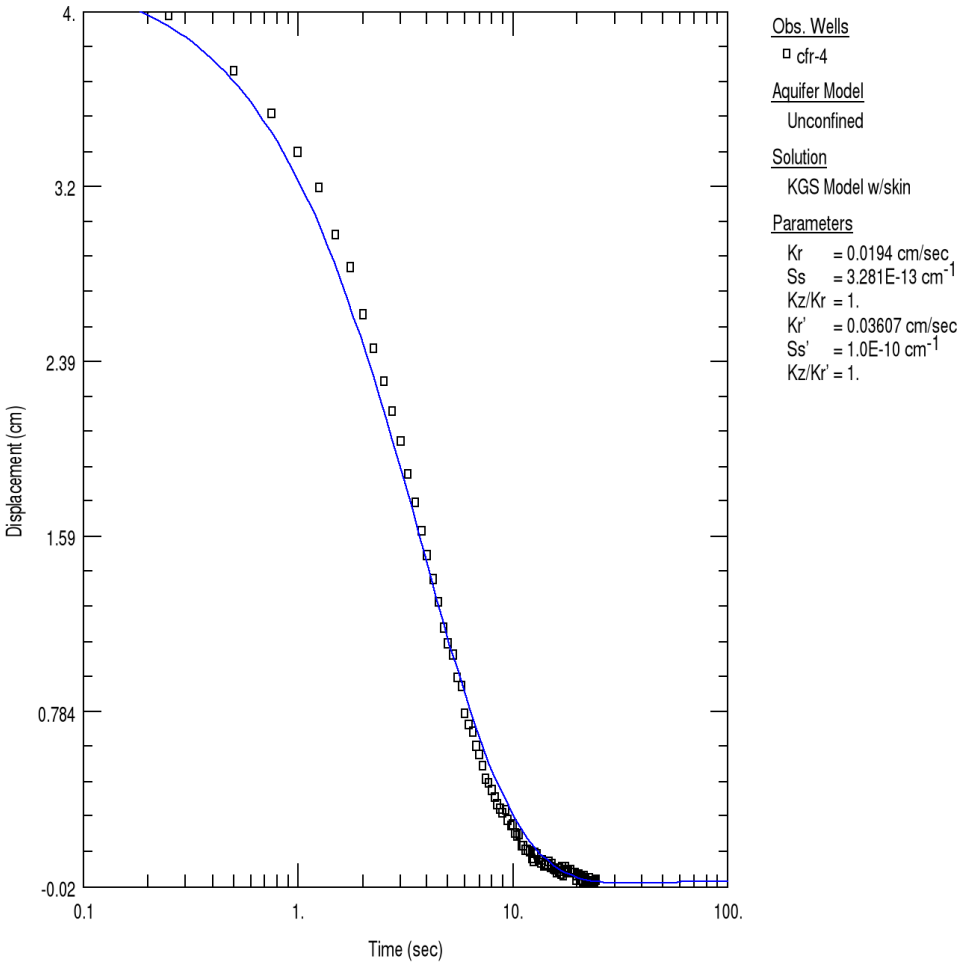

Figure 16: Fit of the KGS model (Hyder et al., 1994) to data collected in well CFR-4 at the Clark Fork River Coalition ranch.

Table 1: Parameter values estimated with the KGS model for the wells at the Miles Crossing site.

Well	K_r (m/s)		S_s (m^{-1})	
	Aquifer	Skin	Aquifer	Skin
JMT-09-1	1.96×10^{-4}	7.40×10^{-4}	2.39×10^{-2}	3.12×10^{-2}
JMT-09-2	4.06×10^{-4}	5.13×10^{-4}	2.13×10^{-2}	2.13×10^{-2}
JMT-09-3	4.48×10^{-4}	1.04×10^{-3}	1.59×10^{-2}	1.0×10^{-8}
JMT-09-4	2.15×10^{-5}	3.38×10^{-5}	6.35×10^{-4}	3.72×10^{-2}
JMT-09-5	5.65×10^{-4}	1.18×10^{-3}	6.56×10^{-2}	1.0×10^{-8}

Table 2: Parameter values estimated with the KGS model for the wells along the Clark Fork River.

Well	K_r (m/s)		S_s (m^{-1})	
	Aquifer	Skin	Aquifer	Skin
ML-1	2.08×10^{-4}	1.04×10^{-3}	7.48×10^{-4}	1.0×10^{-8}
WST-1	6.51×10^{-4}	1.00×10^{-2}	4.26×10^{-5}	1.0×10^{-6}
CFR-4	1.94×10^{-4}	3.61×10^{-4}	6.56×10^{-11}	1.0×10^{-8}

5.1 Mathematical Formulation

The governing equation for flow in the aquifer formation (Malama et al., Manuscript in review)

$$S_{s,i}\frac{\partial s_i}{\partial t} = \frac{K_{r,i}}{r}\frac{\partial}{\partial r}\left(r\frac{\partial s_i}{\partial r}\right) + K_{z,i}\frac{\partial^2 s_i}{\partial z^2} \tag{1}$$

where $i = 1$ for skin and $i = 2$ for the formation, s_i is change in head from the initial static level in the ith flow zone, $K_{r,i}$ and $K_{z,i}$ are the radial and vertical hydraulic conductivities, $S_{s,i}$ is the specific storage of the ith flow zone, and (r, z, t) are the space-time coordinates. The z-coordinate is positive downward from the water table ($z = 0$) into the formation. A schematic of the flow domain is shown in Figure 17.

Pertinent boundary conditions, include mass conservation condition

$$2\pi b K_{r,1}\left(r\frac{\partial s_1}{\partial r}\right)\bigg|_{r=r_w} = \begin{cases} C_w\dfrac{\mathrm{d}H}{\mathrm{d}t} & \forall z \in [d, l] \\ 0 & \text{elsewhere,} \end{cases} \tag{2}$$

and momentum conservation condition (Butler Jr. and Zhan, 2004)

$$\frac{\mathrm{d}^2 H(t)}{\mathrm{d}t^2} + \frac{8\nu L}{r_c^2 L_e}\frac{\mathrm{d}H(t)}{\mathrm{d}t} + \frac{g}{L_e}H(t) = \frac{g}{bL_e}\int_d^l s_1(r_w, z, t)\mathrm{d}z, \tag{3}$$

at test well. Linearized kinematic condition (Neuman, 1972) is used at water table:

$$-K_z\frac{\partial s}{\partial z}\bigg|_{z=0} = -S_y\frac{\partial s}{\partial t}\bigg|_{z=0}, \tag{4}$$

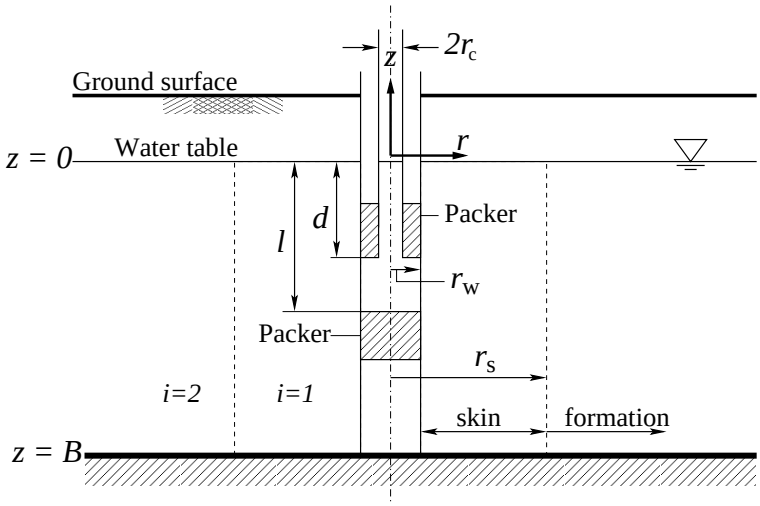

Figure 17: Schematic of slug test set-up.

where S_y is specific yield.

5.2 Solution

The details of the solution procedure can be found in (Malama et al., Manuscript in review). The solution is obtained in Laplace transform space and is given by

$$\overline{\Phi}_{\mathrm{uc}}(p) = \frac{\beta_1 + \beta_2 p + \gamma\overline{\Omega}/2}{1 + p\beta_1 + \beta_2 p + \gamma\overline{\Omega}/2}, \tag{5}$$

where $\overline{\Phi}_{\mathrm{uc}}(p) = \mathcal{L}\{\Phi_{\mathrm{uc}}\}$, $\Phi_{\mathrm{uc}} = H/H_0$ is the normalized source well response, $s_{D,1} = s_1/H_0$ is the normalized skin response, $t_D = t/T_c$, $z_D = z/B$, $r_{D,w} = r_w/B$ are dimensionless time and space coordinates, $\beta_1 = 8\nu L/(r_c^2 g T_c)$, $\beta_2 = L_e/(gT_c^2)$, $T_c = B^2/\alpha_{r,1}$ is a characteristic time, $b_D = b/B$, $d_D = d/B$, and $l_D = l/B$ are dimensionless test-configuration lengths and depths, $\gamma = K_{r,2}/K_{r,1}$,

$$\overline{\Omega}(r_{D,w}, p) = \mathcal{H}_0^{-1}\{\hat{\overline{\Omega}}(a,p)\}|_{r_{D,w}}, \tag{6}$$

$$\hat{\overline{\Omega}}(a,p) = \frac{C_D[1 - \langle\hat{\overline{w}}_D(a,p)\rangle]}{\kappa\eta^2\xi_w \mathrm{K}_1(\xi_w)} \tag{7}$$

$C_D = r_{Dc}^2/(bS_s)$, $\eta^2 = (p + a^2)/\kappa$, $\xi_w = r_{D,w}\sqrt{p}$, and

$$\begin{aligned}
\langle\hat{\overline{w}}_D\rangle &= \frac{1}{b_D\eta\Delta_0}[\Delta_1 \sinh(\eta d_D^*) + (\Delta_2 - 2\Delta_1)\sinh(\eta l_D^*)] \\
\Delta_0 &= \sinh(\eta) + \varepsilon\cosh(\eta) \\
\Delta_1 &= \sinh(\eta d_D) + \varepsilon\cosh(\eta d_D) \\
\Delta_2 &= \sinh(\eta l_D) + \varepsilon\cosh(\eta l_D)
\end{aligned} \tag{8}$$

Additional parameter definitions can be found in Malama et al. (Manuscript in review).

The MWT solution admits specific yield, which governs the effects of the water table. It, in principle, can be used to estimate S_y from slug test data. Preliminary results indicate that model results show sensitivity to S_y over a very narrow range. Where slug tests are performed close to the water table, this should be the model of choice, provided the effects of wellbore skin are negligible.

6 Discussion and Conclusion

Preliminary analysis of field data collected in pneumatic slug tests conducted at several sites in the Butte-Silver Bow area yield estimates of hydraulic conductivity and specific storage at these sites. The estimated parameter values showed only modest variability at individual sites as well as between sites. Additionally, estimates of hydraulic conductivity at the site near Miles Crossing are comparable to those obtained by others from similar tests (Haley, 2010) and with pumping tests. There was greater variability and uncertainty in the estimated values of specific storage, confirming to some degree the long known observation that slug test data do not yield well determined values of aquifer storage parameters.

The analyses of the data were performed with the AQTESOLV implementation of the KGS unconfined aquifer model (Hyder et al., 1994) which does to account for wellbore inertial effects and water table kinematics. This model treats the water table as a constant head boundary, and thus, cannot be used to estimate aquifer specific yield. Hence, a model was developed (Malama et al., Manuscript in review) that uses the linearized kinematic condition at the water table and accounts for wellbore inertial effects. The model, however, was not used to analyse the data collected in the experiments reported herein. Future work will involve reanalyses of the data with the new model.

Acknowledgments

This work was funded by a $13,217 grant provided by the Montana Water Center in conjunction with the U.S. Geological Survey Water Resources Research Program. The author thanks Gretchen Rupp, Director, and Stephen Guettermann, both of the Montana Water Center, Dr. Christopher Gammons of Montana Tech, Geological Engineering Department, Patrick Haley and Chrysten Ngouya, students at Montana Tech, and Dr. Jeanette Abdo of the Montana Bureau of Mines and Geology, for their kind support in accomplishing the objectives of this work.

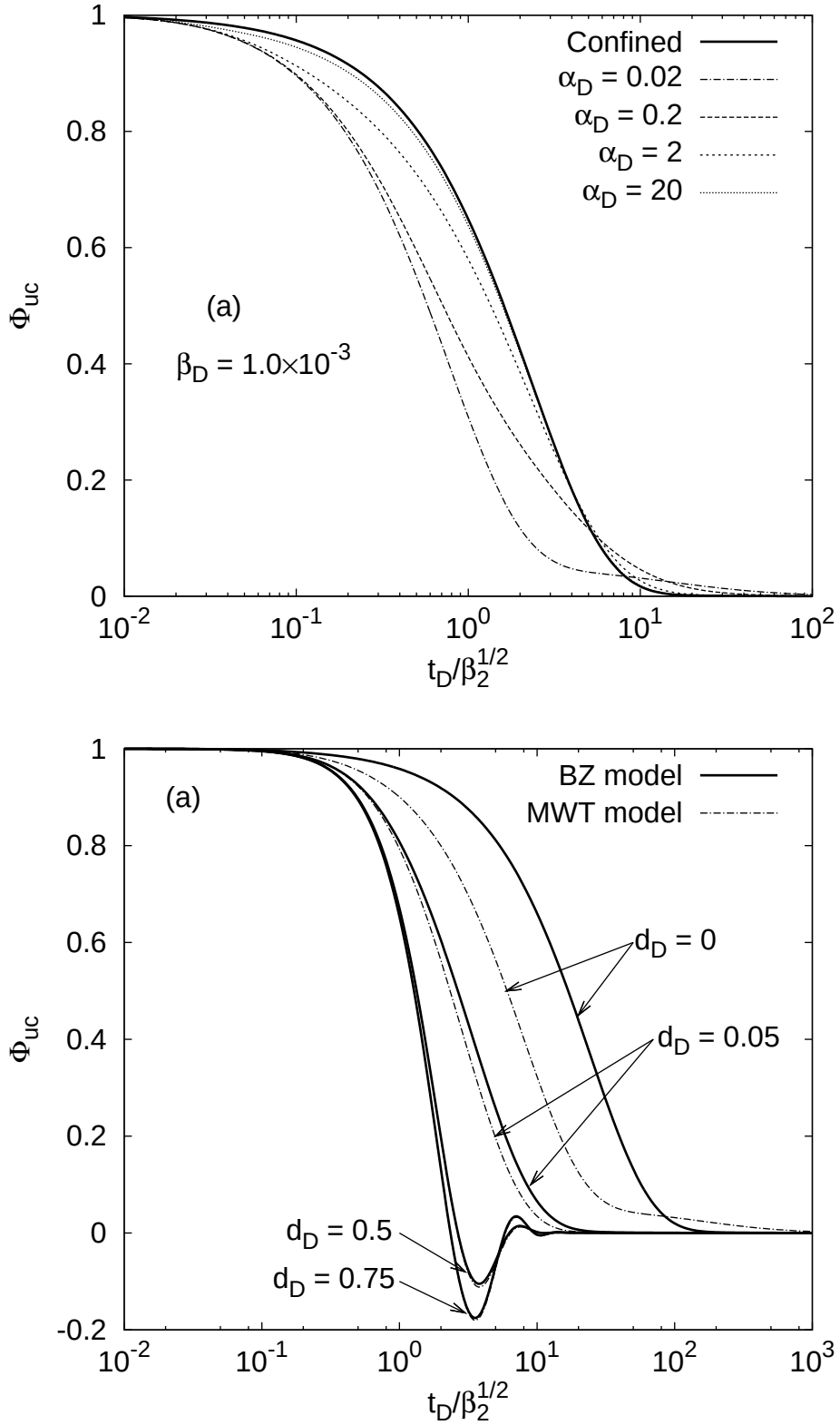

Figure 18: Model predicted behavior showing normalized head $\Phi_{\rm uc}$ plotted against dimensionless time, $t_D/\beta_2^{1/2}$.

References

Bouwer, H., Rice, R., 1976. A slug test for determining hydraulic conductivity of unconfined aquifers with completely or partially penetrating wells. Water Resources Research 12 (3), 423–428.

Bredehoeft, J. D., Papadopulos, I. S., 1980. A method for determining the hydraulic properties of tight formations. Water Resources Research 16 (1), 233–238.

Butler Jr., J. J., 1998. The Design, Performance, and Analysis of Slug Tests. Lewis Publishers, Boca Raton.

Butler Jr., J. J., Zhan, X., 2004. Hydraulic tests in highly permeable aquifers. Water Resources Research 20, W12402.

Cooper, H. H. J., Bredehoeft, J. D., Papadopulos, I. S., 1967. Response of a finite-diameter well to an instantaneous charge of water. Water Resources Research 3 (1), 263–269.

Gammons, C., McGivern, A., December 2010. Hydrogeology and chemistry of groundwater near miles crossing. Final report, Montana Tech, Geological Engineering Department, 1300 W Park St., Butte, MT.

Gordon, L., Dutton, A., Gammons, C., December 2010. Monitoring groundwater in remediated vs. unremediated floodplain sediments along the upper clark fork river. Report, Montana Tech, Geological Engineering Department, 1300 W Park St., Butte, MT.

Haley, P. F., 2010. A study of vertical distribution in hydraulic conductivity values using pneumatic slug testing methods. Undergraduate Research Project Student Report, Montana Tech of the Univ. of Montana.

Hyder, Z., Butler Jr., J. J., McElwee, C. D., Liu, W., 1994. Slug tests in partially penetrating wells. Water Resources Research 30 (11), 2945–2957.

Malama, B., Barrash, W., Cardiff, M., Thoma, T., , Kuhlman, K. L., Manuscript in review. Modeling slug tests in unconfined aquifers taking into account water table kinematics, wellbore skin and inertial effects, submitted to Journal of Hydrology.

McElwee, C. D., Zenner, M. A., 1998. A nonlinear model for analysis of slug test data. Water Resources Research 34 (1), 55–66.

Moench, A. F., 1997. Flow to a well of finite diameter in a homogeneous, anisotropic water table aquifer. Water Resources Research 33 (6), 1397–1407.

Neuman, S. P., 1972. Theory of flow in unconfined aquifers considering delayed response of the water table. Water Resources Research 8 (4), 1031–1045.

Springer, R. K., Gelhar, L. W., 1991. Characterization of large-scale aquifer heterogeneity in glacial outwash by analysis of slug tests with oscillatory response, Cape Cod, Massachusetts. Water Res. Invest. Rep. 91-4034, U.S. Geological Survey.

Zenner, M. A., 2008. Experimental evidence of the applicability of Colebrook and Borda Carnot-type head loss formulas in transient slug test analysis. Journal of Hydraulic Engineering, ASCE 134 (5), 644–651.

Zenner, M. A., 2009. Near-well nonlinear flow identified for various-displacement well response testing. Ground Water 47 (4), 526–533.

Zlotnik, V. A., McGuire, V. L., 1998. Multi-level slug tests in highly permeable formations: 1. modifications of the Springer-Gelhar (SG) model. Journal of Hydrology (204), 271–282.

Ecohydrologic Model Development for the Assessment of Climate Change Impacts on Water Resources in the Bitterroot Valley

Basic Information

Title:	Ecohydrologic Model Development for the Assessment of Climate Change Impacts on Water Resources in the Bitterroot Valley
Project Number:	2010MT216B
Start Date:	3/1/2010
End Date:	2/28/2011
Funding Source:	104B
Congressional District:	At-Large
Research Category:	Climate and Hydrologic Processes
Focus Category:	Hydrology, Models, Ecology
Descriptors:	None
Principal Investigators:	Marco Maneta

Publications

1. • Johnson, A. “Distribution and Movement of Thermal Energy Beneath a Snowpack as Affected by Soil Moisture and Root Water Uptake”. MSc Thesis (Expected completion: Fall 2011)
2. • Pasternack, G. B., Maneta, M. P., Pan, L.-L, Chen, S.-H. , Fogg, G. E., Grismer, M. E., Harter, T., Hopmans, J. W., Puente, C. E., Ustin, S. L., Wallender, W. W. Resiliency of a high-precipitation water supply region to future climatic change in California. Water Resources Research. Submitted March 3, 2011
3. Silverman, N, Johnson, A, Maneta, M. A Spatially Distributed Ecohydrological Model for Forested Catchments. Montana Section of the America Water Resources Association. 2010 Annual Conference: Rivers of change: Science, policy and the Environment. Helena, MT. October 14-15 2010. Poster session
4. Maneta, M. and Wallender, W. (2010), “Propagation of information in a pilot-point based multi-objective calibration exercise for a surface-subsurface distributed hydrologic model”, Abstract H21F-1119 Poster presented at 2010 Fall Meeting, AGU, San Francisco, Calif., 13-17 Dec
5. Silverman, N.L., Maneta, M. (2011, April) "Ecohydrologic Model Validation using Remote Sensing Techniques", The University of Montana Graduate Student and Faculty Research Conference, Missoula, Montana, Poster Session.
6. Silverman, N.L., Maneta, M. (2011, April) "Validation of a Spatially Distributed Ecohydrologic Model using Remote Sensing Techniques", Montana Space Grant Consortium Student Research Symposium, Bozeman, Montana, Poster Session.

Final technical report

ECOHYDROLOGIC MODEL DEVELOPMENT FOR THE ASSESSMENT OF CLIMATE CHANGE IMPACTS ON WATER RESOURCES IN THE BITTERROOT VALLEY

Funding Program: USGS 104(b) Grant, Montana Water Center

PI: Marco P Maneta
Geosciences Dept
University of Montana

May 2, 2011

Funded amount: $11,710

Abstract of original project:

The effect of climate change predictions on local water resources is not yet well understood. This is because climate models provide predictions of changes in the hydrologic cycle at the global or regional scales, which is not adequate to evaluate impacts in the water cycle at the local scale, and hence not adequate for policy action. Downscaling tools that can transfer results from climate models to the local scale are necessary.

An evaluation of the amount of water that will be available in the future under different climate scenarios is only possible with integrated modeling tools that can simulate the system with our best understanding of the relevant processes, including vegetation feedbacks to the hydrologic system.

In this project its is proposed the development of a spatially distributed model that couples a description of the hydrologic system with a forest growth model and an energy balance scheme so the mid-term feedbacks between climate, vegetation and the land phase of the hydrologic system at the local scale can be investigated.

The project involves two components: a model development part, in which the equations that govern energy and mass transfer between the different components of the watershed are programmed in a computer, and a field work component, in which data about the research area is collected and processed to parameterize and validate the model. Data will be collected and the model will be applied in Lost Horse Canyon, a watershed draining to the Bitterroot Valley

1. Status of the main original goals of the project:

a) Develop a ecohydrologic model by coupling together a vertical energy transfer scheme between soil, vegetation and the atmosphere, a hydrologic model and a forest growth model

Model development. **Status: Complete**
A comprehensive computer model (called ECH2O) has been successfully developed in C++ and is under a test stage to evaluate its performance. This model is currently being used by one graduate student as a main tool for his research.

Model parameterization. **Status: Complete**
Data to test the model has been obtained including digital information for the test sites, satellite imagery, land cover parameters and snow and river flow data from the public SNOTEL and river gauging networks.

Model calibration and testing: **Status: Complete**
Three case studies have been used to evaluate the performance of ECH2O including its ability to simulate vertical energy exchanges between the soil and the lower atmosphere and to simulate soil temperature dynamics and its ability to simulate the spatial distribution of the snowpack accumulation and ablation and the dynamics of the forest biomass production as measured by the leaf area index.

b) Fieldwork component

Field site instrumentation: **Status: Complete**
A research site meeting the necessary criteria was located in Lost Horse Canyon in the Bitterroot Valley near Missoula. With the help of two undergraduate students, an experimental plot was installed in the summer of 2010. This plot includes sensors to monitor heat and moisture fluxes into and within the soil as well as sensors to track the activity of trees and a full high precision weather station. This data is forming the base of one of the case studies to validate ECH2O and is the main database one MSc dissertation currently in progress

2. Outcomes derived from project:

2.1. Dissertations

- Johnson, A. "Distribution and Movement of Thermal Energy Beneath a Snowpack as Affected by Soil Moisture and Root Water Uptake". **MSc Thesis** (Expected completion: Fall 2011)

2.2. Reports

- **Maneta, M. P.** "Ecohydrologic model development for the assessment of climate change impacts on water resources in the bitterroot valley**". Final technical report for USGS 104(b) Grant, Montana Water Center (This report). April, 2011**

2.3. Peer-reviewed papers

a. Submitted:

- Pasternack, G. B., **Maneta, M. P.**, Pan, L.-L , Chen, S.-H. , Fogg, G. E., Grismer, M. E., Harter, T., Hopmans, J. W., Puente, C. E., Ustin, S. L., Wallender, W. W. Resiliency of a high-precipitation water supply region to future climatic change in California. *Water Resources Research.* Submitted March 3, 2011

b. In preparation:

- **Maneta, M. P.** and Silverman, N (in preparation). A physics-based ecohydrologic model for forested mountain catchments. *To be submitted promptly to Environmental Modeling and Software*

2.4. Talks, presentations or abstracts at professional meetings,

- One talk to be determined at the 2011 AWRA Montana Section meeting to comply with the grant obligations

- Silverman, N, Johnson, A, **Maneta, M.** *A Spatially Distributed Ecohydrological Model for Forested Catchments*. Montana Section of the America Water Resources Association. 2010 Annual Conference: Rivers of change: Science, policy and the Environment. Helena, MT. October 14-15 2010. Poster session

- **Maneta, M**. and Wallender, W. (2010), "Propagation of information in a pilot-point based multi-objective calibration exercise for a surface-subsurface distributed hydrologic model", Abstract H21F-1119 *Poster* presented at 2010 Fall Meeting, AGU, San Francisco, Calif., 13-17 Dec.

- Silverman, N.L., **Maneta, M.** (2011, April) "Ecohydrologic Model Validation using Remote Sensing Techniques", *The University of Montana Graduate Student and Faculty Research Conference*, Missoula, Montana, Poster Session.

- Silverman, N.L., **Maneta, M.** (2011, April) "Validation of a Spatially Distributed Ecohydrologic Model using Remote Sensing Techniques", *Montana Space Grant Consortium Student Research Symposium*, Bozeman, Montana, Poster Session.

2.5. follow-on grant proposals submitted/funded:

Agency	Title	Amount requested	Status
National Science Foundation	High-resolution impacts of climate change on the land phase of the hydrologic cycle in mountain catchments	$237,305	Pending
US Army Corps of Engineers	Climate change reassessment in the hydrology of the Yuba River catchment, CA	$217,256	Pending
Montana NSF EPSCoR	Watershed Management Strategies under Climate Change Scenarios Using a Spatially Distributed Dynamically Coupled Ecohydrologic Model	$6800	Funded
Montana Space Grant Consortium NASA EPSCoR seed grant	Hydrologic modeling at the watershed scale under climate scenarios with dynamic forest growth and competition using remote sensing and field data	$44,578	Funded

2.6. Other publications

- The project was featured in the February 2011Montana Water News published by the Montana Water center

2.7. Other outcomes

- **Software:** Ecohydrologic model (ECH2O). Current version 2.6b (testing stage). This model will be made publicly available for download online after quality assurance tests have been passed

3. Students involved in this project

3.1. Graduates (3)

Leah Burrell - MSc student – University of Montana

Adam Johnson - MSc student – University of Montana

Nick Silverman - PhD student – University of Montana

3.2. Undergraduates (2)

Andrew Fisher – Senior - University of Montana

Tell Dietzler – Senior - University of Montana

Narrative of project: ECOHYDROLOGIC MODEL DEVELOPMENT FOR THE ASSESSMENT OF CLIMATE CHANGE IMPACTS ON WATER RESOURCES IN THE BITTERROOT VALLEY

1. Introduction

The interconnectedness of the terrestrial, ecologic and atmospheric processes and the importance of the feedbacks has been long recognized (Eagleson, 1978). Also, the need to build a more integrated description of the hydrologic, ecologic and atmospheric processes into our models to capture the feedbacks has been highlighted (Rodriguez-Iturbe, 2000). Yet, most of the available tools used to simulate the hydrologic effects of climate change at local scales do not incorporate a component that describes the vegetation dynamics (The effect of vegetation is simulated using a static set of prescribed parameters). Few of them have a rigorous description of the energy exchanges between the soil, the snowpack, the vegetation and the atmosphere (Liang et al., 1994; Peters-Lidard et al., 1997). While a purely hydrologic description yields good results in short term hydrologic simulations (days to months), the assumption that vegetation will remain static during longer (multi-year to decadal or more) simulations under a changing climate does not hold.

Vegetation activity and energy exchanges in the first top layers of the soil are of especial importance, since transpiration largely drives the soil moisture content in the vadose zone (Laio, 2006), which in turn is a key reservoir that determines recharge rates to the groundwater system (Allison et al., 1994; Warrick et al., 1997), runoff production (Bergkamp, 1998) and hence the response of the entire basin. Vegetation is also a large energy consumer and any energy not dissipated through evapotranspiration will manifest as sensible heat, warming up the air or the soil and increasing snowmelt rates and hence altering the timing of spring flows and the temporal distribution of available water during the year.

Furthermore, resiliency of hydrologic systems is to a large extent dependent on vegetation. Once a transient disturbance in the boundary of a hydrologic system ceases, the system may not return to its original equilibrium point if the disturbance has been long or severe enough to have the vegetation change in response to that disturbance (Peterson et al., 2009).

Few models are available that incorporate a simultaneous description of the hydrology and ecology at the watershed scale. Two examples are Rhessys (Tague and Band, 2004) and Tribs+Veggie (Ivanov et al., 2008; Tague and Band, 2004). The model presented in this document is different from previous efforts in that it simultaneously incorporates a hydrologic model with a conservative energy balance scheme and an ecologic model that allows for the inclusion of vegetation variability at a higher resolution than the computational grid used to solve the energy and hydrologic components.

ECH2O describes intra-pixel surface cover variability in a similar way is the Variable Infiltration Capacity model does (Cherkauer et al., 2003; Liang et al., 1994). In that method, the contribution of the fluxes by each different type of cover to the total pixel value is prorated by their relative area within the pixel. In ECH2O each pixel has P cover types, where p = 1, 2, …, P represent P-1 different vegetation types and P is bare soil. The energy balance is calculated P times per pixel and the results are weighted averaged by the proportion of each of the P cover types in that pixel. A detailed description of the different components of the model (energy balance, hydrologic balance and ecologic component) and two brief case studies follow.

2. Energy balance schemes

2.1. Canopy energy balance:

The energy balance for the canopy level is solved P-1 times, one for each vegetation type except for the P bare soil type. At the canopy level, the available energy is partitioned into latent and sensible heat. The canopy temperature of each of the vegetation types is calculated by solving the energy balance for the canopy temperature T_c. The total energy balance for the pixel is calculated by taking the sum of the fluxes for each of the land cover types weighted by the proportion of the pixel they occupy f_p. Note that since the summation in the energy balance equation is to P-1, the canopy energy balance is not solved for the P (bare soil) vegetation type.

$$\sum_{p=1}^{P-1}\left[R_{n[p]} - \rho_w \lambda_v E_{c[p]} - \rho_w \lambda_v Tp_{c[p]} - H_{[p]}\right] f_p = 0 \qquad 1.$$

Where R_n is net radiation [$ET^{-1}L^{-2}$], ρ_w is water density [ML^{-3}], λ_v is latent heat of vaporization water [EM^{-1}], and $E_{c[p]}$ is evaporation flux [LT^{-1}], $\rho_w\lambda_v E_c$ [$ET^{-1}L^{-2}$] is latent heat flux into the atmosphere due to evaporation, $Tp_{c[p]}$ is transpiration flux [LT^{-1}], $\rho_w\lambda_v E_c$ [$ET^{-1}L^{-2}$] is latent flux into the atmosphere due to transpiration, H is sensible heat flux into the atmosphere [$ET^{-1}L^{-2}$]. The subscript *[p]* indicates that the flux of energy is for the p vegetation type.

Net radiation into the p vegetation type is calculated as the sum of the non-reflected and non-transmitted fraction of incoming shortwave radiation $R_{s\downarrow}(1-\alpha)$ $(1-e^{-kLAI})$[$ET^{-1}L^{-2}$], where α is the albedo of the p vegetation type [-], k is the exponential attenuation coefficient (as per Beer's law) and LAI is the leaf area index of the p vegetation type, incoming longwave radiation $\varepsilon_a R_{l\downarrow}$ [$ET^{-1}L^{-2}$], where ε_a is the emissivity of air [-], minus the longwave radiation leaving the surface $\varepsilon_s \sigma T_s$ [$ET^{-1}L^{-2}$], where ε_s is the emissivity of the p vegetation type [-], σ is the Stefan-Boltzmann constant [$ET^{-1}L^{-2}\Theta^{-4}$] and T_c is the canopy temperature of the p vegetation type [Θ]. The subscript *[p]* applied to brackets indicates that the vegetation properties inside the brackets are evaluated for the p vegetation type but not for the P vegetation type.

$$R_{n[p]} = R_{s\downarrow}(1-\alpha)_{[p]}(1-e^{-k\cdot LAI})_{[p]} + \varepsilon_a R_{l\downarrow} - \left(\varepsilon_s \sigma T_c^4\right)_{[p]} \qquad 2.$$

Latent heat flux between the canopy vegetation type and the atmosphere due to evaporation of intercepted water is calculated as:

$$\rho_w \lambda_v E_{c[p]} = \frac{\rho_a c_a}{r_{av[p]} \gamma} [e_c^*(T_c)_{[p]} - e_a] \qquad 3.$$

In this function, ρ_a is the density of air [ML^{-3}], c_a is the specific heat capacity of air [$EM^{-1}\Theta^{-1}$], γ is the psychrometric function [$FL^{-2}\Theta^{-1}$], r_{av} is the aerodynamic resistance of the p vegetation type [$T^{-1}L$], e_c is the saturation vapor pressure at canopy temperature and e_a is the vapor pressure in the air.

Latent heat flux between the canopy and the atmosphere due to transpiration is calculated from the difference between vapor pressure at canopy temperature and atmospheric vapor pressure:

$$\rho_w \lambda_v Tp_{c[p]} = \frac{\rho_a c_a}{\gamma} g_{c[p]} [e_c^*(T_c)_{[p]} - e_a] \qquad 4.$$

The new symbol in this equation is g_c, which is the canopy conductance of vegetation p to latent heat flux (equation 39), which depends on the soil moisture content and vegetation characteristics.

Sensible heat flux between the p canopy type and the atmosphere is calculated as:

$$H_{[p]} = \frac{\rho_a c_a}{r_{av[p]}} [T_{c[p]} - T_a] \qquad 5.$$

In this last equation, T_a [Θ] is air temperature. The calculation of the psychrometric constant, vapor pressure values and aerodynamic resistance is as indicated in the following section.

2.2. Surface energy balance:

The partition of available energy into energy allocated to evaporate water, reduce the cold content of the snow pack, and heat the air, and heat the ground is calculated by solving the energy balance for surface temperature T_s for each of the p land cover types including this time a solution for bare soil. The total energy balance for the pixel is calculated by taking the sum of the fluxes for each of the land cover types weighted by the proportion of the pixel they occupy f_p:

$$\sum_{p=1}^{P} \left[R_{n[p]} - \rho_w \lambda_v E_{[p]} - H_{[p]} - G_{[p]} - S_{[p]} - LM_{[p]} \right] f_p = 0 \qquad 6.$$

Where R_n is net radiation [$ET^{-1}L^{-2}$], ρ_w is water density [ML^{-3}], λ_v is latent heat of vaporization water [EM^{-1}], and E is flux of water vapor due to soil evaporation [LT^{-1}], $\rho_w\lambda_v E$ [$ET^{-1}L^{-2}$] is latent heat flux into the atmosphere due to soil evaporation, H is sensible heat flux into the atmosphere [$ET^{-1}L^{-2}$], G is ground heat flux [$ET^{-1}L^{-2}$], S is heat flux into the snow pack [$ET^{-1}L^{-2}$] and LM is latent heat of snowmelt [$ET^{-1}L^{-2}$]. The subscript *[p]* indicates that the flux of energy is for the *p* vegetation type including the P (bare soil) vegetation type.

Net radiation into the surface is calculated as the sum of the non-reflected and non intercepted by canopy fraction of incoming shortwave radiation $R_{s\downarrow}(1-\alpha)$ (e^{-kLAI}) [$ET^{-1}L^{-2}$], where α_s is the albedo of the surface under cover type *p* [-]; incoming longwave radiation from the canopy layer of vegetation type *p*, which is the bottom half of the radiation emmited by the canopy*:* $0.5(\varepsilon_c\sigma T_c^4)$ [$ET^{-1}L^{-2}$]. In this equation ε_c is the emissivity of the canopy and 0.5 indicates that only half of the longwave emission of the canopy is directed downwards; incoming longwave radiation $\varepsilon_a R_{l\downarrow}$ [$ET^{-1}L^{-2}$], where ε_a is the emissivity of air [-], minus the longwave radiation leaving the surface $\varepsilon_s\sigma T_s$ [$ET^{-1}L^{-2}$], where ε_s is the emissivity of the surface [-], σ is the Stefan-Boltzmann constant [$ET^{-1}L^{-2}\Theta^{-4}$] and Ts is the surface temperature [Θ]. The subscript [p] applied to brackets indicates that the vegetation properties inside the brackets are evaluated from the *p* vegetation type and are set to zero for the P (bare soil) soil type.

$$R_{n[p]} = R_{s\downarrow}(1-\alpha_{s[p]})(e^{-kLAI})_{[p]} + 0.5\left(\varepsilon_c\sigma T_c^4\right)_{[p]} + \varepsilon_a R_{l\downarrow} - \left(\varepsilon_s\sigma T_s^4\right)_{[p]} \qquad 7.$$

Emissivity of the air and surface are calculated from their temperatures using Swinbank's (1963) empirical relationship:

$$\varepsilon_{\bullet} = 0.92x10^{-5}\left(273.2 + T_{\bullet}\right)^2 \qquad 8.$$

Where temperature is given in degree Celsius.

Latent heat flux between the surface and the atmosphere due to soil evaporation is calculated as:

$$\rho_w\lambda_v E_{[p]} = \frac{\rho_a c_a}{\gamma(r_s + r_{av[p]})}[e_s^*(T_s)_{[p]} - e_a] \qquad 9.$$

In this last equation, ρ_a is the density of air [ML^{-3}], c_a is the specific heat capacity of air [$EM^{-1}\Theta^{-1}$], γ is the psychrometric function [$FL^{-2}\Theta^{-1}$], r_s is the soil resistance to evaporation [$T^{-1}L$], r_{av} is the aerodynamic resistance [$T^{-1}L$], both associated to land cover *p*, e_s is the saturation vapor pressure at the soil temperature T_s under vegetation type p and e_a is the vapor pressure in the air.

Density of air is adjusted for air temperature using the ideal gas relationship

$$\rho_a(T) = \frac{P_a}{R_a T} \qquad 10.$$

Where P_a is air pressure [FL^{-2}], R_a is the gas constant for dry air [$EM^{-1}\Theta^{-1}$].

The psychrometric relationship is a function of atmospheric pressure

$$\gamma(P_a) = \frac{c_a P_a}{0.611\lambda_v} \qquad 11.$$

Vapor pressure is calculated from saturation vapor pressure and relative humidity RH:

$$e = e^* * RH \qquad 12.$$

Saturation vapor pressure in the air and at the surface is function of the respective temperatures

$$e^*(T) = 611 * \exp\left(\frac{17.3T}{T + 237.3}\right) \qquad 13.$$

In this last equation, T is given in degree Celsius and saturation vapor pressure is calculated in Pascals.

Aerodynamic resistance is calculated assuming a vertical logarithmic profile and is assumed to be the same for the vertical transfer of momentum, vapor and energy

$$r_{av} = \frac{\ln\left(\frac{z - z_d}{z_0}\right)^2}{k^2 v_a} \qquad 14.$$

Where k is the von Karman constant (0.4), v_a is wind speed [LT^{-1}], z is the elevation at which wind speed has been measured [L], z_d is a reference elevation (zero plane displacement) [L] and z_0 is the roughness height [L], which is a measure of the unevenness of the surface.

Resistance to exfiltration, r_s, [TL^{-1}], is function soil moisture and soil charactersistics (Eagleson, 1978; Wigmosta, 1994; Tague, 2004);

$$r_s = \left[\left(\frac{\theta - \theta_r}{\eta - \theta_r}\right)^{\frac{1}{2\lambda}+2} \sqrt{\frac{8\eta K_s \psi_{ae}}{3(1+3\lambda)(1+4\lambda)}\Delta t}\right]^{-1} \qquad 15.$$

Where θ is the volumetric soil moisture content [L^3L^{-3}], θ_r is the residual volumetric soil water content [L^3L^{-3}], η is porosity [L^3L^{-3}], Ks is soil saturated hydraulic conductivity [LT^{-1}], ψ_{ae} is the soil air entry pressure [L] and λ is the soil pore size index [-]. The calculation of canopy conductance is given below (eq. 32) when describing the vegetation module.

Sensible heat flux between the surface and the atmosphere is calculated as:

$$H_{[p]} = \frac{\rho_a c_a}{r_{av[p]}}[T_{s[p]} - T_a] \qquad 16.$$

In this last equation, T_s and T_a [Θ] are soil and air temperature, respectively.

Ground heat is calculated using the 1D diffusion equation, for which soil heat capacity c_s [$EM^{-1}\Theta^{-1}$] and soil thermal conductivity K_T [$EL^{-1}\Theta^{-1}$] are averaged for the entire soil profile in the pixel and are functions of the volumetric soil moisture content θ [L^3L^{-3}] .

$$G_{[p]} = \frac{\partial[c_s(\theta)\cdot T]}{\partial t} = -\frac{\partial}{\partial z}\left[K_T(\theta)\frac{\partial T}{\partial z}\right] \qquad 17.$$

Soil heat capacity and soil thermal conductivity are calculated as a weighted sum of the heat capacity and thermal conductivities of the fractions of water, air and solid particles:

$$c_s(\theta) = (1-\eta)c_p + \theta\cdot c_w\cdot\rho_w + (\eta-\theta)c_a\cdot\rho_a \qquad 18.$$

$$K_r(\theta) = (1-\eta)K_p + \theta\cdot K_w\cdot\rho_w + (\eta-\theta)K_a \qquad 19.$$

Where η is soil porosity, c_p, c_w and c_a are the heat capacities of the soil particles, water and air, respectively; and K_p, K_w and K_a are the thermal conductivities of the soil particles, water and air, respectively.

If a snowpack exists, the energy flux into the snowpack is used to increase its average temperature until it reaches the melting point. At melting point, any extra energy input generates snowmelt that carries away latent heat of fusion:

$$S_{[p]} = \begin{cases} c_i\rho_w h_i\dfrac{\partial T_{s[p]}}{\partial t} + R & T_s < T_m \\ -\lambda_f\rho_w\dfrac{dh_i}{dt} & T_s = T_m \end{cases} \qquad 20.$$

In this equation, c_i is the specific heat capacity of frozen water [$EM^{-1}\Theta^{-1}$], h_i is the snow water equivalent of the snowpack [L], λ_f is the latent heat of fusion [EM^{-1}], R is a term holding energy advected by rainfall or run-on from upstream areas [$ET^{-1}L^{-2}$] and T_m is the temperature of the melting point [Θ].

When the snowpack melts, latent heat taken by the melt process is calculated as

$$LM_{[p]} = \begin{cases} \min\left(\dfrac{\rho_w \lambda_f h_{i[p]}}{\Delta t}, \rho_w \lambda_f (T_{s[p]} - T_m)\mu_M \right) & T_{s[p]} > T_m \\ 0 & T_{s[p]} \le T_m \end{cases} \qquad 21.$$

The new symbol μ_M is an empirical melt coefficient [$L\Theta^{-1}$] to account for the sensitivity of the snowpack to sensible heat. The *min* function ensures that no more latent heat of fusion is extracted than the equivalent for the amount of snow in the cell, where $\rho_w \lambda_f h_i / \Delta t$ is the total amount of latent heat needed to melt the current snowpack of depth h_i.

3. Water balance

3.1. Precipitation input

When run at daily time steps, total daily precipitation P_t [LT^{-1}] is partitioned into snowfall P_s [LT^{-1}] and rainfall P_r [LT^{-1}] according to the minimum and minimum temperatures of the day according to the fraction of the temperature range that falls below 0^oC

$$P_s = \begin{cases} P_t & \text{if} \quad T_{a\max} \le 0 \\ 0 & \text{if} \quad T_{a\min} > 0 \\ P_t * \max\left(0, \dfrac{-T_{a\min}}{T_{a\max} - T_{a\min}}\right) & \text{otherwise} \end{cases} \qquad 22.$$

$$P_r = P_t - P_s$$

3.2. Canopy water balance

ECH2O implements a linear bucket approach to simulate canopy interception. The water balance in the canopy layer is solved for each of the P-1 vegetation types

$$\frac{\partial C_{s[p]}}{\partial t} = P_r + P_s - C_{t[p]} - E_{c[p]} \qquad 23.$$

Where C_s is the current canopy water storage [L] and Ct is the canopy water trascolation (dripping from the canopy) [LT^{-1}].

Transcolation occurs at the rate at which canopy storage increases above the maximum canopy storage C_{smax}

$$C_{t[p]} = \frac{\partial (C_{s[p]} - C_{s\max[p]})}{\partial t} \qquad 24.$$

The maximum canopy storage for species *p* is a function of the current leaf area index

$$C_{s\max[p]} = \mathrm{X}_{s\max[p]} * LAI_{[p]} \qquad 25.$$

Where X_{smax} is a species dependent maximum canopy storage parameter [L] that reflects the depth of water that the species can hold per unit leaf area index.

Transcolation from trees is partitioned as snow or as rain using the same approach considered for incident rainfall:

$$C_{s[p]} = \begin{cases} C_{t[p]} & \text{if} \quad T_{a\max} \le 0 \\ 0 & \text{if} \quad T_{a\min} > 0 \\ C_{t[p]} * \max\left(0, \dfrac{-T_{a\min}}{T_{a\max} - T_{a\min}}\right) & \text{otherwise} \end{cases} \qquad 26.$$

$$C_{r[p]} = C_{t[p]} - C_{s[p]}$$

Where C_s is the amount of trascolation happening as snow and C_r is the amount of trascolation happening as rain.

3.3. Surface water balance and fluxes

Precipitation on bare soil and trascolation from trees reach the surface and increase the snowpack storage or the ponding storage depending on weather they reach the ground as snow or as rain, respectively.

The mass balance for the snowpack is

$$\frac{dh_i}{dt} = \sum_{p=1}^{P-1}\left[C_{s[p]} f_p\right] + P_s f_P - \sum_{p=1}^{P}\left[M_{i[p]} f_p\right] = 0 \qquad 27.$$

Where the first P-1 terms on the right hand side is the trascolation as snow from the vegetation types, the P term is the amount of snowfall directly onto the ground and the last P terms is the amount of snowmelt M_i [LT^{-1}] under each of the P land covers.

The mass balance for the surface ponding storage is:

$$\frac{dh_w}{dt} = \sum_{p=1}^{P-1}\left[C_{r[p]} f_p\right] + P_r f_P + \sum_{p=1}^{P}\left[M_{i[p]} f_p\right] + q_{rtn} + q_{up} - I_f = 0 \qquad 28.$$

Where h_w is the depth of surface ponding water [L], the first P-1 terms on the right hand side is the trascolation as rain from the P-1 vegetation types, the P term is the amount of rainfall directly onto the ground, the following P terms is the amount of snowmelt M_i [LT^{-1}] under each of the P land covers, q_{rtn} is return flow rate from subsurface [LT^{-1}], q_{up} [LT^{-1}] is overland run-on into the cell and the last term I_f is the infiltration rate into the soil [LT^{-1}]

The amount of snowmelt is calculated directly from the latent heat of melt:

$$M_{i[p]} = \frac{LM_{[p]}}{\lambda_f \rho_w} \qquad 29.$$

The surface water storage that is not infiltrated becomes overland flow.

The infiltration rate term in [28] is calculated using a form of the Green and Ampt equation for which infiltration capacity is a function of soil moisture:

$$I_f = K_s\left(\frac{\psi_{ae}(1-S_\theta)\eta}{\theta \cdot d_s} + 1\right) \qquad 30.$$

In this equation K_s is saturated hydraulic conductivity [LT^{-1}], ψ_{ae} is the soil air entry pressure [L], η is effective porosity, θ is the average volumetric soil water content for the soil layer and S_θ is effective saturation [i.e. $S_\theta = (\theta - \theta_r)/(\eta - \theta_r)$, where θ_r is residual soil water content]. The depth of water that infiltrates and the associated increase in soil moisture depends on the antecedent moisture conditions and the available water for infiltration h_w . The potential infiltration depth F_p [L] is the lesser between the available water for infiltration on the surface (ponding depth h_w) and the potential infiltration rate integrated over the time before ponding occurs, $t_p \leq \Delta t$:

$$F_p = \min(h_w, I_f t_p) \qquad 31.$$

Actual infiltration depth ΔF [L] increases the average soil moisture of the cell ($\Delta F = \Delta\theta d_s$)

$$\Delta\theta \cdot d_s = F_p + K_s(\Delta t - t_p) - \psi\Delta\theta * \ln\left[\frac{\psi\Delta\theta + \Delta\theta \cdot d_s}{\psi\Delta\theta + F_p}\right] \qquad 32.$$

where t_p is the time at which ponding occurs. This equation is solved iteratively for $\Delta\theta$ using a Newton-Raphson scheme.

The fraction of h_w that does not infiltrate becomes at the end of the time step becomes runoff. Runoff in one cell becomes run-on for the downstream cell, where it may re-infiltrate. The calculation is performed in a cascading form following the local drain direction determined by the steepest descent D8 algorithm performed over a raster DEM until the outlet a cell with a channel or the outlet is reached. Once overland flow reaches a channel, no further losses by reinfiltration are allowed. In the current version, overland flow is assumed to be able to run the entire drainage network each time step (i.e. overland flow exits the basin in one time step).

The flow at each channel cell is the sum of inflows from upstream cells (channel and non-channel cells) plus inflows from the subsurface system, q_{chan}, as explained below.

3.4. Subsurface water balance and fluxes

The theoretical background underpinning ECH2O implementation of the subsurface processes relies on the idea that once the soil profile reaches field capacity, any extra water in the soil will move downslope under the force of gravity.

$$h_g = (\theta - \theta_{fc}) d_s \qquad 33.$$

The movement of water in the subsurface system is simulated using a 1D kinematic wave approach in which groundwater fluxes are assumed to be proportion to the slope of the bedrock and to some effective hydraulic conductivity value:

$$\frac{\partial h_g}{\partial t} + K_{eff} S_x \frac{\partial h_g}{\partial x} + q_{rch} - q_{rtn} - q_{cap} - q_{chan} = 0 \qquad 34.$$

Where h_g is the water depth in the soil free to move downslope [L], K_{eff} is an *effective* conductivity of the soil [LT^{-1}], S_x is the slope of the bedrock in the downslope direction [LL^{-1}], q_{rch} is the amount of recharge to the saturated layer [LT^{-1}], q_{rtn} is return flow rate to the surface system when groundwater exceeds the soil storage capacity [LT^{-1}], q_{cap} is the rate of water transfer from the groundwater system to the vadose zone system due to capillary rise [LT^{-1}] and q_{chan} is the rate of water transfer from the subsurface system to the channel.

Recharge to the groundwater system is assumed to be the water in the vadose zone system that is in excess of the soil field capacity (gravitational water)

$$q_{rch} = \max(0.0, (\theta - \theta_{fc}) \frac{d_s}{\Delta t} \qquad 35.$$

Where the max function ensures no negative recharge happens when the current soil moisture in a pixel is below field capacity.

Return flow happens when groundwater exceeds the soil storage at a rate governed by the soil effective conductivity and the groundwater balance

$$q_{rtn} = -(\eta - \theta) d_s \left(1 + K_{eff} S_x \frac{\Delta t}{\Delta x}\right) + h_g{}^{i}_{j+1} \left(K_{eff} S_x \frac{\Delta t}{\Delta x}\right) + h_g{}^{i+1}_{j} + q_{rtn} - q_{cap} - q_{chan} \qquad 36.$$

And capillary fluxes into the vadose zone system are assumed be driven by the vadose zone soil moisture deficit until it the vadose zone reaches field capacity. The transfer is governed by the soil effective conductivity

$$q_{cap} = h_g{}^{i}_{j+1} \left(K_{eff} S_x \frac{\Delta t}{\Delta x}\right) + h_g{}^{i+1}_{j} + q_{rch} - q_{rtn} - q_{chan} - h_g{}^{i+1}_{j+1} \left(1 + K_{eff} S_x \frac{\Delta t}{\Delta x}\right) \qquad 37.$$

The transfers of water from the subsurface to the channel are calculated using an exponential decay controlled by an empirical parameter b [L^{-1}]:

$$q_{chan} = K_{eff}\, h_g\, (1 - e^{-b \cdot h_g}) \qquad 38.$$

4. Ecological processes

4.1. Forest growth

A multiplicative production function is the backbone of the forest growth module included in ECH_2O. The function is based on that proposed in 3PG, which relates gross primary production (GPP [ML^{-2}]) to the amount of photosynthetically active radiation (R_{par} [EL^{-2}]), the status of the tree (age, leaves) and environmental factors:

$$GPP_{[p]} = \varepsilon_{c[p]} \cdot R_{par} \cdot LAI \cdot f_{GPP}(age_{[p]}) \cdot f_{GPP}(T_a) \cdot f_{GPP}(\theta) \qquad 39.$$

Where ε_c is the quantum efficiency of the tree [ME^{-1}], which prescribes how much mass of carbon is assimilated per unit of energy absorbed, R_{par} is assumed to be 47% of $R_{s\downarrow}$ and $f_{GPP}(age)$, $f_{GPP}(T_a)$ and $f_{GPP}(\theta)$ are the environmental efficiency factors that modulate maximum potential growth and that are functions of the tree age, air temperature and soil moisture, respectively.

$$f_{GPP}(age_{[p]}) = \begin{cases} 0.7 + 0.3\dfrac{age_{[p]}}{0.2age_{\max[p]}} & age < 0.2age_{\max} \\ \dfrac{1}{1 + \max\left[0, \left(\dfrac{age_{[p]} - 0.2age_{\max[p]}}{0.95age_{\max[p]}}\right)^3\right]} & \text{otherwise} \end{cases} \qquad 40.$$

$$f_{GPP}(T_a) = \left(\frac{T_a - T_{\min[p]}}{T_{opt[p]} - T_{\min[p]}}\right)\left(\frac{T_{\max[p]} - T_a}{T_{\max[p]} - T_{opt[p]}}\right)\left(\frac{T_{\max_{[p]}} - T_{opt_{[p]}}}{T_{opt_{[p]}} - T_{\min_{[p]}}}\right) \qquad 41.$$

$$f_{GPP}(\theta) = \min\left(\frac{g_{c[p]}}{g_{c\max[p]}}, \frac{1}{1 + \left(\dfrac{1 - f_p(\theta - \theta_{fc})}{Wc}\right)^{Wp}}\right) \qquad 42.$$

Where age is the age of the tree patch (years) and $age_{\max}$ (years) is the maximum age a tree of its species can achieve, T_{min}, T_{max} and T_{opt} are the minimum, maximum and optimal temperatures, respectively, for trees of species p, g_c is canopy conductance, g_{cmax} is potential canopy conductance under unrestricted conditions and Wp and Wc are empirical soil parameters.

Canopy conductance is calculated using a Jarvis multiplicative. In this model canopy conductance is proportional to LAI and affected by the environmental factors embedded in the efficiency functions (solar radiation, air temperature, vapor pressure deficit and available soil moisture):

$$g_{c[p]} = g_{c\max[p]} \cdot LAI_{[p]} \cdot \varsigma \cdot f_{gc}(R_{s\downarrow}) \cdot f_{gc}(T_a) \cdot f_{gc}(e_a) \cdot f_{gc}(\theta) \quad 43.$$

Where ς is a shelter factor [0-1] that accounts for the shade that leaves project on each other and $f_{gc}(R_{s\downarrow})$, $f_{gc}(T_a)$, $f_{gc}(e_a)$ and $f_{gc}(\theta)$ are the efficiency factors related to solar radiation, air temperature, vapor pressure and soil moisture, respectively. These factors are calculated as follows:

$$f_{gc}(R_{s\downarrow}) = \frac{R_{s\downarrow}}{C_{s\downarrow} + R_{s\downarrow}} \quad 44.$$

$$f_{gc}(T_a) = f_{GPP}(T_a) \quad 45.$$

$$f_{gc}(e_a) = \exp(-C_{ea}(e_a^* - e_a)) \quad 46.$$

$$f_{gc}(\theta) = \min\left(1.0, \frac{\theta - \theta_{wp}}{\theta_{fp} - \theta_{wp}}\right) * \left(C_\theta - \min\left(1.0, \frac{\theta - \theta_{wp}}{\theta_{fp} - \theta_{wp}}\right)\right) \quad 47.$$

Where $C_{s\downarrow}$, C_{ea} and C_θ are empirical coefficients, θ_{wp} and θ_{fc} are the volumetric soil moisture content at wilting point and at field capacity, respectively.

Net primary productivity (NPP, [ML^{-2}]) is considered to be a constant ratio of GPP

$$NPP_{[p]} = C_{NPP} GPP_{[p]} \quad 48.$$

Where C_{NPP} is the proportionality constant found to be 0.47±0.04 for a wide range of forests.

Allocation of assimilated carbon to leaves, roots and stem is done assuming that trees will allocate more carbon to roots when the environmental conditions are less favorable to capture more resources rather than using the resources to grow the stem. The partition of NPP is thus done as

$$\Delta M_{root} = NPP * \eta_r \quad 49.$$

$$\Delta M_{stem} = NPP * \eta_s \quad 50.$$

$$\Delta M_{leaf} = NPP * \eta_f \quad 51.$$

Where η_r, η_s, η_f ($\eta_r + \eta_s + \eta_f = 1$) are the partition factors to allocate NPP to roots, stem and leaves, respectively. The calculation of these factors is as follows:

$$\eta_r = \frac{0.5}{1 + 2.5 * f_{GPP}(age_{[p]}) f_{GPP}(T_a) f_{GPP}(\theta)} \quad 52.$$

$$\eta_s = \frac{1 - \eta_r}{1 + p_{fs}} \quad 53.$$

$$\eta_f = 1 - \eta_r - \eta_s \qquad 54.$$

Where p_{fs} is a partition function dependent on species parameters

$$p_{fs[p]} = \frac{F_{prn[p]} * F_{pra[p]}}{S_{prn[p]} * S_{pra[p]}} DBH_{[p]}^{(F_{prn[p]} - S_{prn[p]})} \qquad 55.$$

Where F_{prn}, F_{pra}, S_{prn} and S_{pra} are species dependent empirical parameters and DBH is the total diameter at breast height of the sum of the individual trees of species [p] in the pixel [L].

Once carbon is allocated, LAI, roots mass and the size of the tree are updated. The increment of the leaf area index is

$$\Delta LAI_{[p]} = \sigma_{LAI[p]} \cdot \Delta M_{leaf[p]} - \delta_{f[p]} \cdot \Delta t \cdot LAI_{[p]} \qquad 56.$$

Where σ_{LAI} is the specific leaf area index [L^2M^{-1}], δ_f is the leaf turnover rate [T^{-1}] and Δt the time step size [T].
The increment in root mass is calculated by

$$\Delta Root_{[p]} = \Delta M_{root[p]} - \delta_{r[p]} \cdot \Delta t \cdot Root_{[p]} \qquad 57.$$

Where Root is the root mass [ML^{-2}] and δ_r is the root turnover rate [T^{-1}].

The growth of the tree derived from carbon allocation to the stem (which includes branches) is calculated using the allometric relationships proposed in TREEDYN3. Tree diameter is incremented according to the following expression:

$$\Delta DBH_{[p]} = \frac{4\breve{\rho}_{t[p]}}{\rho_{wood[p]} \pi DBH_{[p]}^2 \left(2\frac{H_{t[p]}}{DBH_{[p]}} + F_{hd[p]} \right)} \qquad 58.$$

And tree height is incremented according to:

$$\Delta H_{t[p]} = F_{hd} \Delta DBH \qquad 59.$$

In the last two equations, $\breve{\rho}_t$ is the average mass increment per individual tree in patch [p] with units of mass per tree [M $tree^{-1}$], which is calculated by dividing total stem mass [ML^{-2}] by the stem density (number of trees per area of the patch, [tree L^{-2}] in patch [p]. ρ_{wood} is the density of wood [ML^{-3}], π is the constant (3.14159…), H_t is the average tree height [L] in the patch and F_{hd} is a growth factor that depends on the height to diameter ratio of the tree and the conditions of the patch:

$$F_{hd[p]} = \begin{cases} \mathrm{F}_{\mathrm{hdmin}[p]} & \text{if} \quad \dfrac{H_{[p]}}{D_{[p]}} \geq \mathrm{F}_{\mathrm{hdmin}[p]} \;\&\; Stc_{[p]} < 1 \\ \mathrm{F}_{\mathrm{hdmin}[p]} & \text{if} \quad \dfrac{H}{D} \leq \mathrm{F}_{\mathrm{hdmax}[p]} \;\&\; Stc_{[p]} \geq 1 \;\&\; age_{[p]} < \dfrac{age_{\max[p]}}{2} \\ \mathrm{F}_{\mathrm{hdmax}[p]} & \text{if} \quad \dfrac{H}{D} \leq \mathrm{F}_{\mathrm{hdmax}[p]} \;\&\; Stc_{[p]} \geq 1 \;\&\; age_{[p]} > \dfrac{age_{\max[p]}}{2} \\ \mathrm{F}_{\mathrm{hdmax}[p]} & \text{if} \quad \dfrac{H_{[p]}}{D_{[p]}} < \mathrm{F}_{\mathrm{hdmin}[p]} \\ 0.5\mathrm{F}_{\mathrm{hdmin}[p]} & \text{if} \quad \dfrac{H_{[p]}}{D_{[p]}} > \mathrm{F}_{\mathrm{hdmax}[p]} \\ 0 & \text{if} \quad age_{[p]} > 0.7 age_{\max[p]} \end{cases} \qquad 60.$$

In this last equation, F_{hdmin} and F_{hdmax} are the maximum and minimum growth factors allowed for a given species and *Stc* is a crowding factor that is depends on the density of trees in the patch and the crown coverage:

$$Stc_{[p]} = 0.25\pi\left(\varpi_{[p]} DBH_{[p]}\right)^2 N_{trees[p]} \qquad 61.$$

Where ω is the crown to stem diameter ratio and N_{trees} is the number of trees in patch [p]

5. Field site

5.1. Site description and monitorization

As part of the development and goals of this project, an experimental field site has been identified and instrumented. The chosen site is located at an elevation of 1950m in the head of the Lost Horse drainage of the Bitterroot Mountains, approximately 29 km southwest of Hamilton, MT. The site lies within the Forest Service designated Lost Horse Research Natural Area (RNA) adjacent to the Selway-Bitterroot Wilderness Figure 2.

To monitor local energy exchanges between the soil, the vegetation and the atmosphere, a plot is heavily instrumented including an array of soil sensors, sap flow probes and meteorological stations (Figure 1). The soil sensor array is organized in a series of twelve pits arranged in four arms of three pits extending outward ~10 meters in four directions from a mature Engelmann Spruce, roughly aligned with the cardinal directions and are deep enough to reach bedrock. Pits have been instrumented at 15cm, 30cm, and 45cm depths in order to adequately represent the soil profile. The layout of the pits is designed to provide both lateral and vertical data. Initial site installation included two pits instrumented with thermocouples and five Decagon Device (Echo 5 model) soil moisture probes to record soil moisture content. Each pit includes a Hukseflux thermal flux plate to determine net sensible heat flux through the profile including upwards loss into the snowpack. The soil heat flux plates measure the direction and magnitude of sensible heat flux by measuring the thermal gradient between two thermocouples

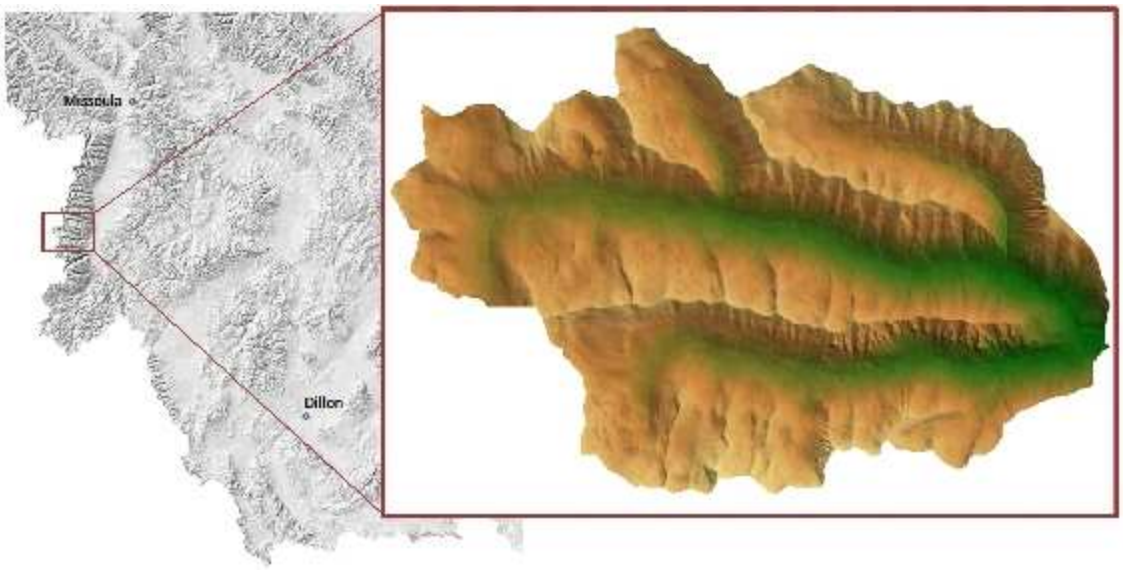

Figure 2 Location of Lost Horse Canyon within the west range of the Bitterroot valley.

separated by thermopile of known conductivity. At a second instrumentation stage, ten additional pits, with three probes per pit, were installed with two additional Hukseflux thermal flux plates and soil moisture probes produced by Decagon Devices (5TE model) which simultaneously record temperature, soil moisture and electrical conductivity.

A sap-flow monitoring system (Dynamax Thermal Dissipation Probe) has been installed on a mature Engelmann Spruce to monitor root water uptake rates from the soil. The system utilizes a dual needle probe that is inserted 3 cm into the tree. The top needle is heated while the other, inserted a known distance below the heated needle, measures the heat dissipation as heat is carried downstream (upwards) by sap. In order to quantify the volume of transpiration core samples of the tree trunks provide the thickness of the sapwood from which to calculate cross-sectional

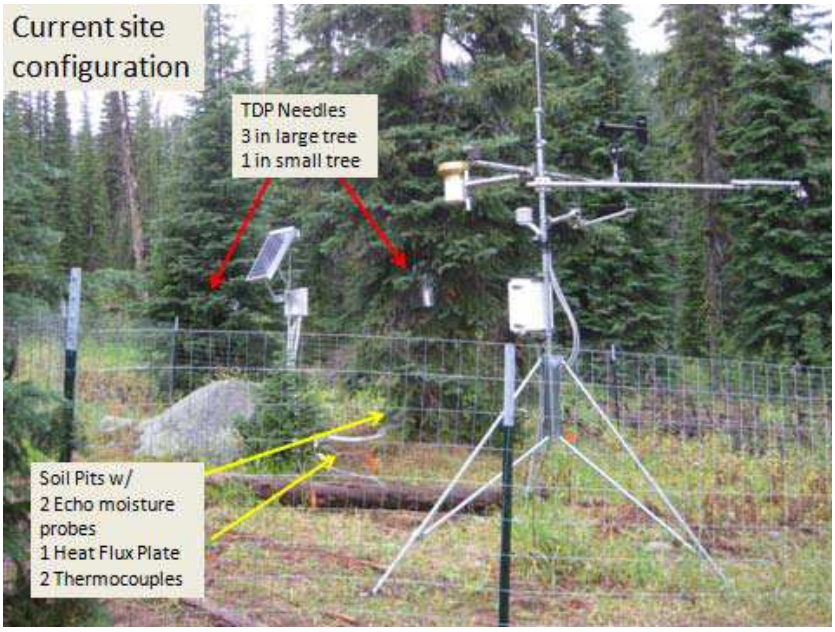

Figure 1 Instrumentation of the study site with locations of TDP needles, soil pits, and of the meteorological array mounted to a 10' tripod. View is looking northwest.

sap wood area which multiplied by sap velocity will yield volume of sap translocation in the tree which is directly related to rates of root water uptake required for photosynthesis. A young Engelmann Spruce has a single heat dissipation probe installed in order to monitor differential transpiration between saplings and mature spruces throughout the year.

A tripod mounted meteorological station is used to monitor on-site atmospheric conditions. The station is equipped with relative humidity and temperate sensors mounted in a radiation shield, a barometric pressure sensor, rain gauge for liquid precipitation, a sonic ranger for acoustic snow depth measurement and a wind anemometer, recording both wind velocity and direction. In addition, a silicone pyranometer used to monitor incoming solar radiation and a net radiometer measuring the balance of incoming radiation to outgoing radiation.

Each system is operated and recorded via a Campbell Scientific CR-1000 data-logger (3 total) mounted in weather proof enclosures on site. The soil array and sap-flow system also utilize Campbell Scientific Am 16/32 multiplexers to allow for the large number of sensors. Due to the large amount of data generated, each data-logger contains a compact flash expansion allowing for the storage of over three weeks' worth of data.

In addition to this instrumentation, two SNOTEL sites, operated by the Natural Resources Conservation Service (NRCS), are located at two different elevations within the canyon providing historic atmospheric and snow data beginning in 1978.

5.2. Data

The instrumentation described above allows us to monitor a wide array of environmental variables: precipitation, air temperature, air h,umidity, air pressure, short wave radiation, net radiation, wind speed, wind direction, snow depth, soil moisture, soil temperature, soil heat flux, soil electrical conductivity and sap flow. Data is being collected at a 10 minute resolution. The monitoring started on August 15th 2010 and the site is planned to be kept for research and teaching purpose while financial support exists.

Information from this site will provides us with an exceptionally rich data set with valuable information to investigate soil, vegetation and atmosphere water and energy transfers and will provides us with accurate information to test and calibrate the model. It will also serve as a site for instruction to graduate and undergraduate students about environmental monitoring and assessment.

6. Tests

6.1. Case study: radiation balance

Thirteen days of data from August 20th, 2010 through September 1st, 2010 were used to test the radiative component of the model for Lost Horse Canyon. The data were aggregated hourly constituting a record of 311 hours of information. The time series for air temperature, and

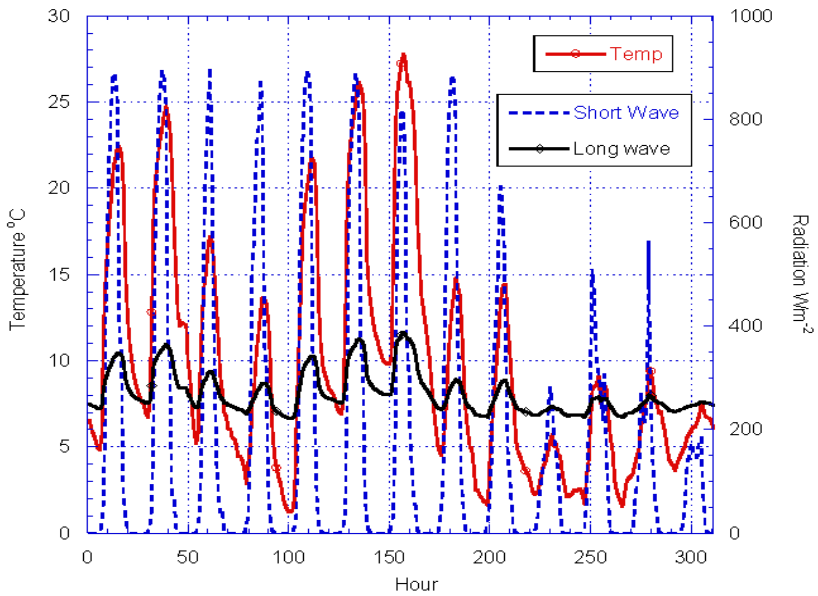

Figure 3Temperature and radiation input data collected in the study site and used as forcing for the demonstration run described in the next section.

incoming long and short wave radiation can be shown in Figure 3 The performance of the radiative and hydrologic component of the model was evaluated through a study comparing net radiation and soil temperature data from the Lost Horse Canyon site with model output. Values for albedo, thermal conductivity of the soil, and the aerodynamic roughness coefficient specific to study were calibrated. The soil temperature sensor used for calibration was an average of the sensors at a 15 cm depth. Net radiation was calculated by the radiometer mounted on the meteorological station.

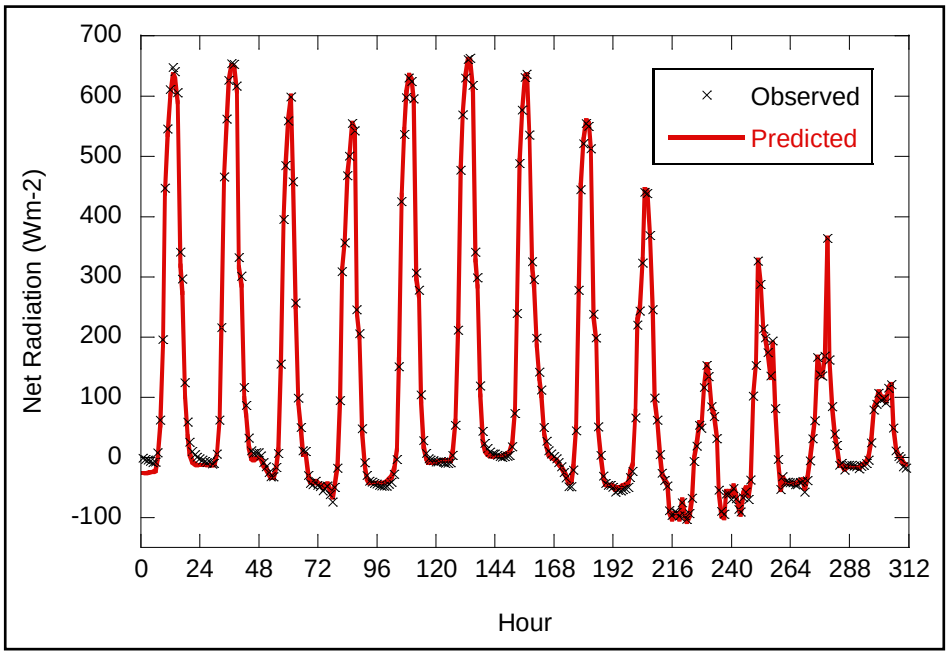

Figure 4. Predicted and observed net radiation for the Lost Horse Canyon study site in late August, 2010. Measurements were recorded at one-hour intervals over a 13-day timespan.

Other atmospheric conditions collected from the meteorological station; such as precipitation, air temperature, relative humidity, and wind speed were used to drive the model. This data was used as input to calculate predictions of soil temperature and net

radiation to be compared with our observed data. Average values during our study for precipitation was 2.55 mmd^{-1}, windspeed was 0.46 ms^{-1}, daytime high temperature was 10.4 ^{o}C, nighttime low temperature was 0.91 ^{o}C, and relative humidity was 64%.

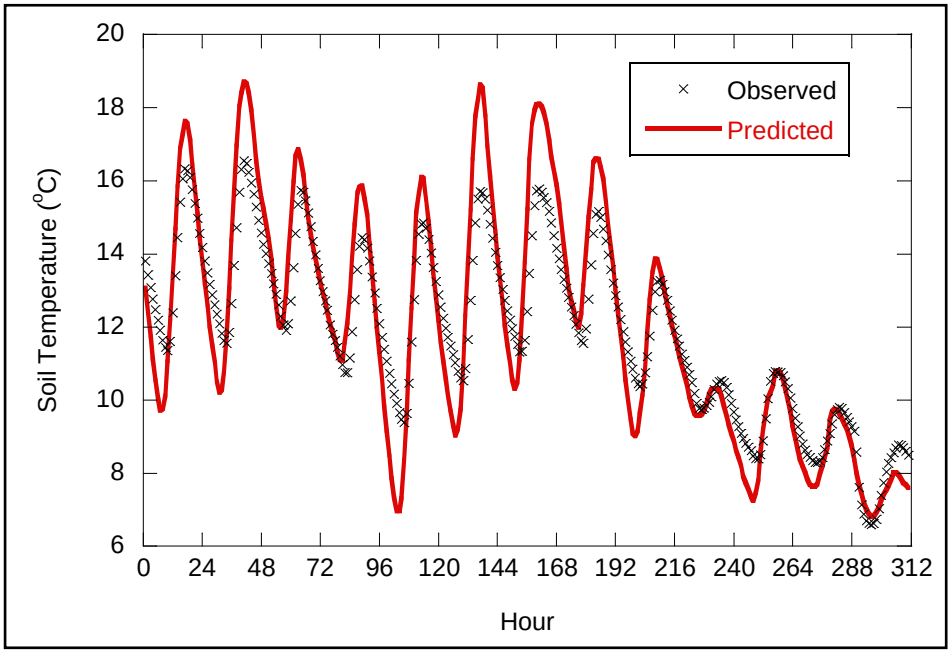

Figure 5. Predicted and observed soil temperature for the Lost Horse Canyon study site.

We used PEST software (Doherty, 2004) as the parameter estimation tool to run the model calibration. Using PEST we found the optimal values of albedo, soil thermal conductivity and aerodynamic roughness that minimized the discrepancies between measured and model estimates of soil temperature and net radiation.

Results of the model run are illustrated in Figures 3 and 4. Predicted values of net radiation match observational data throughout the study. Residual values were consistently around 14 Wm^{-2} with the maximum difference coming at the nighttime minimums. The soil temperature results show most of the error occurs at the daily minimum and maximum values but have an accurate rate of change during heating and cooling stages. Average residual value for the soil temperature is approximately one degree. Overall, the performance of the model is very satisfactory.

6.2. Case study: distributed hydrologic processes

A qualitative evaluation of the behavior of the hydrologic component and its sensitivity to the ecologic components is demonstrated here. Six snapshots of the dynamics of SWE during a model run focused on the calculation of accumulation and melt of snow in Lost Horse Canyon is shown in Figure 6. The snapshots span a period from October 26 to May 15th. Even though the assessment of the model performance is only qualitative at this point, the physically plausible behavior of the model indicates that implementation of the methods in the code is likely correct.

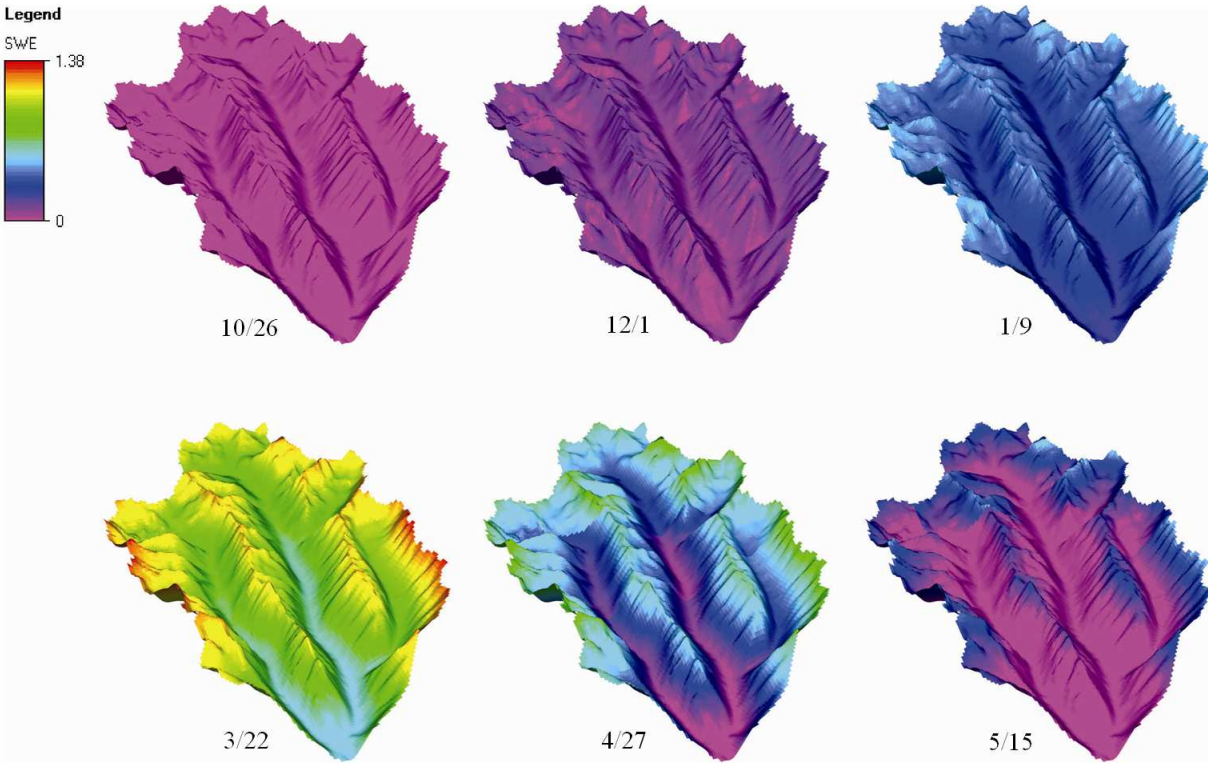

Figure 6.Snow water equivalent (SWE) dynamics for Lost Horse Canyon. The figure shows the calculated SWE for six days during the snow accumulation and snow ablation season. SWE scale is in meters.

Currently a calibration run using SNOTEL and satellite-derived information on snow accumulation and coverage is being performed.

The time-series of SWE at a point midslope in the basin is shown in Figure 7. Three model runs with different initial leaf area indices (LAI) were performed to evaluate the sensitivity that greener vegetation had on the snow dynamics. While one may expect that increased vegetation reduces SWE on the ground by intercepting more snowfall that can be subsequently sublimated, our preliminary results indicate that the shading of trees on snow may be a bigger factor, keeping the snow on the ground lower. We see in the figure that the accumulation of snow during the three scenarios is almost identical, but that the SWE dynamics starts being different once the snowpack peaks and the ablation stage starts. This reinforces the idea that sheltering effect of vegetation may be beneficial to reduce the snowmelt rates, keeping the snowpack longer in the mountain and reducing the risk of flood derived from sudden spring snowmelt-runoff events. Further investigation is needed to conclude what are the actual effects of vegetation on the dynamics of the snowpack, including further validation of the model.

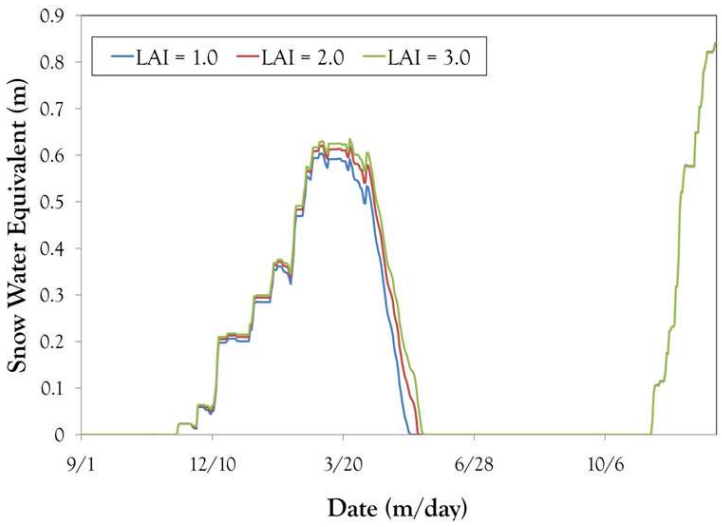

Figure 7.Snow water equivalent (SWE) dynamics for Lost Horse Canyon. The figure shows the calculated SWE for six days during the snow accumulation and snow ablation season. SWE scale is in meters.

7. Conclusions

An ecohydrologic model has been developed and implemented and a experimental site has been set, as originally proposed. The model is currently in its quality assurance stage and so far has demonstrated robustness in reproducing the observations collected for Lost Horse Canyon. A description of the model with further tests is being currently written and is expected to be submitted for publication in Journal of Environmental Software. The model will be made publicly available online after the quality assurance tests have passed.

8. References

Allison, G.B., Gee, G.W., Tyler, S.W., 1994. VADOSE-ZONE TECHNIQUES FOR ESTIMATING GROUNDWATER RECHARGE IN ARID AND SEMIARID REGIONS. Soil Science Society of America Journal, 58(1): 6-14.

Bergkamp, G., 1998. A hierarchical view of the interactions of runoff and infiltration with vegetation and microtopography in semiarid shrublands. Catena, 33(3-4): 201-220.

Cherkauer, K.A., Bowling, L.C., Lettenmaier, D.P., 2003. Variable infiltration capacity cold land process model updates. Global and Planetary Change, 38(1-2): 151-159.

Doherty, J., 2004. PEST: Model-independent parameter estimation: User manual. Watermark Numerical Computing. Brisbane, QLD, Australia.

Eagleson, P.S., 1978. CLIMATE, SOIL, AND VEGETATION .1. INTRODUCTION TO WATER-BALANCE DYNAMICS. Water Resources Research, 14(5): 705-712.

Ivanov, V.Y., Bras, R.L., Vivoni, E.R., 2008. Vegetation-hydrology dynamics in complex terrain of semiarid areas: 1. A mechanistic approach to modeling dynamic feedbacks. Water Resources Research, 44(3).

Laio, F., 2006. A vertically extended stochastic model of soil moisture in the root zone. Water Resources Research, 42(2): 10.

Liang, X., Lettenmaier, D.P., Wood, E.F., Burges, S.J., 1994. A simple hydrologically based model of land-surface water and energy fluxes for general-circulation models. Journal of Geophysical Research-Atmospheres, 99(D7): 14415-14428.

Peters-Lidard, C.D., Zion, M.S., Wood, E.F., 1997. A soil-vegetation-atmosphere transfer scheme for modeling spatially variable water and energy balance processes. J. Geophys. Res., 102.

Peterson, T.J., Argent, R.M., Western, A.W., Chiew, F.H.S., 2009. Multiple stable states in hydrological models: An ecohydrological investigation. Water Resour. Res., 45(3): W03406.

Rodriguez-Iturbe, I., 2000. Ecohydrology: A Hydrologic Perspective of Climate-Soil-Vegetation Dynamics. Water Resour. Res., 36.

Tague, C.L., Band, L.E., 2004. RHESSys: Regional Hydro-Ecologic Simulation System-An Object-Oriented Approach to Spatially Distributed Modeling of Carbon, Water, and Nutrient Cycling. Earth Interactions, 8.

Warrick, A.W., Wierenga, P.J., Pan, L., 1997. Downward water flow through sloping layers in the vadose zone: Analytical solutions for diversions. Journal of Hydrology, 192(1-4): 321-337.

Addressing computational paradigms in modeling the impacts of climate variability on watershed yield

Basic Information

Title:	Addressing computational paradigms in modeling the impacts of climate variability on watershed yield
Project Number:	2010MT217B
Start Date:	3/1/2010
End Date:	2/28/2011
Funding Source:	104B
Congressional District:	At-Large
Research Category:	Climate and Hydrologic Processes
Focus Category:	Hydrology, Models, Methods
Descriptors:	None
Principal Investigators:	Lucy Marshall

Publications

1. Mashamba, A. Bayesian Uncertainty and Sensitivity Analysis for Complex Environmental Models, with Applications in Watershed Management. Montana State University Electronic Dissertation.
2. Mashamba, A., L. A. Marshall. Bayesian Constrained Optimization and Uncertainty Analysis Using Radial Basis Random Local Fitting. The Modeling and Optimization: Theory and Application (MOPTA) conference. Lehigh University, PA. August 2010.

Final Report for USGS 104b Grant: Addressing computational paradigms in modeling the impacts of climate variability on watershed yield

Principal Investigator:

Lucy Marshall, Assistant Professor of Watershed Analysis, Department of Land Resources and Environmental Sciences, Montana State University.

Student Researchers:

Able Mashamba, PhD, Industrial Engineering, Montana State University.

Paddy Stoy, Land Resources and Environmental Sciences, Montana State University.

Abstract

This project was aimed at linking complex conceptualizations of watershed processes with statistical tools for representing uncertainty in models and simulated scenarios. We demonstrate the feasibility of using radial basis approximating functions in Bayesian optimization and uncertainty analysis of the Distributed Hydrology Soil-Vegetation model (DHSVM). DHSVM is a physically based model that models the dynamics of hydrology, vegetation, soil and topographical interactions to predict sediment yields, water balance and channel discharge. The modeling framework enabled scenario analysis related to climatic variability and change. We implemented these methods at the Tenderfoot Creek Experimental Forest (TCEF) in central Montana, an experimental watershed with multi-scale field observations and a complexity of environmental processes due to complex terrain, seasonal variability in climatic forcing, and diversity in physical characteristics affecting watershed processes (vegetation, aspect, topographic convergence/divergence, geology) across nested sub-watersheds.

This project helped support training for two graduate students in field hydrology methods, modeling and statistical analysis. Several presentations and reports disseminated the main scientific findings of this project to the greater scientific community.

1. Introduction

Recent research has illustrated the variability of snowpack accumulation and melt in the Montana region and its links to climate change trends (Gillan et al., 2009; Mote, 2006). The long term availability and reliability of regional water resources may be significantly impacted by potential future changes in climate. Recent studies have highlighted probable impacts on water resources in the western US due to shifting climatic patterns, including increasing variability in precipitation, average earlier spring snowmelt, decreased winter snowpack, and corresponding changes in the timing and availability of streamflow (Barnett et al., 2004; Hamlet et al., 2005; Leung et al., 2004). Given the reliance in the inland northwest region on the availability of water stored as snowpack there is a strong desire to better understand the potential long term impact of climatic variability on local downstream watershed response and water yield. Recent efforts have focused on the use of downscaled projections of temperature, precipitation, and other climatic variables, and have linked these to watershed scale

simulation models. Watershed models can facilitate testing our understanding of the watershed response to climatic variables, whether it is to elucidate more information on the unobservable processes occurring, or to simulate past or future scenarios for better water resource management.

Increased computing power now permits modelers to use more complex physically-based distributed modeling paradigms that have more realistic detail and descriptive power than the traditional lumped or basin averaged approaches (Beven and Binley 1992). These distributed hydrologic models describe the effect of spatial heterogeneity and locality of catchment processes to fully represent sub-basin hydrology. The biggest hurdle facing widespread adoption of process based models is the computational burden associated with model simulations and analysis of model outputs. Physically based models have a large number of parameters and lengthy run times. This burden can inhibit efforts to better understand forecast uncertainties, to undertake scenario analysis, and to understand process sensitivities. Recent efforts in developing model emulators (which are fast statistical surrogates for the simulation model) could help enhance process-based watershed modeling to better undertake different modeling scenarios.

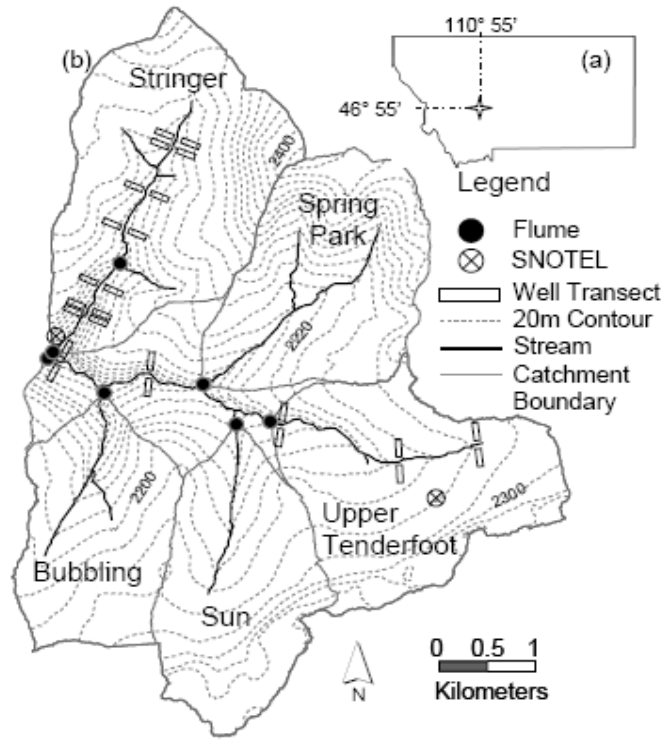

Figure 1. Site location and instrumentation of the TCEF catchment. (a) Catchment location in the Rocky Mountains, MT. (b) Catchment flumes, well transects, and SNOTEL instrumentation locations. Transect extents are not drawn to scale.

2. Overview of Project Objectives

We implemented a physically based model that simulates the dynamics of hydrology, vegetation, soil and topographical interactions to predict sediment yields, water balance and channel discharge (the Distributed Hydrology Soil-Vegetation model, DHSVM). For model optimization and calibration, we explored the use of surrogate models that avoid having to run the 'expensive' model during the many optimization iterations that may be necessary makes automatic calibration feasible. By way of a test case study, we assessed the ability of the calibrated model to implement multiple climate change scenarios and assess their potential impact on available water yield and timing of streamflow events.

Research was conducted at Tenderfoot Creek Experimental Forest (TCEF). The TCEF was established in 1961, and consists of seven gauged watersheds in central Montana (Figure 1). The forest is representative of the vast expanses of lodgepole pine found east of the continental divide and is the only USDA experimental forest formally dedicated to research on subalpine forests on the east slope of the northern Rocky Mountains.

The overall objectives of this project included:

1. To implement a physically based mechanistic watershed model, and develop emulators for efficient model calibration, uncertainty analysis, and other advanced computational tasks.
2. To apply the model to a mountainous watershed to assess the potential impacts of climatic variability on current water resources.

3. Methodology

Our analysis focused on three main activities: development of the process based complex model for describing hydrologic processes (DHSVM), implementation of surrogate models for model calibration and uncertainty analysis, and test application to derived climate scenarios. In addition, student researchers involved in the project continued with field data monitoring and installation of field equipment.

3.1. Model Development and Implementation

The Distributed Hydrology Soil Vegetation model (DHSVM, Doten et al., 2006; Thyer et al., 2004) provides an ideal modeling framework in which to test the utility of advanced mathematical tools and for implementing climate scenario analysis. DHSVM has gained wide acceptance and use in climate change scenario analysis (Leung and Wigmosta 1999), forest management (Storck, Bowling et al. 1998) and land use and land cover studies (Thanapakpawina, Richeyb et al. 2007) as they relate to hydrologic processes. DSHVM has its roots in the hydrology-vegetation model (Wigmosta, Vail et al. 1994) that originally modeled canopy interception, evapotranspiration and snow accumulation and melt, as well as runoff generation via the saturation excess mechanisms.

DHSVM is a fully distributed model that is typically used to represent spatial scales of 10-200 meter grid cells and time steps of 1-24 hours. Model inputs include Geographic Information System (GIS) datasets describing watershed boundaries, meteorology, watershed topography, soils data, vegetation, stream and road networks and initial watershed states (e.g. snow water equivalent and soil water content or storage). The main outputs of DHSVM include channel flow, surface runoff, water balance, sediment yields, evapotranspiration, soil storage, road and channel interception, canopy storage, snow water equivalent, and other snow and soil hydrology. Channel flow can be used to predict flooding or critical low-flows; sediment yields indicate extent of soil erosion and river siltation; higher canopy storage increases evapotranspiration; snow characteristics affect surface runoff and channel wetting and recession patterns; and watershed storage affects base-flow and vegetation.

The DHSVM model for this study was setup to simulate the discharge of the Tenderfoot Creek Experimental Forest (TCEF) watershed. The TCEF watershed encompasses 3693 hectares (9,125 acres) on the Lewis and Clark National Forest in Meagher Country, Montana. The main channel of TCEF, the Tenderfoot Creek, is a headwater tributary of the Missouri River that drains the Little Belt Mountains of central Montana in a westerly direction as shown in Figure 1. The TCEF watershed is heavily forested with few access roads. Lodgepole pine (Pinus contorta) and mixed lodgepole pine with Engelmann spruce (Picea engelmannii) and subalpine fir (Abies lasiocarpa) stands are the dominant forest types and occupy about 95% (3,514 ha) of the experimental forest. The most extensive soil groups are loamy

skeletal, mixed Typic Cryochrepts and clayey, mixed Aquic Cryoboralfs. The watershed has a montane continental climate and the elevation weighted mean annual precipitation of 800 mm. Almost 70% of the annual precipitation falls as snow, which accumulates in the watershed between November and May.

DHSVM was setup for our case study watershed using climate and 10 meter grid Geographic Information System (GIS) data for the Lower Tenderfoot Creek sub-watershed. A single six hourly time-step simulation needed 6 seconds per simulated day on an Intel Core 2 Quad with 2 x 2.83 GHz processor speed and 4MB RAM 64-bit desktop machine.

3.2. Response Surface Modeling and Model Optimization

As with other fully distributed modeling paradigms, there have been few published routines for automatic calibration and predictive uncertainty analysis for the DHSVM model (Yao and Yang 2009). The computational burden of repeated model simulations generally means that automatic calibration routines are considered computationally prohibitive. For instance, we calculated it would take over 25 days to execute 1000 DHSVM calibration iterations using 1 year of observed data at 6-hourly time-steps for the Lower Tenderfoot Creek sub-basin at 10 meter spatial resolution on an Intel Core 2 Quad with 2 x 2.83 GHz processor speed and 4MB RAM 64-bit desktop machine. It is thus desirable to reduce the automated calibration time required for such computationally expensive models. Other than parallel processing, substituting expensive model runs with a faster fitted response surface model (RSM) is a feasible way of reducing long automatic calibration times. Response surface methodology (RSM) is a collection of statistical and mathematical techniques useful for developing, improving, and optimizing processes through the exploration of relationships between several explanatory variables and one or more response variables (Myers and Montgomery 1995). In this approach, a suitable measure of model error or performance is computed for a carefully selected and limited set of parameter values (design points) using the expensive actual model simulations. From the resulting parameter-residual set, RSM approximating functions, such as the radial basis, kriging or multiple linear regression models, can be developed to replace further expensive model evaluations.

To the best of our knowledge there is no published research that uses RSM fitting for automated calibration and uncertainty assessment of the DHSVM model or of other distributed hydrologic models in general. Thus the main objective of this project task was to use radial basis function fitting for Bayesian calibration and uncertainty analysis of the case study DHSVM model. The purpose of this is to demonstrate that RSM fitting could be successfully used for automated calibration of DHSVM or other similar distributed models. While a Bayesian MCMC algorithm is used for uncertainty analysis, other uncertainty routines may be used. A secondary objective was to perform automated sensitivity analysis of the parameters affecting stream channel discharge. As mentioned above, sensitivity analysis is useful for pruning insensitive parameters so as to minimize the fitting dimensions in the RSM model.

DHSVM parameters that can be calibrated are related to catchment soil properties, vegetation properties, and climatic constants such as rainfall and snowmelt leaf area index multipliers, and snow threshold and water capacity. Most of the approximated parameter values were set based on literature

research and knowledge of the case study watershed. As DHSVM is actively used in hydrologic modeling research, thirteen unique parameters were identified as most sensitive to discharge. Note that depending on the number of soil and vegetation types identified in the model application the number of actual parameters to be optimized would increase. Of these thirteen parameters, five were specifically considered for automatic calibration by (Yao and Yang 2009). Thus, for this case study, lateral hydraulic conductivity, exponential decrease, field capacity, and minimum stomatal resistance were selected for automatic calibration while all other parameters were calibrated manually. These parameters generally are expected to control the characteristics of the wetting and recession periods of the hydrograph.These parameters would have different values for different soil and vegetation types. To minimize the total number of distributed parameters for automatic calibration only the two most significant soils and vegetation types were automatically adjusted for. Hence effectively 8 distinct distributed parameters were used to automatically calibrate the DHSVM for discharge.

Modeling Optimization Methodology

Current research that uses RSM methods within hydrologic modeling has been in model calibration and, more usefully, uncertainty analysis of computationally time expensive models (Bliznyuk et al., 2008; Regis and Shoemaker, 2004; Regis and Shoemaker, 2007). The RSM method as applied to Bayesian optimization and uncertainty analysis within modeling can be summarized in the following steps (Bliznyuk et al., 2008; Buhmann, 2003; Regis and Shoemaker, 2004; Regis and Shoemaker, 2007; Ye et al., 2000);

1. Calibrate the model using a global optimization routine (Evolutionary Algorithm, Dynamically Dimensioned Search, Greedy search, etc) and observed data, y, so as to approximate the HPD region, the near optimum region of the parameters of the model (Bliznyuk et al., 2008).
2. Sample some RSM design points, x, at which the response or objective function of the expensive model is evaluated often using symmetric Latin hypercube sampling design, SLHD, from the HPD region for unbiased sampling (Regis and Shoemaker, 2004; Ye et al., 2000).
3. Evaluate the objective function on the selected RSM design points.
4. Fit a second order, or nth order, least squares multiple linear regression function or a radial basis function to the best responses of a subset of the RSM design points evaluated in 3. As much as all, or just the minimum nearest neighbors may be used for fitting.
5. Run a Bayesian MCMC optimization and uncertainty (or any other optimization) routine, evaluating on the fitted function for N number of cycles.
6. Evaluate the actual response for the final Bayesian MCMC parameter set after the N cycles in 5 and append to the RSM design points.
7. Repeat 4 to 6 until there are no further systematic improvements to the responses being evaluated. Bayesian MCMC convergence to the optimum.
8. Use the parameter values drawn after Bayesian convergence to characterize the uncertainty and optimality of the model.

In this study, we used a radial basis function (RBF) for approximating the response surface of the DHSVM model (Bliznyuk et al., 2008; Buhmann, 2003; Mugunthan et al., 2005; Regis and Shoemaker, 2005; Regis

and Shoemaker, 2004; Regis and Shoemaker, 2007). Other methods often applied may include multiple linear regression (Regis and Shoemaker, 2005), kriging (Davis and Ierapetritou, 2009) and the more involved neural networks (Zorzettoa et al., 2001). A radial basis function (RBF), $S_n(x)$, is a real-valued function whose value depends only on the distance x from the origin or from some given point (called a center).Given n distinct points $x_1, \ldots, x_n \in R^d$ whose function values $f(x_1), \ldots, f(x_n)$, are known, the RBF then is an interpolant of the form as in Equation (1).

$$S_n(x) = \sum_{i=1}^{k} \omega_i \, \phi(\|x - x_i\|) + p(x), \; x \in R^d \qquad (1)$$

where $\|.\|$ is the Euclidean norm, $\omega_i \in R$ for i = 1, …, n, $p \in \Pi_{\mathrm{m}}^{\mathrm{d}}$ (a linear space of polynomials in d variables of degree less than or equal to m), and ϕ may take the forms $\phi(r) = r^2 \log r, r > 0$ and $\phi(0) = 0$ (thin plate spline), $\phi(r) = r^3$ (cubic), $\phi(r) = \sqrt{r^2 + \gamma^2}$ (multi-quadratic), or $\phi(r) = e^{-\gamma r^2}$, $r \geq 0$ and γ is a positive constant (Gaussian) (Regis and Shoemaker 2004). The ω_i is a weight showing how the Euclidean distance for point x_i from a sampled point x contributes to the approximation of the response at point x. The tail of the radial basis function, $p(x)$, is often linear with respect to the explanatory variables, but higher order polynomials could also be used. The thin plate spline and the quadratic functions have been reported to have good fitting performance for applications to complex models (Bliznyuk et al., 2008; Buhmann, 2003; Regis and Shoemaker, 2005; Regis and Shoemaker, 2004). Further detail on how to obtain the ω_i and $p(x)$ radial basis coefficients from a system of linear algebra matrices can be obtained from recent RSM literature (Bliznyuk et al., 2008; Regis and Shoemaker, 2005; Regis and Shoemaker, 2004; Regis and Shoemaker, 2007).

The radial basis function approximation used as the surrogate model for DHSVM in the Bayesian MCMC calibration and uncertainty analysis in this research depends heavily on a fitting approach called the random local fitting (RLF) algorithm (summarized in Figure 2). RLF improves the fitting performance of previously evaluated parameter sets (design points), compared to other local or global fitting methods. This is because RLF starts by global fitting, which helps in locating the region of global optimality, before eventually fitting to a local region, which improves the fitting. Initially the sampling scheme involves symmetric Latin hypercube sampling of 300 design points. The lower shaded region of Figure 2 shows how these 300 parameter design points are firstly evaluated (simulated) using DHSVM (Route 1). The RLF algorithm uses the exact likelihoods calculated from the DSHVM runs and fits random local points into the approximating radial basis function RSM model. Route 2 represents subsequent updates to the RSM model during MCMC chains by use of new neighborhood points. When not updating the RSM, Route 3 is used to approximate the Bayesian likelihood. The top region of Figure 2 represents the Bayesian MCMC calibration and uncertainty assessment routine. The specific details of the scheme used for this case study are beyond the scope of this report, but may be found in Mashamba, 2010.

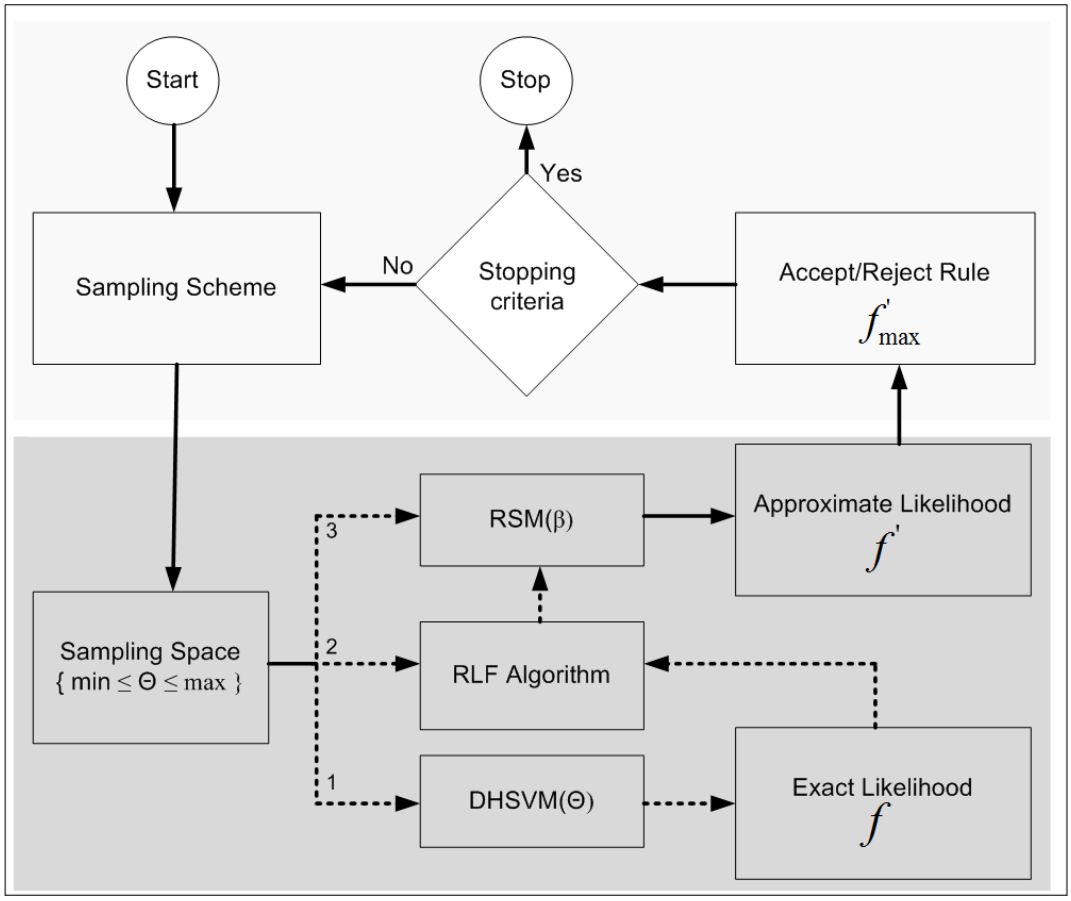

Figure 2. Flowchart of model optimization and uncertainty analysis methodology via use of Response Surface Model (RSM).

Modeling Results

Due to the high (10 meter) spatial resolution used for the DHSVM model and the 6-hour time step, we limited the calibration period to 7 months (March – September 2008), so as to minimize the calibration time while capturing the spring runoff period and hydrologic dynamics of the entire year. A further two years, 2006 and 2007, were used for model assessment. The 300 DHSVM runs used for fitting the likelihood during MCMC calibration took about 4.46 days, running at 6 seconds per day. By comparison, 20000 fitted runs using the response surface model only take about 3 minutes on average. Typically, 30 meter grids are considered reasonable resolution for distributed modeling (VanShaar, Haddeland et al. 2002). Using 10 meter resolution for this research was however desirable in connection with further work using the same model and given the total catchment size.

Figure 3 shows three hydrographs of Tenderfoot Creek during the analysis period, April – September 2008. The observed, simulated (manual calibration) and simulated (automated calibration) hydrographs show relatively very low base flow followed by snow-melt driven peak flow from early May to early July. Automated Bayesian MCMC calibration on a fitted radial basis response function improved the simulated discharge from a Nash Sutcliffe Efficiency (NSE) (Nash and Sutcliffe, 1970) of 0.83, after

manual calibration, to 0.89. The high prior knowledge of the TCEF watershed coupled to the uncomplicated features of the hydrographs enabled a manual calibration with an NSE of 0.83, which could be considered satisfactory (Eckhardt et al., 2005). Nonetheless, the optimized simulation shows improved recession characteristics (with a faster falling recession period) and a slower wetting up period.

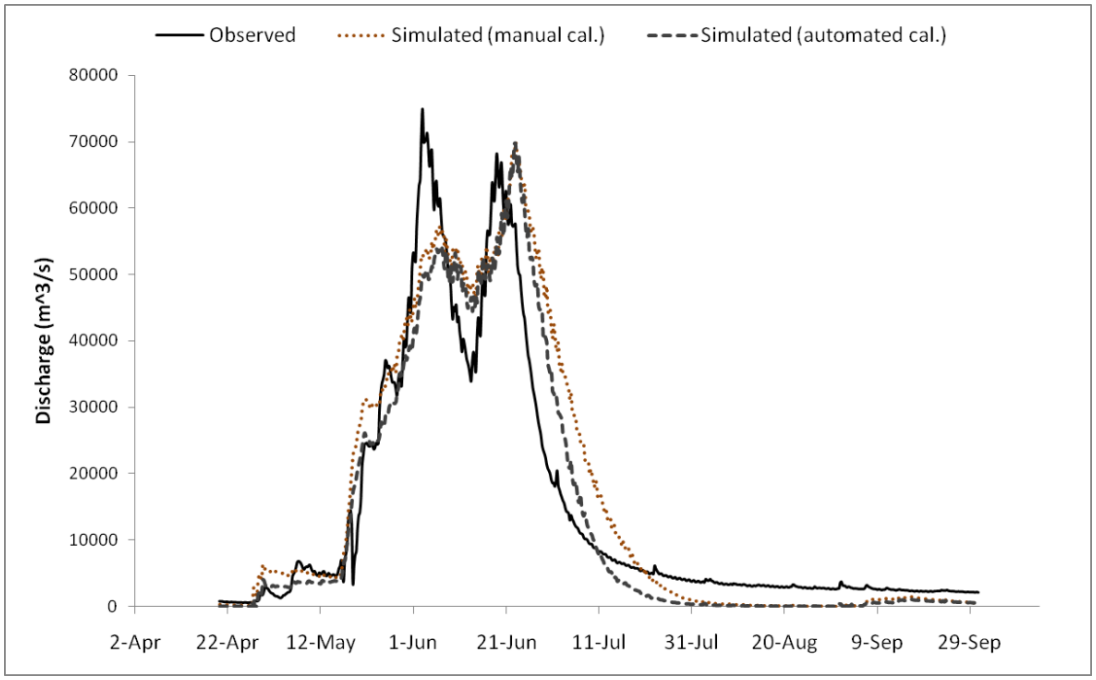

Figure 3: Observed Vs simulated discharge for Tenderfoot Creek for the year 2008Figure 4 shows the observed, simulated (manual calibration) and simulated (automated calibration) hydrographs for the Tenderfoot Creek from March to September of 2006 (4a) and 2007(4b) validation periods. The 3 peak flows correspond to the May-June snowmelt periods for the two years.

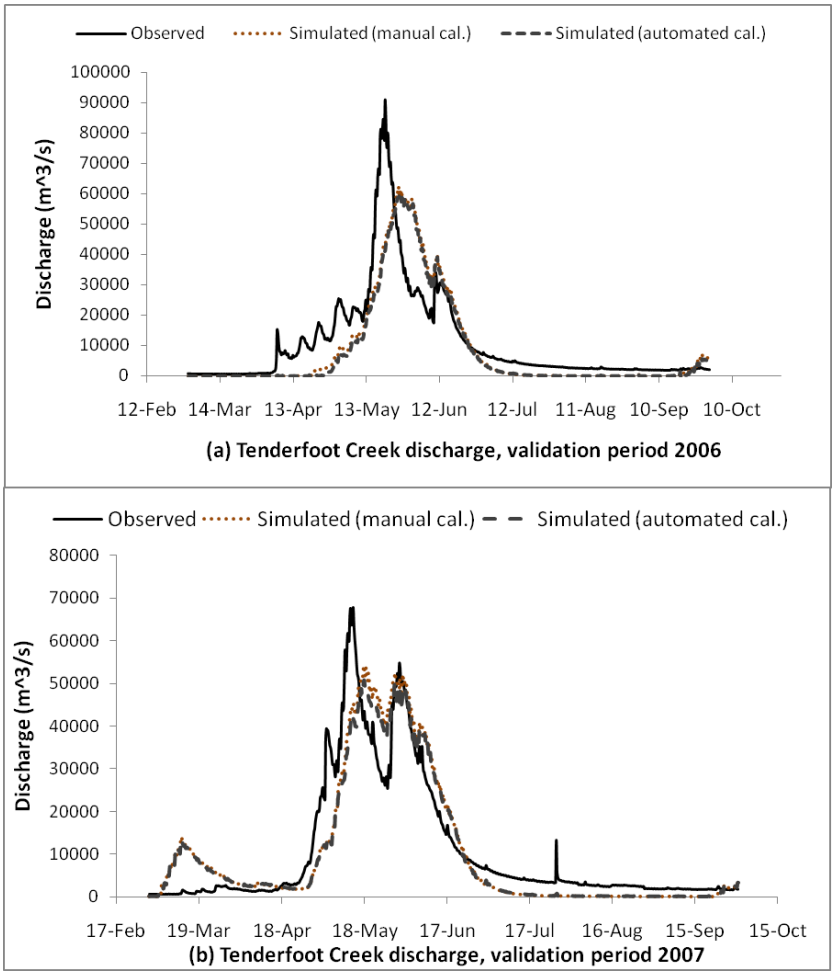

Figure 4: Observed Vs simulated discharge for Tenderfoot Creek for the validation period 2006-2007

The NSE numbers for the simulated discharge after manual and automated calibration are 0.796 and 0.765 respectively. This supports the view that automated calibration slightly over-fitted the model parameters to the calibration period in Figure 3, and thus performing slightly poorer over other periods. Over-fitting of model parameters to a calibration period can occur regardless of the calibration method. The model assessment supports the view that the model calibration and robustness would be improved by a multi-year calibration.

shows the optimization and uncertainty assessment results summary of the 8 sensitive parameters that were studied. All the other DHSVM parameters were manually calibrated from existing knowledge of the TCEF watershed.

results were compiled from the converged last half (10000 iterations) of the MCMC chain. The standard deviations and 95% confidence intervals (CI) represent the posterior distribution of the 'Bayesian MCMC on fitted radial basis function' scheme (Figure 2). The parameter posterior distributions are relatively narrow, indicating the likely limited uncertainty and high sensitivity of he selected parameters.

Parameter	95% CI		Std dev	Mean	Optimal
	Min				
Lateral conductivity for loam soil, K_6	0.141578	0.141579	3.55E-06	0.141579	0.141582
Exponential decrease for loam soil, ExD_6	1.046850	1.046854	9.94E-05	1.046852	1.046937
Field capacity for loam soil, FC_6	0.295196	0.295201	1.21E-04	0.295199	0.295306
Lateral conductivity for silty clay soil, K_11	0.019528	0.019529	1.85E-05	0.019528	0.019512
Exponential decrease for silty clay soil, ExD_11	1.888893	1.888934	1.04E-03	1.888914	1.888701
Field capacity for silty clay soil, FC_11	0.413995	0.414003	2.01E-04	0.413999	0.413700
Minimum stomatal resistance for evergreen needle leaf, Rmin_1	379.98574	380.02519	1.01E+00	380.00546	381.63633
Minimum stomatal resistance for grassland, Rmin_10	236.05224	236.07605	6.07E-01	236.06415	236.28526

Table 1: Uncertainty and calibration summary

3.3. Scenario Analysis

A variety of recent research efforts have investigated the use of watershed scale simulation models for predicting the impacts of climate change on watershed yield, including those using dynamically downscaled and statistically downscaled climate change scenarios (e.g. (Fowler et al., 2007; Groves et al., 2008). In particular, DHSVM has shown to be useful for assessing potential climate change related impacts (Leung and Mark, 1999). We implemented a simple case study as a test of the feasibility of the model for scenario analysis. Using downscaled General Circulation Model (GCM) projections we tested the impact of potential future changes in precipitation and temperature on model simulations at TCEF.

Data was obtained from the World Climate Research Programme's (WCRP's) Coupled Model Intercomparison Project phase 3 (CMIP3) multi-model dataset. Available data consisted of bias-corrected and spatially downscaled climate projections derived from CMIP3 data and served at: http://gdo-dcp.ucllnl.org/downscaled_cmip3_projections/, described by Maurer et al (2007). Multiple projections were used to represent the uncertainty in derived climatic scenarios (10 models in total, Table 2). We obtained monthly estimates of precipitation and temperature at roughly a 12km resolution

for our site for the year 2099 under the IPCC's A1b scenario which describes a linear increase in CO2 concentration until stabilization in 2100 at 720 ppm.

Modeling Group, Country	WCRP CMIP3 I.D.
Bjerknes Centre for Climate Research	BCCR-BCM2.0
Canadian Centre for Climate Modeling & Analysis	CGCM3.1 (T47)
Meteo-France / Centre National de Recherches Meteorologiques, France	CNRM-CM3
CSIRO Atmospheric Research, Australia	CSIRO-Mk3.0
US Dept. of Commerce / NOAA / Geophysical Fluid Dynamics Laboratory, USA	GFDL-CM2.0
NASA / Goddard Institute for Space Studies, USA	GISS-ER
Institute for Numerical Mathematics, Russia	INM-CM3.0
Institut Pierre Simon Laplace, France	IPSL-CM4
Meteorological Institute of the University of Bonn, Meteorological Research Institute of KMA	ECHO-G
National Center for Atmospheric Research, USA	CCSM3

Table 2. Downscaled GCM data used in scenario analysis.

We used simple regression analysis to bias-correct our data for elevation effects. GCM data for the current water year were compared to available TCEF observations to correct for these potential biases under future derived scenarios. We disaggregated monthly GCM variables to 6 hourly data using current water year precipitation and temperature dynamics. Data were then used as inputs to our calibrated DHSVM model framework.

Via our 10 GCM derived scenarios, we were able to characterize the uncertainty in our model projections. Figure 5 shows the range of GCM simulations for the year 2099, along with the base DHSVM simulation for the 2008 water year (as derived under Section 3.2).

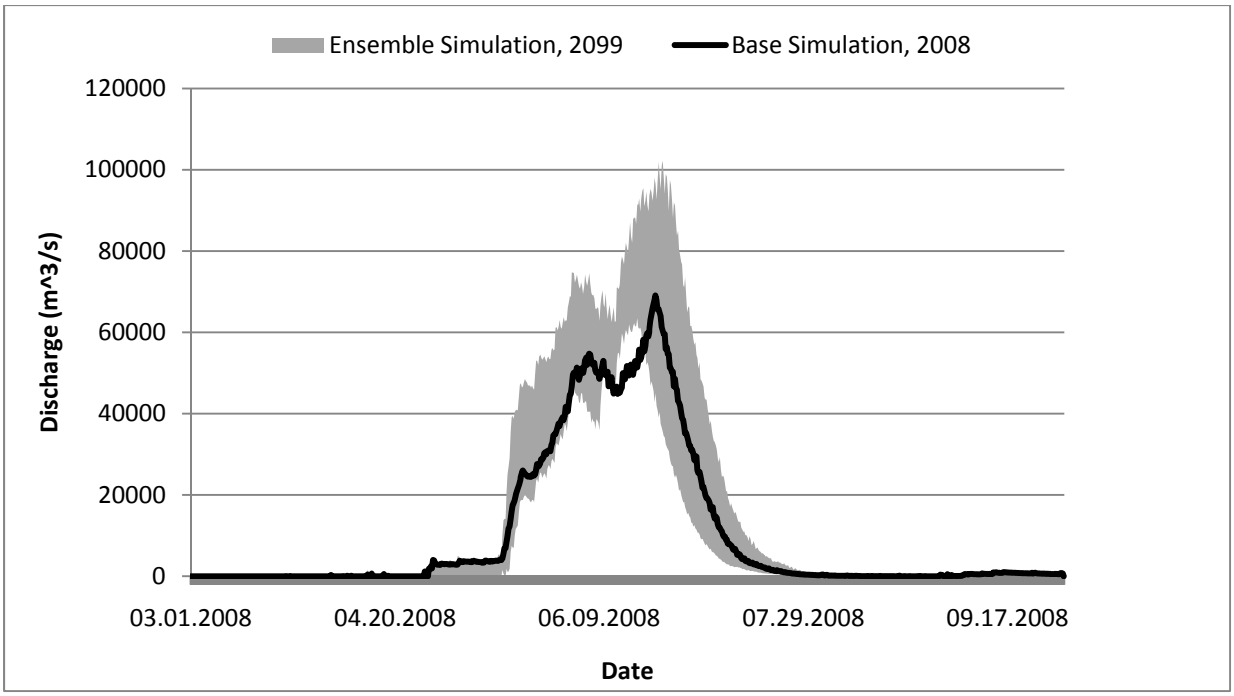

Figure 5. Downscaled GCM-DHSVM simulations (2099) and original DHSVM base simulation (2008).

In general, our climate scenarios supported earlier studies which have found increasing variability in precipitation, and average earlier spring snowmelt. In particular, GCM simulations which show lower input precipitation resulted in earlier spring runoff (Figure 5). Simulations with higher precipitation amounts showed a variable pattern to snowmelt, with increasing rates of early runoff, but similar timing for maximum snowmelt runoff. In general, we observed highly variable precipitation rates depending on the GCM used to derive model inputs, suggesting that the uncertainty associated with input scenarios exceeds that of the hydrologic model uncertainty.

It is recognized that this analysis provides an initial testing of the feasibility of the model for assessing the impacts of future climate variability on watershed yield and hydrologic response. The simple bias-corrections made here warrant further analysis, as do the data disaggregation methods. However, the methods developed here provide a foundation on which further research questions can be addressed. In particular, we aim to examine the model simulations beyond streamflow outputs under these climate scenarios, including impacts on vegetation dynamics and sediment yield.

3.4. Hydrologic Data Collection

This project additionally helped support student researchers to undertake field visits and monitor instrumentation. Under this project, continuing data monitoring included:

Stream flow

Monitored discharge at the outlets of 7 nested watersheds
Monitored real time specific conductance and temperature at 8 locations and installed 4 new specific conductance probes

Wells and piezometers

Installed 12 new wells and monitored existing wells (for real-time water level data collection)

Field Work

Two field trips were conducted per month over the period December 2010- February 2011 to download water content (WC) probes and flume specific conductance probes. Multiple WC probes and flume data loggers failed due to extreme cold and battery issues, and student researchers assisted in maintaining and repairing field equipment during this time.

4. Results and Conclusions

Overall, the project was successful and productive from three main viewpoints: scientific merit and furthering scientific understanding, graduate student training, and disseminating results via publications and presentations. These areas are detailed following.

4.1. Scientific Merit

The methods developed under this project fill a critical niche in the computational tools available for model optimization and uncertainty analysis, and the corresponding utility of complex models for predicting the impacts of climatic variability on available water resources. We implemented multi-tiered activities focused on: implementation of a physically based watershed model specified with multiple data types; development of surrogate models that can efficiently characterize watershed model response and model uncertainty; undertaking scenario analysis to better understand the probability of different hydrologic responses due to changes in climate. Understanding the potential impact of climate variability on regional watersheds is critical to long term planning for water resources management, as climate variability and change has the potential to have severe consequences for watershed ecosystems. The scenarios and tools implemented in this project will help provide a protocol in which similar modeling exercises may be carried out and may consequently provide a platform in which to address potential climatic impacts at other mountainous regional watersheds.

It is expected that the application of these methods will ultimately enhance the computational efficiency and widespread adoption of more complex models to help resolve water resource problems. While this project emphasized model implementation and development of statistical methods rather than the case study application, ultimately the tools developed under this project will enhance other modeling applications including those related to water resources management, assessing the impacts of land use change, and real time forecasting.

While the research undertaken in this project has been focused at a local test-site, the methods and models developed are broad reaching and could be applied to other watersheds. This research should have significant impact for better understanding of the link between model reliability and predictive uncertainty in streamflow forecasting for mountainous snow driven watersheds, and for conceptualizing watershed response based on topographic structure.

4.2. Student Training

Two students received training and support under this project. Able Mashamba recently completed a PhD degree in the department of Industrial Engineering at Montana State University and was advised by

Dr Lucy Marshall. Able successfully defended his PhD thesis, and is now pursuing publication of the work undertaken in this project. Additionally, Paddy Stoy undertook field work and helped collate data related to the model implementation. Paddy recently commenced a Master's degree in the department of Land Resources and Environmental Sciences at MSU and will continue to pursue research questions at the study site.

4.3. Publications

Several journal papers and presentations resulted out of this project:

Mashamba, A., L. Marshall. 2010. A case study examining factors affecting the performance of response surface modeling during Bayesian optimization and uncertainty analysis of hydrologic models. Environmental Modeling and Software, Undergoing Revisions.

Mashamba, A. Bayesian Uncertainty and Sensitivity Analysis for Complex Environmental Models, with Applications in Watershed Management. Montana State University Electronic Dissertation.

Mashamba, A., L. A. Marshall. Bayesian Constrained Optimization and Uncertainty Analysis Using Radial Basis Random Local Fitting. The Modeling and Optimization: Theory and Application (MOPTA) conference. Lehigh University, PA. August 2010.

Acknowledgements

We acknowledge the modeling groups, the Program for Climate Model Diagnosis and Intercomparison (PCMDI) and the WCRP's Working Group on Coupled Modelling (WGCM) for their roles in making available the WCRP CMIP3 multi-model dataset. Support of this dataset is provided by the Office of Science, U.S. Department of Energy.

References Cited

Barnett, T. et al., 2004. The Effects of Climate Change on Water Resources in the West: Introduction and Overview. Climatic Change, 62(1): 1-11.

Beven, K. and Binley, A.M., 1992. The future of distributed models: Model calibration and uncertainty prediction. Hydrological Processes, 6: 279-298.

Bliznyuk, N. et al., 2008. Bayesian Calibration and Uncertainty Analysis for Computationally Expensive Models Using Optimization and Radial Basis Function Approximation. Journal of Computational and Graphical Statistics, 17(2): 270–294.

Buhmann, M.D., 2003. Radial Basis Functions: Theory and Implementations. Cambridge Monographs on Applied and Computational Mathematics. Cambridge Unversity Press, 272 pp.

Davis, E. and Ierapetritou, M., 2009. A kriging-based approach to MINLP containing black-box models and noise. Industrial and Engineering Chemistry Research, 47(16): 6101-6125.

Doten, C.O., Bowling, L.C., Lanini, J.S., Maurer, E.P. and Lettenmaier, D.P., 2006. A spatially distributed model for the dynamic prediction of sediment erosion and transport in mountainous forested watersheds. Water Resour. Res., 42(4): 1-15.

Eckhardt, K., Fohrer, N. and Frede, H.-G., 2005. Automatic model calibration. Hydrological Processes, 19(3): 651-658.

Fowler, H.J., Blenkinsop, S. and Tebaldi, C., 2007. Linking climate change modelling to impacts studies: recent advances in downscaling techniques for hydrological modelling. International Journal of Climatology, 27(12): 1547-1578.

Gillan, B.J., Harper, J.T. and Moore, J.N., 2009. Timing of Present and Future Snowmelt from High Elevations in Northwest Montana. Water Resources Research, In Press.

Groves, D.G., Yates, D. and Tebaldi, C., 2008. Developing and applying uncertain global climate change projections for regional water management planning. Water Resour. Res., 44.

Hamlet, A.F., Mote, P.W., Clark, M.P. and Lettenmaier, D.P., 2005. Effects of Temperature and Precipitation Variability on Snowpack Trends in the Western United States&#042. Journal of Climate, 18(21): 4545-4561.

Leung, L.R. and Mark, S.W., 1999. Potential climate change impacts on mountain watersheds in the Pacific Northwest. Journal of the American Water Resources Association, 35(6): 1463-1471.

Leung, L.R. et al., 2004. Mid-Century Ensemble Regional Climate Change Scenarios for the Western United States. Climatic Change, 62(1): 75-113.

Leung, L. R. and M. S. Wigmosta (1999). "Potential climate change impacts on mountain watersheds in the pacific northwest." Journal of American Water Resources Association 35(5): 1463–1471.

Mashamba, A. Bayesian Uncertainty and Sensitivity Analysis for Complex Environmental Models, with Applications in Watershed Management. Montana State University Electronic Dissertation.

Maurer, E. P., L. Brekke, T. Pruitt, and P. B. Duffy (2007), 'Fine-resolution climate projections enhance regional climate change impact studies', Eos Trans. AGU, 88(47), 504.

Mote, P.W., 2006. Climate-Driven Variability and Trends in Mountain Snowpack in Western North America. Journal of Climate, 19(23): 6209-6220.

Mugunthan, P., Shoemaker, C.A. and Regis, R.G., 2005. Comparison of Function Approximation, Heuristic and Derivative-Based Methods for Automatic Calibration of Computationally Expensive Groundwater

Bioremediation Models. Water Resour. Res., 41(W11427).

Nash, J.E.a. and Sutcliffe, J.V., 1970. River flow forecasting through conceptual models part I — A discussion of principles. Journal of Hydrology, 10(3): 282–290.

Regis, R.G. and Shoemaker, C.A., 2005. Constrained global optimization using radial basis functions. Journal of Global Optimization, 31: 153-171.

Regis, R.G.a. and Shoemaker, C.A., 2004. Local Function Approximation in Evolutionary Algorithms for the Optimization of Costly Functions. IEEE Transactions On Evolutionary Computation, 8(5): 490-505.

Regis, R.G.a. and Shoemaker, C.A., 2007. Improved strategies for radial basis function methods for global optimization. Journal of Global Optimization, 37: 113–135.

Storck, P., L. Bowling, et al. (1998). "Application of a GIS-based distributed hydrology model for prediction of forest harvest effects on peak stream flow in the Pacific Northwest." Hydrological Processes 12(6): 889–904.

Thanapakpawina, P., J. Richeyb, et al. (2007). "Effects of landuse change on the hydrologic regime of the Mae Chaem river basin, NW Thailand " Journal of Hydrology 334(1-2): 215-230.

Thyer, M., Beckers, J., Spittlehouse, D., Alila, Y. and Winkler, R., 2004. Diagnosing a distributed hydrologic model for two high-elevation forested catchments based on detailed stand- and basin-scale data. Water Resour. Res., 40(1): 1-20.

Wigmosta, M. S., L. W. a. Vail, et al. (1994). "A distributed hydrology-vegetation model for complex terrain." Water Resour. Res. 30(6): 1665-1679.

Yao, C. and Z. Yang (2009). "Parameters optimization on DHSVM model based on a genetic algorithm." Frontiers of Earth Science in China 3(3): 374-380.

Ye, K.Q., Li, W.a. and Sudjianto, A., 2000. Algorithmic Construction of Orthogonal Symmetric Latin Hypercube Designs. Journal of Statistical Plannning and Inference, 90: 145-159.

Zorzettoa, L.F.M., Maciel Filho, R. and Wolf-Macielb, M.R., 2001. Processing modelling development through artificial neural networks and hybrid models Computers and Chemical Engineering, 24(2-7): 1355-1360.

Assessing hydrologic response to channel reconfiguration: Science to inform the restoration process, Silver Bow Creek, Montana

Basic Information

Title:	Assessing hydrologic response to channel reconfiguration: Science to inform the restoration process, Silver Bow Creek, Montana
Project Number:	2010MT220B
Start Date:	3/1/2010
End Date:	2/27/2011
Funding Source:	104B
Congressional District:	At-large
Research Category:	Ground-water Flow and Transport
Focus Category:	Groundwater, Hydrology, Geomorphological Processes
Descriptors:	None
Principal Investigators:	Geoffrey Poole, Brian Leonard McGlynn

Publication

1. Kurt-Mason, Seth - 2010 M.S. Thesis: "Hydrologic response to channel reconfiguration on Silver Bow Creek: Science to inform the restoration process." Land Resources and Environmental Sciences; Montana State University, Bozeman, MT

Assessing hydrologic response to channel reconfiguration: Science to inform the restoration process, Silver Bow Creek, Montana.

Final Report

Prepared for:

United States Geological Survey

and

Montana Water Center
101 Huffman Building
Montana State University
Bozeman, MT 59717

Prepared by:

Seth J.K. Mason
Montana State University
334 Leon Johnson Hall, PO Box 173120
Bozeman, MT 59717-3120

March 1, 2011

Table of Contents

I. USGS 104(b) Grant Information 1
Summary 1
II. Final Report 2
1. Problem Statement 2
2. Methods 3
3. Principle Findings 4
3.1 Hydrogeomorphic Comparisons 4
3.2 Geostatistical Comparisons 6
3.3 Stream Tracer Experiments 10
3.4 Hydrologic Gains and Losses 12
4. Significance 13
5. Conclusion 14
References Cited 15
III. Tracking 16
Student Support 16
Citations 16
Notable Awards and Achievements 17

I. USGS 104(b) Grant Information

Project Title: Assessing hydrologic response to channel reconfiguration: Science to inform the restoration process, Silver Bow Creek, Montana.
Project Type: Research
Focus Categories: GW, HYDROL, GEOMOR
Research Category: Groundwater Flow and Transport
Keywords: Groundwater-surface water interactions, restoration, hydrology, geomorphology
Start Date: March 1, 2010
End Date: February 28, 2011
Principal Investigator: Geoffrey Poole, Department of Land Resources and Environmental Sciences, Montana State University, Bozeman, MT, (406) 994-5564, gpoole@montana.edu
Co-Principal Investigator: Brian McGlynn, Department of Land Resources and Environmental Sciences, Montana State University, Bozeman, MT, (406) 994-7690, bmcglynn@montana.edu
Congressional District: At large

Summary

The real-dollar, social, and aesthetic value gained from stream restoration through increased quality of use by wildlife, anglers, agricultural users, and municipalities is inextricably tied to the stream's ecological, biogeochemical, and hydrologic functioning. Interactions between the physical structure of streambeds and the hydraulic characteristics of overlying surface-waters govern storage and exchange processes responsible for transporting water and solutes among the stream, riparian zone, and alluvial aquifer. Such hydrologic transport and retention mechanisms create vertical, lateral and longitudinal linkages among the surface and subsurface biotic communities distributed along stream corridors. The timing, direction, and magnitude of these interactions influence habitat for fish, and the food web upon which fish depend by buffering temperature extremes and influencing the stream's assimilation capacity for excess nutrients, heavy metals, and other pollutants. Assessment of hydrologic behavior along the Silver Bow Creek corridor elucidated the relationships between restoration actions, channel morphology, and hydrologic storage and exchange processes. Restoration increased advective transport times by increasing sinuosity, decreasing channel slope, and introducing frequent slow-moving pools. Observed decreases in transient storage following restoration coincided with reduced spatial complexity in velocity fields and increased hydraulic efficiency in designed channels. Thus, the realignment of degraded stream channels is not guaranteed to immediately increase rates of biogeochemical cycling, temperature buffering, etc. that are associated with transient storage processes. We suggest that enhanced understanding of the primary controls on hydrologic behavior along restored streambeds will lead to more efficient and cost effective restoration approaches, while providing new avenues for improving long-term habitat quality, water quality, ecological and economic value of restored rivers and streams across the region.

II. Final Report

1. Problem Statement

Complex interactions between the physical structure of the streambed and the hydraulic characteristics of overlying surface-waters govern storage and exchange processes responsible for transporting water and solutes among the stream, riparian zone, and alluvial aquifer [*Brunke and Gonser*, 1997; *Poole et al.*, 2008]. Importantly, these interactions may influence water temperature extremes [*Arrigoni et al.*, 2008] and the in-stream retention and transformation of pollutants [*Findlay and Sobczak*, 1996] (e.g., nitrate, pesticides, pharmaceuticals, etc.). Exchanges between the stream channel, surface dead-zones, hyporheic zones, and groundwater exist at multiple spatial (centimeter to kilometer) and temporal (seconds to months) scales and are most prevalent where channel morphology is complex (e.g., high sinuosity, frequent side channels and mid-channel bars, well-formed pool/riffle sequences, and variable channel slope). Degraded streams tend to have simplified channel patterns and therefore exhibit reduced rates of exchange, yielding associated losses in habitat complexity, depressed capacity for buffering against temperature and discharge fluctuations, and cumulative or synergistic effects from downstream advection of pollutants. Thus, we hypothesize that channel response to dynamic hydrologic exchange, transport, and storage mechanisms along the streambed and across the floodplain are critical controls on restoration's success.

Despite well-documented linkages between individual channel structures/features, hydrologic retention, water quality, and in-stream habitat quality, the influence of reach-scale channel reconfiguration on the complex interactions between streambed structure, channel hydraulics, and hydrologic behavior are not well characterized. Therefore, designing restoration efforts to enhance hydrologic retention across a range of spatial and temporal scales remains difficult.

Here, we report measured changes in channel hydrology and solute transport resulting from a massive stream restoration project on Silver Bow Creek (SBC), Montana (Figure 1)**.** We predicted that channel realignment would alter streambed topography, velocity fields and, consequently, patterns of water and solute movement. Specifically, we anticipated that: (1) measures of hydrogeomorphic channel complexity would be greater in restored channel segments at a range of spatial scales, resulting in (2) lower advective transport velocities and increased transient storage. We tested these predictions by conducting hydrogeomorphic surveys and stream tracer experiments on multiple channel segments prior to and following realignment of the stream channel.

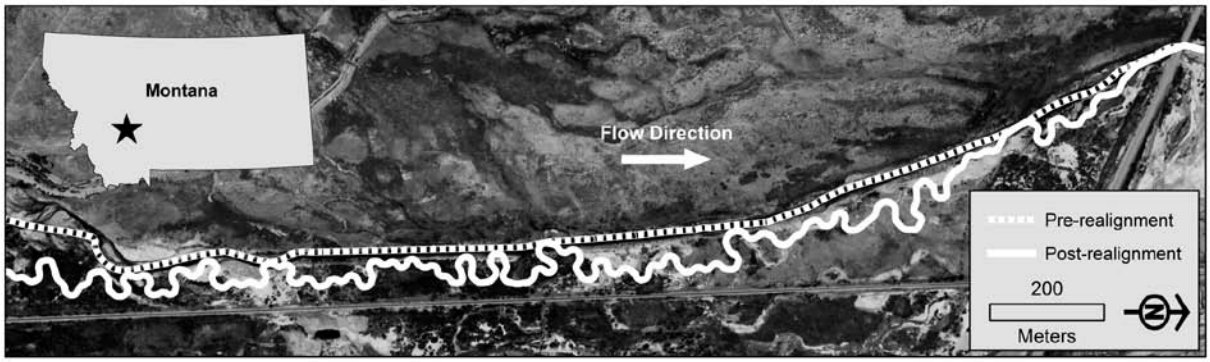

Figure 1. Silver Bow Creek study area

2. Methods

We conducted geomorphic and hydraulic comparisons of pre- and post-realignment channel segments on SBC. Digitization of thalweg lines from aerial photos and planform channel design plans within a GIS identified changes in channel sinuosity following restoration. Comparison of pre-restoration floodplain surveys and design plans for restored channels identified changes in reach-averaged channel slope. A StreamPro (Teledyne RD Instruments, Poway, California, USA) acoustic Doppler current profiler (ADCP) mounted on a floating platform measured water velocity fields and vectors of stream depth. We operated the instrument in the field by attaching a long aluminum handle to the downstream side of the floating platform and pushing it at a constant rate both perpendicular to the main direction of flow (cross-sectional profiles) and along the channel thalweg (longitudinal profiles). Direct comparison of ADCP data collected from 27 randomly selected cross-sections on each of two adjacent channel segments—one pre-realignment and one post-realignment—during summer baseflow conditions ($Q \approx 800$ l/s) identified changes in channel width, cross-sectional area, hydraulic depth, wetted perimeter, hydraulic radius, and Froude number. Frequency distributions of stream depth collected along the channel thalweg and along individual cross-sections were calculated by summing the lengths of streambed that fell within various depth ranges and dividing by the total measured thalweg or cross-sectional length. Frequency distributions of stream velocity were calculated by summing the measured longitudinal and cross-sectional profile area fractions falling within various velocity ranges and dividing by the total measured profile area. Aggregation of cross-sectional data collected along a given channel segment yielded a single distribution.

We investigated spatial patterns of velocity and depth data through application of geostatistical methods. We used experimental semivariograms to explore the spatial organization of measured depth and velocity values at three flow states: 800 l/s, 1100 l/s, and 1400 l/s. Data collected from 400 m long pre- and post-realignment channel segments produced longitudinal velocity and depth semivariograms. Aggregation of semivariance values calculated at various lag distances from multiple cross-sections within a single channel segment yielded cross-sectional semivariograms. We quantified differences in spatial structure by fitting spherical covariance model structures or pure nugget effect model structures to the data. We related each component of the semivariogram (as described by model parameters) back to the physical organization of stream topography or velocity fields.

We conducted 58 stream tracer experiments on pre-realignment (n=35) and post-realignment (n=23) study reaches during the summer and fall of 2009. We selected reach lengths for tracer experiments such that RTDs could be compared across similar channel distances, valley distances, and average in-channel residence times. To carry out RTD comparisons, we calculated modal stream channel velocity, modal down-valley velocity (down-valley travel rate, excluding sinuosity), and an index of transient storage. We calculated the modal stream channel velocity as the time to RTD peak divided by the thalweg distance between the injection and observation points. We calculated the modal down-valley velocity as the time to RTD peak divided by the straight line distance between the injection and observation points. The relationship between the time to RTD peak and the time at which 99% of the recovered tracer mass passed by the solute observation point provided an index of transient storage. We used ANCOVA methods to assess the significance of observed differences in transport characteristics between pre- and post-realignment data sets for channel distance, valley distance, and residence time comparisons. We tested four model structures (single-mean, two-means, parallel-lines, and separate-lines) for each between-group comparison and used F-tests to identify the most parsimonious model.

Connections between floodplain groundwater systems and the stream channel directly influence the magnitude and timing of stream discharge observed at various points along the stream corridor. We used modified synoptic discharge measurement techniques and conservative tracer recovery estimates to assess the timing and magnitude of gross gains and losses to and from the alluvial aquifer along our study reaches [see *Covino and McGlynn*, 2007; *Harvey and Wagner*, 2000; *Payn*, 2009]. Gross losses of stream water indicated long spatio-temporal exchange and storage mechanisms not readily apparent from RTD analysis alone.

3. Principle Findings

3.1 Hydrogeomorphic Comparisons

Comparisons of channel geometry and frequency distributions of stream depth and stream velocity for pre- and post-realignment channels highlighted the distinct changes in longitudinal and cross-sectional structure evident in Figure 2. Shifts in cross-sectional channel geometry are presented in Figure 3. Generally, restoration produced narrower, deeper channels. Prior to restoration, the distribution of longitudinal stream depths was unimodal and very peaked, reflecting the relatively planar morphology at the channel-unit scale (10^0 to 10^1 meters) (Figure 4c). Conversely, restoration produced bimodal longitudinal depth distributions that exhibited a larger overall variance. The bimodal behavior of these distributions coincided with the distinct differences in the depth of engineered riffle-run sequences and pools. Cross-sectional depth distributions mirrored those collected along the channel thalweg (Figure 4d).

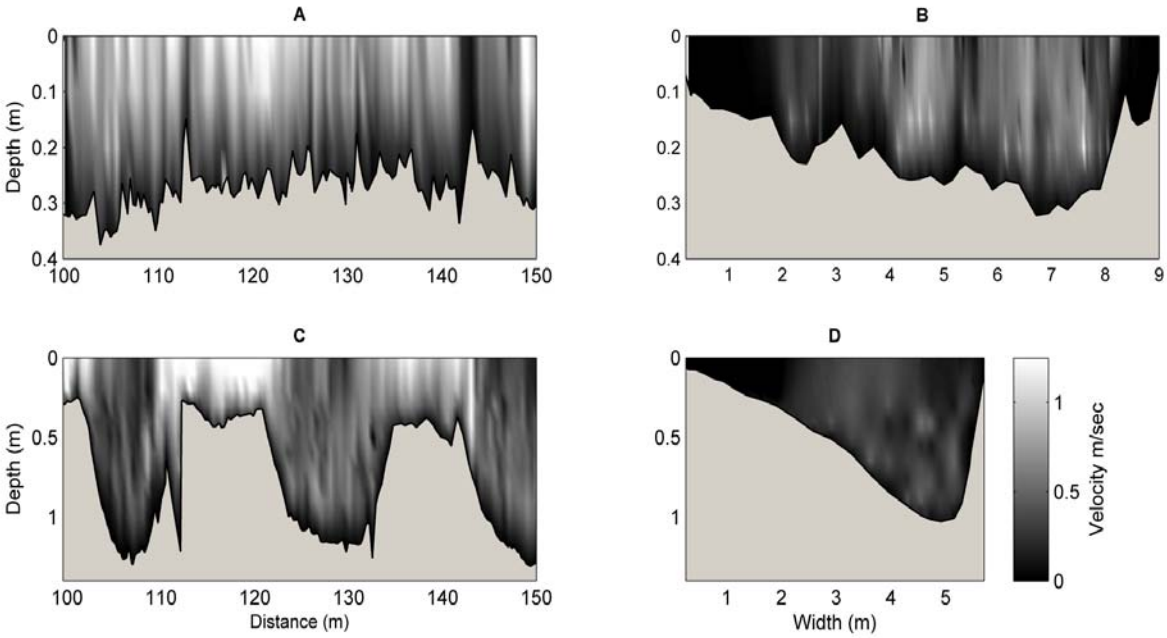

Figure 2. Pre-realignment velocity and depth profiles collected (A) along the channel thalweg and (B) from a representative cross-section. Post-realignment velocity and depth profiles collected (C) along the channel thalweg and (D) from a representative cross-section. Continuous velocity surfaces were kriged with the spatial covariance structures defined by a best-fit spherical model for each data set's experimental semivariogram. Depth data was linearly interpolated between measured points. Vertical axes are scaled for clarity.

We observed correlations between differences in channel form and the characteristics of velocity distributions. In pre-realignment reaches, longitudinal and cross-sectional distributions of channel velocities were near Gaussian (Figure 4a and 5c). Post-realignment longitudinal velocity distributions exhibited a lower mean and a characteristic positive skew that reflected the large fraction of stream volume contained in deep pools. Post-realignment cross-sectional velocity distributions did not exhibit this characteristic, which likely resulted from a random sampling strategy that selected a greater number of riffles and runs than pools. Variability in stream discharge did not affect general conclusions reached from comparisons of velocity distributions. While mean velocity values increased with discharge in both pre- and post-realignment channels, the patterns of differences in mean, variance, and skewness illustrated in Figure 4 remained relatively unchanged.

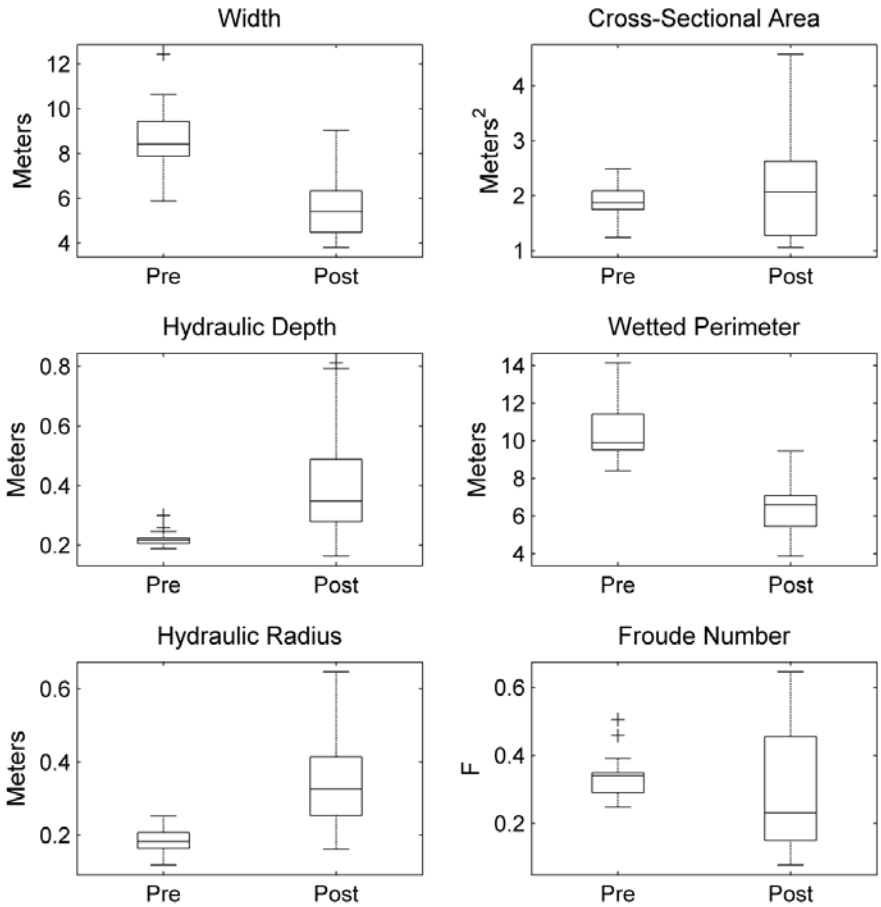

Figure 3. Characterization of cross-sectional channel geometry. Data was collected from pre- and post-realignment stream channels during summer baseflow conditions (n=27 pre-restoration cross-sectional profiles and 27 post-restoration profiles).

3.2 Geostatistical Comparisons

Experimental semivariograms for depth and velocity profiles elucidated differences in hydrogeomorphic structure at a range of spatial scales (Figure 5). We fit a pure nugget effect model to the longitudinal stream depth semivariance data from pre-realignment channels (Table 1). The very low sill, reflecting a low overall variability in depth, was corroborated by depth frequency distributions (Figure 4c). We fit a spherical covariance model structure to the longitudinal depth semivariance data from post-realignment reaches (Table 1). The large sill coincided with the introduction of riffle/pool/run morphology. The greatest semivariance in longitudinal depth in these channels occurred at thalweg distances approximating the average spacing of riffle/run sequences and pools (15-20 m). Restoration increased the semivariance in stream depth at the cannel-unit scale but decreased calculated semivariance values for lag distances between 0 and 10 cm ($\gamma = 1.13*10^{-4}$) when compared to pre-realignment channels ($\gamma = 3.41*10^{-4}$), indicating that more fine-scale variability existed in channel bedform structure before restoration took place. We expect that the semivariogram-derived differences in channel bed roughness are conservative because large absolute changes in depth occurring in the relatively

smooth transition zones between channel units likely produced a significant portion of the observed semivariance at lag distances less than one meter in restored channels. Cross-sectional depth semivariograms displayed similar characteristics to their longitudinal counterparts (Figure 5h). Pre-realignment data exhibited a low sill that reflected the low overall variance in cross-sectional stream depth in these channels (Table 1). Post-realignment data exhibited a much higher sill and a range value that approximated the average width of restored channels (≈ 4m).

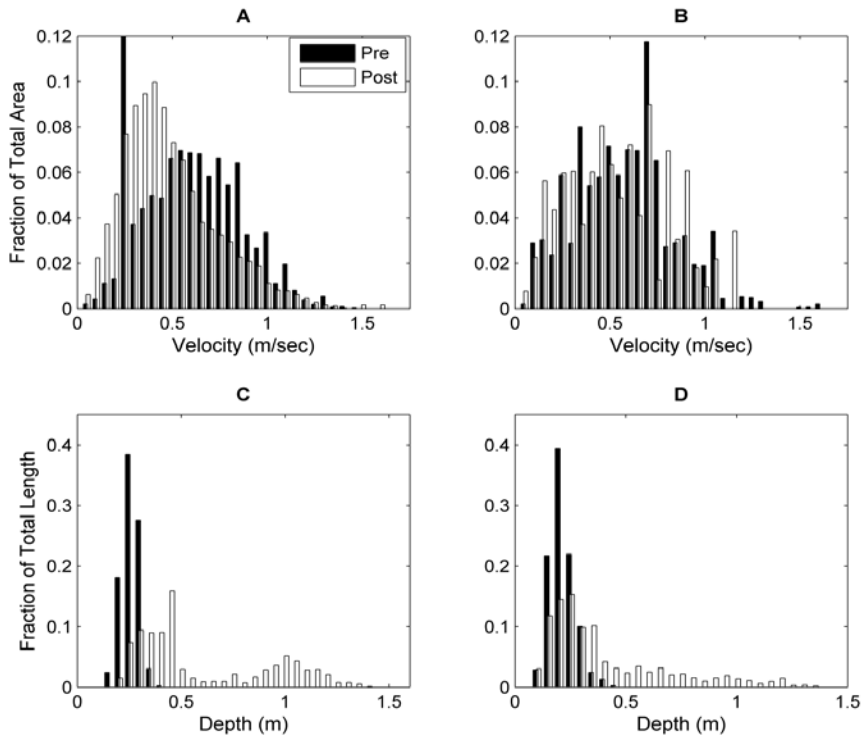

Figure 4. Frequency distributions of (A) longitudinal velocity, (B) cross-sectional velocity, (C) longitudinal depth, and (D) cross-sectional depth collected during summer baseflow conditions. Cross-sectional distributions represent aggregated data from 12 pre-realignment cross-sections and 12 post-realignment cross-sections.

Spatial patterns illustrated by velocity and depth semivariograms for both pre- and post-realignment channels indicated strong relationships between velocity fields and the characteristics of streambed topography (Figure 5). We fit longitudinal velocity semivariograms from both pre- and post-realignment channels with spherical covariance model structures (Table 2). The sill characterizing data from both channels was similar across all three observed flow states. Prior to restoration, longitudinal velocity fields exhibited a large nugget effect and a range that increased with discharge. Longitudinal velocity fields in post-realignment channels exhibited range values that remained relatively constant and approximately equal to average channel unit spacing across all three flow states. Semivariograms and modeling results suggested that spatial correlation existed in longitudinal velocity fields at a coarser scale in post-realignment reaches than in pre-realignment reaches. Differences in cross-sectional semivariograms were similar to those observed in longitudinal data structures (Figure 5). Both

pre- and post-realignment cross-sectional data were fit with spherical covariance model structures (Table 3). Pre-realignment cross-sectional data exhibited a higher nugget and larger sill than post-realignment cross-sections at low flow, indicating spatial correlation existed across larger distances following restoration. The respective values of these parameters for pre- and post- channels converged as discharge increased.

Table 1. Semivariance modeling results for longitudinal and cross-sectional depth profiles collected along 400 m of channel thalweg and 27 randomly selected cross-sections on both pre- and post-realignment channel segments.

Profile Type	Channel Type	Covariance Model	nugget g(h)	range (m)	sill g(h)
Longitudinal	Pre	Nugget	-	-	0.003
	Post	Spherical	0.0006	11.326	0.124
Cross-Sectional	Pre	Nugget	-	-	0.003
	Post	Spherical	0	3.953	0.075

Table 2. Semivariance modeling results for longitudinal velocity profiles collected at three flow states.

Channel Type	Q (l/sec)	Model	nugget g(h)	range (m)	sill g(h)
Pre	800	Spherical	0.043	2.127	0.060
	1100	Spherical	0.048	5.107	0.058
	1400	Spherical	0.053	8.032	0.065
Post	800	Spherical	0.015	16.531	0.056
	1100	Spherical	0.032	12.671	0.070
	1400	Spherical	0.023	15.241	0.070

Table 3. Semivariance modeling results for aggregated cross-sectional velocity data collected at three flow states.

Channel Type	Q (l/sec)	# of x-sections	Model	nugget g(h)	range (m)	sill g(h)
Pre	800	12	Spherical	0.060	4.995	0.077
	1100	8	Spherical	0.044	4.724	0.078
	1400	12	Spherical	0.038	3.711	0.070
Post	800	12	Spherical	0.013	1.477	0.042
	1100	8	Spherical	0.030	3.275	0.060
	1400	12	Spherical	0.042	4.935	0.098

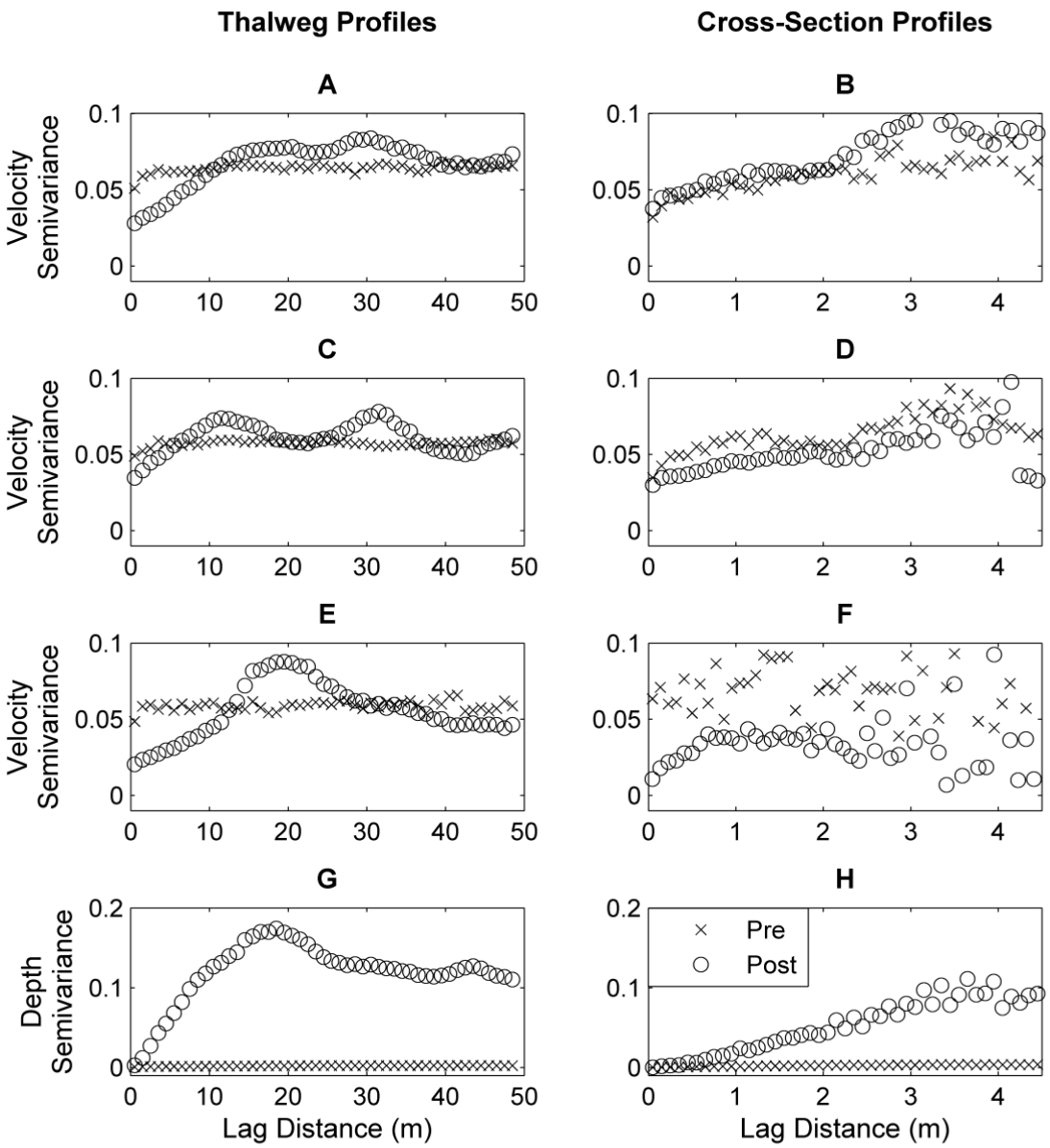

Figure 5. Experimental semivariograms of longitudinal (A) and cross-sectional (B) velocity observed at Q=1400 l/s; longitudinal (C) and cross-sectional (D) velocity observed at Q=1000 l/s; longitudinal (E) and cross sectional (F) velocity observed at Q=800 l/s; longitudinal (G) and cross-sectional (H) depth.

3.3 Stream Tracer Experiments

Direct comparisons of hydrologic RTDs provided insights into changes in hydrologic transport and retention resulting from restoration for a given channel length, a given valley length, and a given channel residence time. We plotted modal stream velocity against discharge for 58 stream tracer experiments and grouped data by channel type (Figure 6a). A parallel lines model adequately characterized trends in the data (Table 4). The model estimated modal stream velocity to be 0.11 m/sec greater in pre-realignment channels across all observed flow states. This difference is illustrated in Figure 6b by plotting individual RTDs from each channel type that characterize solute transport over a given thalweg distance at a given discharge. A similar approach compared differences in hydrologic transport over a given valley length. We plotted modal valley velocity against discharge for the same 58 stream tracer experiments (Figure 7a). A parallel lines model adequately characterized trends in the data (Table 4). The model estimated modal valley velocity to be 0.27 m/sec greater in pre-realignment channels at any given discharge. Plots of individual RTDs for each channel type that characterized solute transport over a given valley length at a given discharge further illustrated these differences (Figure 7b). We assessed differences in RTD tailing by plotting the modal hydrologic residence time against the time at which 99% of the recovered tracer mass passed by the solute observation point for all 58 tracer experiments (Figure 8a). This comparison yielded an index of transient storage reflecting the persistence of RTD tailing as a function of the average solute residence time in the stream channel. A separate lines model best described the differences in the data trends (Table 4).

Table 4. Results from ANCOVA comparisons of solute transport data

ANCOVA Comparison	Test	F-stat	p-value	Selected Model	Channel Type	Intercept	Slope
Discharge vs. Modal Stream Velocity	Same Line vs. Parallel Lines	220.26	≈ 0	Parallel Lines	Pre	0.345	0.0002
					Post	0.236	0.0002
Discharge vs. Modal Valley Velocity	Same Line vs. Parallel Lines	816.4	≈ 0	Parallel Lines	Pre	0.317	0.0002
					Post	0.052	0.0002
Mean Transport Time vs. Time to 99% Mass Recovery	Parallel Lines vs. Separate Lines	28.62	4.48E-07	Separate Lines	Pre	4.832	1.326
					Post	6.516	1.139

The interactive effect in this model suggested that transient storage affected hydrologic RTDs differently in pre- vs. post-realignment channels. The modeled slope that best characterized pre-realignment data was greater than the slope that best characterized post-realignment data, indicating a more pronounced tailing effect in the RTD of pre-restoration channels. This indicates that, for every unit of time water resided in the channel, there were higher rates of transient storage in the pre-restoration channel than the post-restoration channel. Plots of RTDs from pre- and post-realignment channels that exhibited the same median solute residence time in the stream channel illustrated these differences in tailing behavior (Figure 8b).

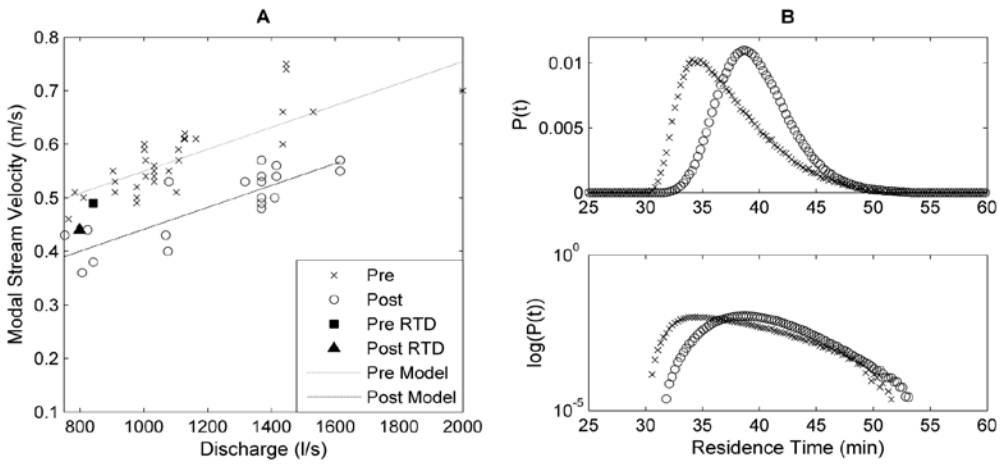

Figure 6. (A) Average solute transport time calculated for the length of the thalweg between the upstream solute injection point and the downstream observation point in pre- and post- channels across a range of flow states. (B) Pre- and post-realignment RTDs observed after injected solute traversed approximately 1000 m of thalweg length in a pre-realignment and a post-realignment channel segment during baseflow conditions. RTDs are displayed in normal and semi-log space.

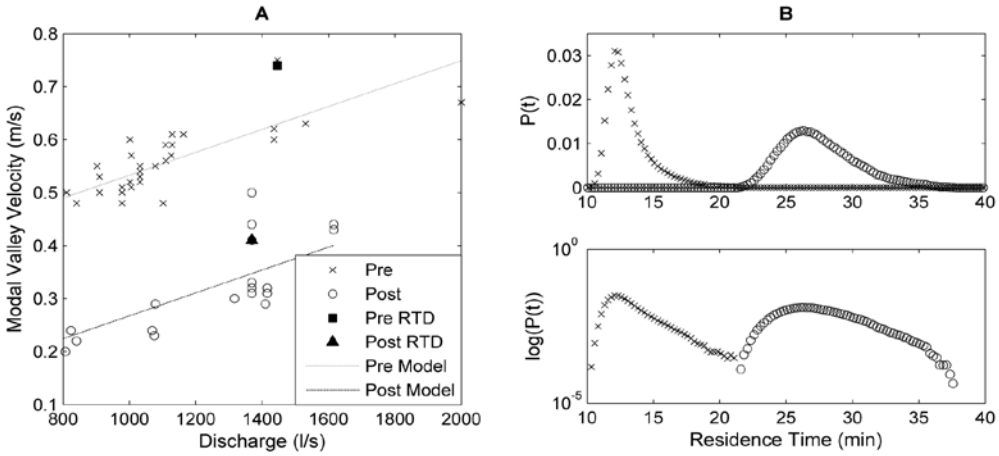

Figure 7. (A) Average solute transport times calculated for the straight-line distance between the upstream solute injection point and the downstream observation point in pre- and post- channels across a range of flow states. (B) Pre- and post-realignment RTDs observed after injected solute traversed approximately 500 m of valley length in a pre-realignment and a post-realignment channel segment. RTDs are displayed in normal and semi-log space.

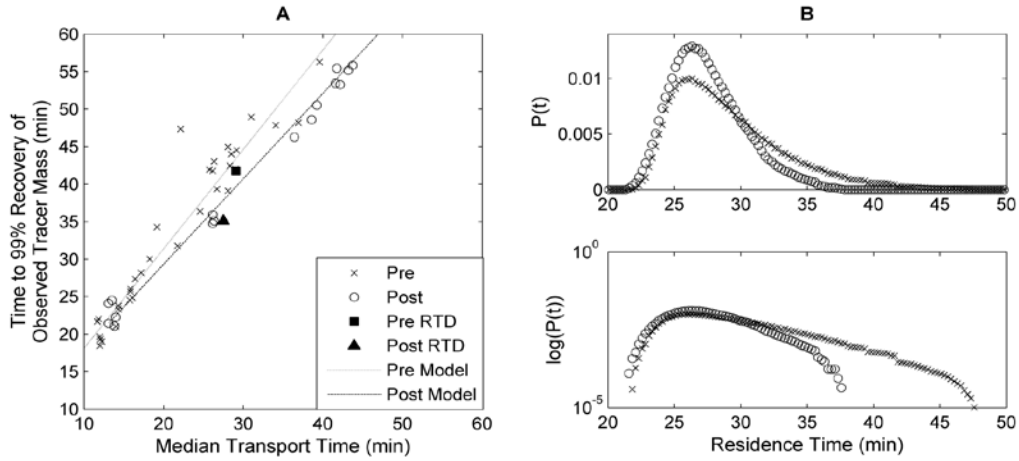

Figure 8. (A) Index of transient storage as a function of average channel residence time in pre- and post-realignment channels. (B) RTDs observed after approximately 27 minutes of downstream transport in a pre-realignment and a post-realignment channel segment. RTDs are displayed in normal and semi-log space.

3.4 Hydrologic Gains and Losses

Measurement of gross stream gains and losses provided a means for assessing concurrent hydrologic exchanges not easily resolved using RTD analysis alone. A Mann-Whitney U-test showed the median hydrologic loss on pre-realignment reaches (88%, n=35) was significantly different than median loss on post-realignment reaches (97%, n=23) (two-sided p-value = 0.022). Thus, a greater fraction of stream water in pre-realignment reaches interacted with the alluvial aquifer at spatio-temporal scales greater than that of individual tracer experiments on the selected study segments on SBC. Our methodology occasionally produced mass recovery estimates greater than 100% (Figure 9). This likely resulted from the compounded error of individual discharge measurements at the upstream and downstream ends of a given reach and from small errors in tracer concentration measurements recorded by individual probes. Alternatively, incomplete solute mixing due to channel geometry and hydraulics may have produced some erroneous measurements; although field observation of fluorescent dye tracers indicated adequate horizontal and vertical mixing over the reach lengths typical to our experiments.

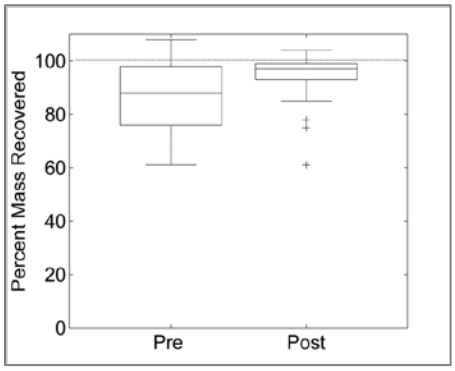

Figure 10. Comparison of mass recovery during tracer experiments on pre-realignment (n=35) and post-realignment (n=23) study reaches. Values greater than 100% (dashed line) result from compounded discharge and tracer concentration measurement error.

4. Significance

The strong relationships observed between semivariograms of channel bed structure and velocity fields (Figure 5) indicated a tight coupling between streambed topography to velocity field complexity. Legleiter [2007] utilized a similar geostatistical approach to identify correlations between stage, streambed topography and the organization of overlying velocity fields. The shallow channel and high bed-roughness present in pre-realignment channels produced velocity fields with very short correlation lengths (Figure 2), while increases in stage and discharge reduced the relative size of roughness elements and increased spatial correlation lengths (Figure 5). Conversely, the regular channel-unit spacing, a hydraulically efficient channel geometry, and reduced bedform roughness present in post-realignment channels strengthened spatial correlations in velocity fields up to the scale approximating the average spacing of pool-riffle sequences (Figure 5). Thus, our findings support Legleiter's conclusion that channel geometry—specifically, stream depth relative to the height of roughness elements in the streambed—is a fundamental control on velocity field structure. It follows from this result that: 1) the physical structure of the streambed is a critical control on the arrangement of surface-water flowpaths, and 2) multi-scale alteration of streambed topography via stream restoration is likely an important mechanism influencing patterns of water and solute movement.

It is probable that elements of channel design generated the reduced RTD tailing observed in restored channels. Channel realignment re-oriented the flow to a primarily downstream direction over relatively smooth bed surfaces, which produced nearly laminar velocity fields characterized by long spatial correlation lengths. Conversely, the presence of large (relative to channel depth) roughness elements in shallow pre-realignment channels significantly shortened velocity field spatial correlation lengths (Figure 5). Thus, enhanced exchange with transient storage zones associated with streambed roughness elements may have produced some portion of the observed differences in RTD tailing behavior. The relationship between bed structure and transient storage is reported by others. A meta-analysis of tracer experiments conducted on streams across the U.S. showed transient storage was positively correlated with channel friction factor, a measure to bed roughness [*Harvey and Wagner*, 2000]. Roughness can affect transport dynamics by creating opportunities for solute storage in boundary layer vortices and eddies located behind large elements in the streambed. Irregular bed surfaces also facilitate advective pumping mechanisms that lead to surface-subsurface exchange [*Wörman et al.*, 2002]. Tracer mass recovery results on SBC lend weight to this conjecture, suggesting that a greater degree channel-aquifer exchanges existed prior to restoration. The reduction of streambed slope and reduced bedform topographic variability in restored channels likely weakened hydraulic head gradients at the bedform scale, limiting the frequency of hyporheic flow along short spatio-temporal subsurface flowpaths. Although the introduction of large pool-riffle sequences and meander bends likely produced an abundance of longer hyporheic flowpaths, the methodological sensitivities typical to our experiments and the ratio of stream discharge to the volume/rate of water conveyed along these flowpaths likely made their presence and influence on RTD tailing difficult to detect. Reductions in the size of the stream-streambed interface (i.e. wetted perimeter) relative to the volume of water conveyed through the stream channel at any given time and/or changes in the hydraulic properties of the streambed may have further reduced rates of exchange between the channel and subsurface storage zones.

Our results may indicate pathways for improving the effect of stream restoration on hydrologic transport processes. Channel realignment on SBC increased advective transport times along a given channel length and a given downstream-valley length. These increases in water and solute retention should benefit biotic uptake of solutes, but decreased bed roughness and velocity fields exhibiting long correlation lengths are apt to at least partially offset the beneficial effects of slower advective velocities by limiting transient storage. Incorporation of roughness elements that produce turbulent velocity fields into channel designs that inherently slow water velocity through increased sinuosity, decreased channel slope, and enhanced channel-unit variability could further enhance contact time between solutes, bio-reactive streambed sediments, and microbial assemblages in surface-water storage zones. Such approaches could, thus, provide additional ecological benefits over traditional channel realignment techniques that frequently aim to enhance hydraulic conveyance by making channels narrower, deeper, and by reducing the roughness of the streambed.

5. Conclusion

Restoration of stream segments on SBC slowed advective transport velocities for a given stream length and across a given valley length by reducing average streambed gradient and increasing stream length. Restoration was more efficient at retarding transport across a given valley length than a given stream length, indicating that adding sinuosity to stream channels is an important component of restoration design where slowing the advective transport of water and solutes along the stream corridor is a stated or implied goal. Despite increased water and solute retention due to changes in advective velocities, channel restoration reduced the influence of transient storage on hydrologic residence time distributions in our study reaches. Our findings caution that the benefits of increased residence time associated with enhanced sinuosity and pool frequency may be offset to some extent by a loss in surface-zone storage and near-channel hyporheic exchange in restored channels. Considering stream-bed complexity and the hydrologic effects of channel roughness and topographic heterogeneity may be a critical but commonly overlooked factor in the design of those stream restoration projects that incorporate channel realignment.

References Cited

Arrigoni, A. S., et al. (2008), Buffered, lagged, or cooled? Disentangling hyporheic influences on temperature cycles in stream channels, *Water Resources Research*, *44*, W09418.

Brunke, M., and T. Gonser (1997), The ecological significance of exchange processes between rivers and groundwater, *Freshwater Biology*, *37*(1), 1-33.

Covino, T. P., and B. L. McGlynn (2007), Stream gains and losses across a mountain-to-valley transition: Impacts on watershed hydrology and stream water chemistry, *Water Resources Research*, *43* (W10431).

Findlay, S., and W. V. Sobczak (1996), Variability in Removal of Dissolved Organic Carbon in Hyporheic Sediments, *Journal of the North American Benthological Society*, *15*(1), 35-41.

Harvey, J. W., and B. Wagner (2000), Quantifying hydrologic interactions between streams and their subsurface hyporhiec zones, *in Streams and Groundwaters*, edited by J.B. Jones and P. Mulholland, Academic Press, San Diego.

Legleiter, C. J., et al. (2007), Geostatistical analysis of the effects of stage and roughness on reach-scale spatial patterns of velocity and turbulence intensity, *Geomorphology*, *83*(3-4), 322-345.

Payn, R. A., M.N. Gooseff, B.L. McGlynn, S.M. Wondzell, K.E. Bencala (2009), Longitudinal distribution of channel water balance through summer discharge recession in a Rocky Mountain headwater stream, Montana, USA. , *Water Resources Research.* .

Poole, G. C., et al. (2008), Hydrologic spiraling: the role of multiple interactive flow paths in stream ecosystems, *River Research and Applications*, *24*(7), 1018-1031.

Wörman, A., et al. (2002), Effect of flow-induced exchange in hyporheic zones on longitudinal transport of solutes in streams and rivers, *Water Resources Research*, *38*(1), 2.1-15.

III. Tracking

Student Support

$6,400 of the grant total funded one graduate student ($1600 per month over 4 months) during the final phases of a project on Silver Bow Creek, Montana. The student (Seth Kurt-Mason) led field data collection efforts, parameterized hydrologic models, and performed multiple statistical tests to identify patterns and trends between stream complexity and hydrologic behavior. The student presented results at numerous academic conferences and compiled findings from this project in a thesis document (see below).

Citations

1) Title: Hydrologic response to channel reconfiguration on Silver Bow Creek: Science to inform the restoration process. (Thesis)
   Institution: Montana State University, Bozeman, MT
   Submission Date: November 18, 2010

2) Title: Hydrologic behavior in restored streambeds: Does function follow form? (Oral Presentation)
   Location: 2010 Annual Meeting of the American Water Resources Association Montana Section, Helena, MT
   Date: October 14-15, 2010
   Primary Audience: Researchers and water resource managers

3) Title: Assessing hydrologic response to channel reconfiguration. (Poster Presentation)
   Location: 2010 Annual Meeting of the North American Benthological Society, Santa Fe, NM
   Date: June 6-12, 2010
   Primary Audience: Researchers

4) Title: Assessing hydrologic response to channel reconfiguration. (Poster Presentation)
   Location: 2010 River Restoration Northwest Annual Symposium, Stevenson, WA
   Date: February 1-4, 2010
   Primary Audience: Researchers, water resource managers, stream restoration practitioners

5) Title: Assessing groundwater-surface water interactions before and after stream channel reconstruction: science to inform the restoration process, Silver Bow Creek, Montana. (Poster Presentation)
   Location: 2009 Annual Meeting of the American Water Resources Association Montana Section, Missoula, MT
   Date: October 1-2, 2009
   Primary Audience: Researchers and water resource managers

Notable Awards and Achievements

1) Award: 2nd Place Oral Presentation
   Presenter: Seth J.K. Mason
   Location: 2010 Annual Meeting of the American Water Resources Association Montana Section, Helena, MT
   Date: October 14-15, 2010

2) Award: Best Student Poster Presentation
   Presenter: Seth J.K. Mason
   Location: 2009 Annual Meeting of the American Water Resources Association Montana Section, Missoula, MT
   Date: October 1-2, 2009

Student Fellowship: Potential Meltwater Contributions from the Glaciers in Glacier National Park, Montana

Basic Information

Title:	Student Fellowship: Potential Meltwater Contributions from the Glaciers in Glacier National Park, Montana
Project Number:	2010MT221B
Start Date:	3/1/2010
End Date:	12/31/2010
Funding Source:	104B
Congressional District:	At-large
Research Category:	Climate and Hydrologic Processes
Focus Category:	Surface Water, None, None
Descriptors:	None
Principal Investigators:	Adam Clark

Publications

There are no publications.

QUANTIFYING GLACIER-DERIVED SUMMER RUNOFF IN NORTHWEST MONTANA

Adam M. Clark
M.S. Candidate
The University of Montana
Department of Geosciences
Faculty Advisor: Joel Harper

Project Summary:

Glacier National Park in northwest Montana contains the second largest concentration of mountain glaciers in the Rocky Mountains of the United States. Observations over the past 100 years have shown a marked recession in glacier extent in this region, which has been primarily attributed to a warming climate. An important consequence of glacier retreat is the decline and/or complete loss of glacier-melt runoff during the typically hot and dry summer months that frequently occur in this region. Although Glacier National Park has received much attention lately for its climate change research programs, there are currently no studies that have quantified glacier meltwater production despite this region's relatively high amount of glacier-covered area.

This study will calculate the glacier-derived component of summer runoff in Glacier National Park using a spatially distributed snow and ice melt model. The output from this model can then be used to determine the spatial and temporal input of glacier meltwater for any stream or river in this region that drains a basin with some amount of glacier-covered area.

Progress to Date:

In order to calibrate the melt model, we committed an entire field season beginning in early June, 2010 and ending in late October, 2010 in order to measure temperature, solar radiation, and melt on 5 different glaciers in Glacier National Park. On each of the 5 glaciers, a weather station was mounted on a support structure drilled into the ice. In addition, we installed 2-7 ablation stakes into each glacier to further examine melt rates and to create a set of reference points which will later be used to evaluate the melt model's output. Installing and maintaining this network of weather stations proved to be a major logistical effort. More than a dozen different people carried 500 pounds of equipment over 380 total miles into (and out of) of this steep mountainous terrain.

The 2010 field season was a success, and we now have a new dataset from 5 different glaciers in Glacier Park. Prior to this study, only one glacier in this region had meteorological measurements coupled with ablation measurements. With the addition of four more glaciers, we can now study the spatial variability of glacier melt by examining how topographic factors such as elevation, aspect, slope angle, and cirque-wall shading combine to influence glacier melt. Additionally, by capturing over 100 days of the melt season, we can also investigate how glacier melt varies from the late spring through the early fall.

Future Work:

The primary effort at the moment is to develop the melt model coefficients by using regression analysis. The ultimate goal is to come up with coefficients that would be applicable to the entire study area for the whole duration of the melt season. In order to determine if this is a realistic proposition, the weather station data is systematically being analyzed on multiple spatial and temporal scales. Once the melt model has been developed, the glacier-melt contribution to local streams and rivers can be quantified and compared to the base flows. Overall, this study will create two new research products. The first will be a much a better understanding of the role of glacier meltwater in this region's hydrograph. The second will be the development of new methodology for quantifying glacier-derived runoff in mountainous regions worldwide.

Student Fellowship: Fine Sediment Infiltration and Sediment Routing in the Clark Fork River, Montana

Basic Information

Title:	Student Fellowship: Fine Sediment Infiltration and Sediment Routing in the Clark Fork River, Montana
Project Number:	2010MT224B
Start Date:	3/1/2010
End Date:	2/28/2011
Funding Source:	104B
Congressional District:	At-Large
Research Category:	Climate and Hydrologic Processes
Focus Category:	Geomorphological Processes, Sediments, Surface Water
Descriptors:	None
Principal Investigators:	Elena Evans

Publications

There are no publications.

Fine Sediment Infiltration in a Gravel-Bedded River

Elena Evans, The University of Montana

Summary

Pulses of fine sediment in gravel-bedded rivers can cause extensive fine sediment infiltration, potentially altering river morphodynamics and aquatic ecosystems. Fine sediment infiltration occurs when sand and silt are deposited into void spaces between gravel at the riverbed. This study takes advantage of a dam-removal that caused the release of contaminated fine sediment into a gravel-bed river to investigate the magnitude, duration, and spatial pattern of infiltration. Comparison of metal concentrations of fine sediment collected in TSS samples, infiltration bags, and freeze cores suggests that these samples were supplied from different source populations; the fine grained sediment in transport is largely unseen at depth in the freeze core data. Variation of freeze core samples, spatially and at depth, indicate that reworking of sediment largely dictated infiltration of contaminated reservoir sediments through this reach.

Work to date

There are three phases of my research on fine sediment infiltration: field work, metal analysis and modeling. Fieldwork and metal analysis have been completed. Modeling with this data will be completed during the upcoming Spring semester.

Fieldwork consisted of bulk sampling, suspended sediment collection, infiltration bags installation and freeze cores. On average, Freeze core samples had the lowest metals concentration, with higher concentration in infiltration bag samples. Concentrations were the highest in the suspended sediment samples. This distribution indicates that at the time of the sediment pulse resulting from the erosion of contaminated sediment in the Milltown reservoir, there was little available pore space in the field area. The suspended sediment sample demonstrates that sediment moving through the system contains contaminates. Infiltration bags indicate that if pore space is made available the sediment in transport will deposit.

Future Work

Variation of metal concentrations among the freeze core and infiltration bag data will be investigated in the context of a 2-D model. Local flow variation over the course of the hydrograph could dictate pore space creation and thus explain areas of higher metal concentration.

This work has been presented at the 2010 American Geophysical Union Conference (http://adsabs.harvard.edu/abs/2010AGUFM.H31E1052E). Once modeling is complete, findings will be submitted to a peer-reviewed journal.

Student Fellowship: Fisheries Restoration Potential of the Clark Fork River Superfund Site: Habitat Use and Movement in Relation to Environmental Factors

Basic Information

Title:	Student Fellowship: Fisheries Restoration Potential of the Clark Fork River Superfund Site: Habitat Use and Movement in Relation to Environmental Factors
Project Number:	2010MT225B
Start Date:	3/1/2010
End Date:	12/31/2010
Funding Source:	104B
Congressional District:	At-Large
Research Category:	Ecological Processes
Focus Category:	Toxic Substances, Solute Transport, Acid Deposition
Descriptors:	None
Principal Investigators:	Mariah Mayfield

Publications

There are no publications.

Mariah Mayfield

Fisheries Restoration Potential of the Clark Fork River Superfund Site: Survival, Habitat Use and Movement of Trout in Relation to Environmental Factors

Large scale heavy metal contamination of the upper Clark Fork River from mining deposits has created significant damage to aquatic habitat in the drainage, leading to its classification as the largest Superfund site in the United States. Trout populations were largely eliminated from much of the basin during the early 1900's, but recent surveys show evidence of recovery in response to remediation efforts with trout density at about 10% of expected. Agencies are embarking on a large scale fisheries restoration program, but little is known about critical trout habitat within this drainage. Such information is vital to designing recovery efforts and maximizing recovery success. The objectives of this study are to identify key spawning, summer rearing, and over-wintering habitat areas and to identify conditions continuing to limit trout populations, such as the environmental effects caused by increased heavy metal concentrations.

After pilot studies conducted during the summer of 2009, it became evident that one of the factors potentially limiting trout populations in the upper Clark Fork River basin is increased mortality rates during periods of poor water quality. Through data collected by USGS, we know that during spring run-off periods heavy metal concentrations exceed recommended standards. This is also a time period where we have observed increased radio-tagged fish mortality. Additionally, water temperature in the late summer often exceeds the optimal rearing temperature for trout, potentially causing a spike in mortality rates that has been observed during this time period. Based on these initial observations, for 2010 we increased the amount of water quality data being collected throughout the study area. Basic water quality parameters (dissolved oxygen, temperature, pH, and conductivity) were collected at least twice a month throughout the summer at a total of 22 sites on the mainstem Clark Fork River and major tributaries. Once a month and during high flow events, water samples were collected at six mainstem locations and were sent to a laboratory for total recoverable heavy metal concentration analysis. Greater care was also taken to monitor when and where fish mortalities occurred. The new radio tags placed in fish during 2010 all had mortality sensors built in to help us do this. Additionally, we did our best to recover mortality tags as soon as possible, in order to attempt to identify possible cause of death. In fall 2010, 50 additional trout were tagged in the mainstem and two major tributaries, in order to analyze the different mortality patterns between mainstem and tributary fish and to determine if tagging fish in the spring (right before run-off) may be leaving them more susceptible to the mortality effects of heavy metal contamination.

Although the data is still being analyzed, we did observe a few trends during summer 2010. We once again saw increased mortality rates during spring run-off (Figure 1). This mortality is not likely related to potential tagging injury because there was a large percent of fish tagged in 2009 that also died during this 2010 run-off period. The pattern of increased fish mortality during late summer was also observed in 2010, for fish tagged in both study years. Fish tagged in the fall have shown an increased survival rate, although we observed another spike in mortality rates for brown trout in late fall, most likely due to post-spawning mortality. We have not yet begun to analyze if there is a spatial difference in mortality rates, but this will be something that we investigate thoroughly in conjunction with our habitat analysis.

Understanding the factors that are limiting trout populations in the upper Clark Fork River is essential for successful remediation of the fishery. Although this data is still preliminary, there is evidence that heavy metals may not be the only environmental factor leading to reduced trout populations; high water temperature and associated poor water quality may also be a limiting factor. With one more year of this study and a plan for increased monitoring of water quality, it is our goal that we will be able to show the relationship between poor water quality and survival rates more clearly.

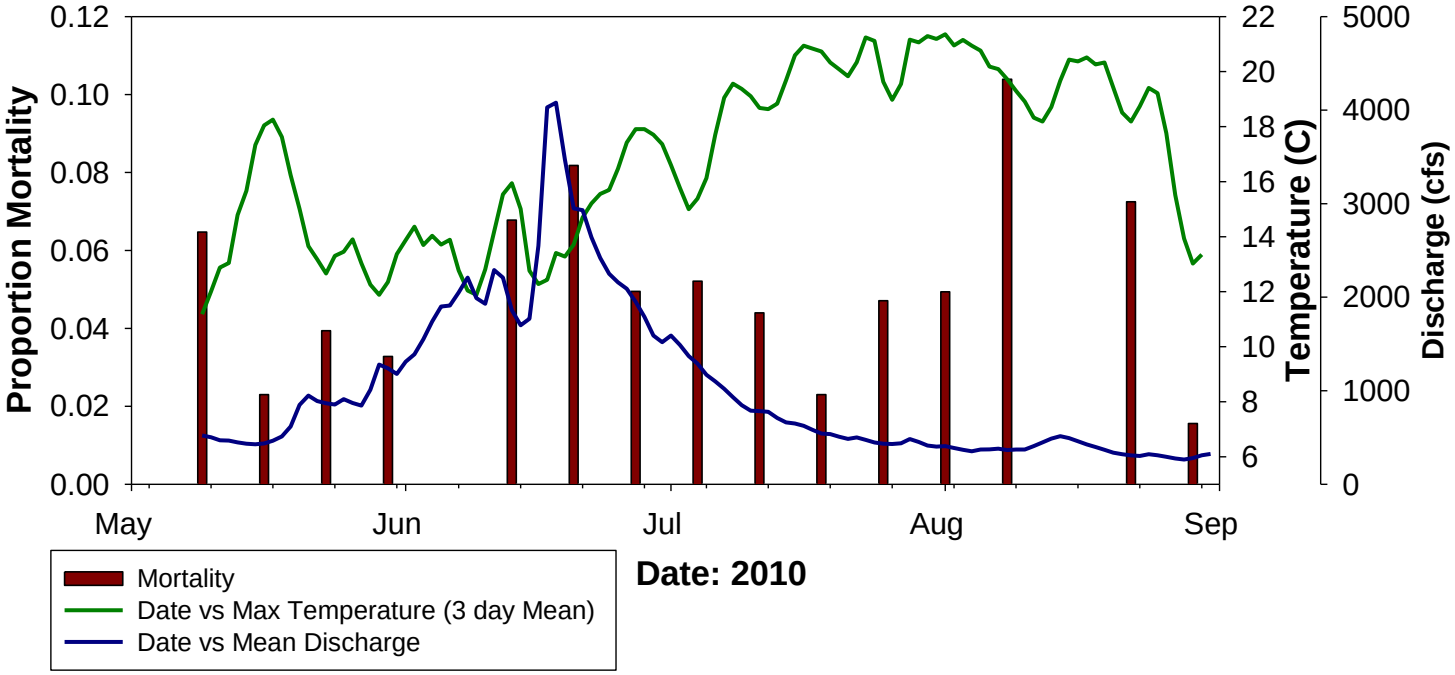

Figure 1: Mortality rates and environmental factors, summer 2010. Note the spikes in mortality rates during the spring run-off period and in late summer.

Student Fellowship: Rapid detection of pathogens in water using a combination of molecular techniques

Basic Information

Title:	Student Fellowship: Rapid detection of pathogens in water using a combination of molecular techniques
Project Number:	2010MT228B
Start Date:	3/1/2010
End Date:	12/31/2010
Funding Source:	104B
Congressional District:	At-large
Research Category:	Water Quality
Focus Category:	Water Quality, Methods, None
Descriptors:	None
Principal Investigators:	Kien Lim

Publications

There are no publications.

Kien Lim

1/5/11

Water Center fellowship Research Summary

Tyramide signal amplification (TSA) on FISH probed *Escherichia coli* (*E. coli*) was optimized to produce fluorescence intensity close to that of SYBR green stained *E. coli* cells.

With the technique optimized, *Legionella pneumophila* was used as the first candidate to test if the optimized technique can produce the same result when compared to *E. coli*. *Legionella pneumophila* ATCC 33153 powder form was resuspended in BCYE broth and incubated at 37°C until a film of growth (white) was observed at the bottom of the BCYE broth tube. When growth was observed, the suspension was mixed on a vortex to resuspend growth evenly in the BCYE broth, before streaking the suspension onto several BCYE plates.

Legionella pneumophila growth on BCYE plates was used to test if the optimized technique for *E. coli* will work for *Legionella pneumophila*. *Legionella* FISH and Eubacterial FISH probes were used. *Legionella pneumophila* and *E. coli* cells were used and both were labeled with *Legionella* FISH and Eubacterial FISH probes so that there is a control for comparison.

E. coli cells probed with Eubacterial FISH probes were positive with fluorescing cells and *E. coli* cells probed with *Legionella* FISH probes were negative with no fluorescing cells. *Legionella pneumophila* cells probed with Eubacterial FISH probes were positive with fluorescing cells, but *Legionella pneumophila* cells probed with *Legionella* FISH probes were negative with no fluorescing cells.

It can be observed that the *E. coli* optimized technique works on both *E. coli* and *Legionella pneumophila*. It seems like the cause of *Legionella pneumophila* cells probed with *Legionella* FISH probes to not work, lies on the probes itself.

The first thing, we did was to find out the concentration of all the probes. Based on NANO drop readings, all probes were around 85ng/µl. The concentrations were what we expected them to be, the next thing we have to check is the sequence of the *Legionella* probe.

Once the sequence of the *Legionella* probe is verified and labeling *Legionella pneumophila* with *Legionella* probes work, we can expect to carry out the technique on several other water pathogens that were listed in the initial proposal.

Student Fellowship: Distinguishing anthropogenic influences on a changing flow regime of the Upper Smith River, Meagher County, Montana

Basic Information

Title:	Student Fellowship: Distinguishing anthropogenic influences on a changing flow regime of the Upper Smith River, Meagher County, Montana
Project Number:	2010MT229B
Start Date:	3/1/2009
End Date:	12/31/2010
Funding Source:	104B
Congressional District:	At-large
Research Category:	Ground-water Flow and Transport
Focus Category:	Geomorphological Processes, Surface Water, Water Quantity
Descriptors:	None
Principal Investigators:	Andrea Stanley

Publications

There are no publications.

Final project summary for Montana Water Center Student Research Fellowship Program (2010 research year):

Investigation of hydrologic regime change in an evolving semi-arid agricultural watershed, Upper Smith River, Montana

Andrea Stanley, University of Montana, Missoula

My research seeks information critical to effective water management in Montana's semi-arid climate including: the degree to which current agricultural land and water use affects the hydrologic regime; where and when the effects of this use are most prominent; and how future changes may affect future water availability for agricultural, recreational, and ecological use. My specific research questions and objectives are:

(1) How is agricultural water use currently affecting the flow regime of the Smith River?
(2) What are the potential effects of future changes in land and water use on flow regimes in the Smith River?

The advent of agricultural water and land use in the Smith River watershed predates local stream gage, climate, and vegetation land-cover records. Therefore a natural flow regime will be created artificially using the calibrated and tested precipitation-runoff model of the area, current climatic conditions, and artificially created watershed parameters to simulate a non-agricultural watershed.

I have built a preliminary watershed model and produced hydrographs according to current agricultural and climate conditions using a distributed watershed model. The modeling software used is the U.S. Geological Survey's Precipitation Runoff Modeling System (PRMS; Leavesley, 1983). Eventually, after refinement and calibration, I will use this model to test the sensitivity and resilience of a semi-arid hydrologic regime to agricultural land and water use.

Several methods will be employed to create non-agricultural watershed parameters for the model and projected future conditions, including modification of vegetation types such as irrigated areas, grasslands, forest, and wetlands, and removal of water development structures such as reservoirs.

Flow metrics of particular focus include frequency of low flow spells, duration of low flow pulses, and the Julian date of annual minimums. Analyses include stream discharge data acquired from the USGS, and stream discharge data simulated using PRMS.

Thank you for your support,
Andrea Stanley

Information Transfer Program Introduction

The Montana Water Center fills the unique role of coordinating Montana University System (MUS) water-related research, and disseminating and applying its findings for the benefit of the people of the state. And, as Montana is a headwaters state to two of the nation's major river drainage basins: the Missouri and the Columbia, how Montana manages its water and aquatic plants and animals can have far ranging impacts downstream. Obviously these are not closed systems. Montana's aquatic resources are also impacted by what comes into the state, be it acid rain, drought, aquatic nuisance species, or wind carried dust and debris that can increase snowpack melt.

Of course, climate change is a growing concern and, as research is being done to determine the impact this will have on Montana, the Montana Water Center is part of a multi-disciplinary effort to prepare for inevitable change. To prepare, people need to be informed, and the Center uses some of its USGS funding to provide forums and outlets for information exchange. During the period March 1, 2010 through February 28, 2011, the Montana Water Center drew on its USGS support to conduct outreach activities and programs listed under the Statewide Education and Outreach project.

Statewide Education and Outreach

Basic Information

Title:	Statewide Education and Outreach
Project Number:	2010MT236B
Start Date:	3/1/2010
End Date:	2/28/2011
Funding Source:	104B
Congressional District:	At-Large
Research Category:	Not Applicable
Focus Category:	Education, Water Quality, Water Quantity
Descriptors:	drinking water, climate change, small public drinking water systems, native fish, stream restoration, aquatic nuisance species, wetlands, hydrology, water law
Principal Investigators:	Steve Guettermann, Mary Jo Nehasil

Publications

1. Montana Water Center, 2010, Saving Water & Energy in Small Water Systems, Web-based: http://watercenter.montana.edu/training/savingwater/default.htm
2. Montana Water Center and Montana Department of Environmental Quality, 2010, Decision-maker's Guide to Montana's Water - Wetlands. Web-based: http://watercenter.montana.edu/training/decisions/wetlands/default.htm

Supporting students to become water science professionals is a core mission of the Montana Water Center. To that end, the center worked closely this year with faculty researchers to engage students in water-related research, and subsequent reports and published papers. Center staff frequently encouraged aquatic science, engineering and students in related disciplines to apply for student fellowships. This outreach increased the diversity of students with whom the center worked. Faculty researchers who received research funding from the Water Center are required to actively mentor students in the research projects. The Water Center also encouraged students engaged in water resource studies to present at conferences. Staff also led an upper level seminar class for environment science students.

In addition to working with faculty and students, Water Center programs reached thousands of other water resource professionals, teachers, farmers, ranchers, engineers, drinking water and wastewater system operators and other professionals throughout the state. Specific information transfer activities include the following.

* Published twelve Montana Water e-newsletters and distributed them monthly to almost 1,800 professionals, students and decision makers concerned with water resource management. Newsletter archives are posted at http://water.montana.edu/newsletter/archives/default.asp.

* Continued the web information network MONTANA WATER, at http://water.montana.edu. Known as Montana's clearinghouse for water information, this website includes an events calendar, news and announcement updates, an online library, water-resource forums and water source links, an expertise directory, water facts and more.

* With Federal stimulus money administered through the Montana Department of Natural Resources and Conservation, is completing production of seven water science training modules for local Montana elected officials and state legislators. Surveys show that often decision makers are asked to make decisions that impact water quality and quantity, but frequently have no or little education, or understanding of, basic hydrology or other relevant water science topics that might be helpful for them to make informed decisions. These modules help fill some of the gaps. Its major topics are 1) wetlands, 2) water quality, 3) basic hydrology, 4) floodplain and riparian zone management, 5) Montana land use changes and water resources, 6) water data and modeling and 7) Montana water law. Three modules have been presented via webinars and other trainings, including a hydrology training to state legislators early in the 2011 legislative session. The four other modules are in the final stages of production and webinars and live trainings are being scheduled.

* With funding from the EPA, the Montana Water Center is in the final stages of production of a training CD for small drinking water systems titled *Arsenic and Radionuclides: Small Water System Treatment Experiences*. The Center is working with five drinking water systems to profile their issues of choosing treatment protocols and the subsequent operating of their systems to meet drinking water standards for arsenic or radionuclides. The purpose of the training is to enhance the technical capacity among small water utility personnel and those who provide

technical assistance, funding or regulatory oversight; provide a better understanding of the advantages and pitfalls of various options for dealing with source waters having elevated concentrations of arsenic or radionuclides and mitigation of hazard from treatment residuals.

* Maintained and circulated a small library of paper documents related to Montana water topics.

* Conducted the statewide water research conference on October 14-15 in Helena, Montana. The theme of the 27th annual meeting was Rivers of Change: Science, Policy and the Environment. It was a joint conference with the Montana Section of the American Water Resources Association. A field trip led by Montana Bureau of Mines and Geology researchers and a private engineering firm concentrated on the Ten Mile Creek area, an area negatively impacted by historic mining and which is being reclaimed. The conference attracted over 175 Montana researchers and policy makers and 25 students. Over forty researchers presented information on their latest findings along with nearly 30 poster displays. The web-based archive of this meeting is found at http://awra.org/state/montana/events/conf_archives.htm.

* Responded to numerous information requests on water topics ranging from invasive aquatic species to water rights to streamside setbacks to contaminants and pollutants in Montana's surface and ground water, and ways to better manage ground and surface water.

* Assisted elected and appointed officials, particularly those serving on the Montana Legislative Environmental Quality Council, the Water Policy Interim Committee (WPIC), and the Governor's Drought Advisory Committee, with water resource issues.

* Sponsored and participated in Montana's 77th Annual Water School October 4-7, 2010 at Montana State University for 300 staff members of water and wastewater utilities. The school primarily helps prepare new system operators to pass the certification exam, and familiarizes participants with other resources they may find helpful in the future.

* Created and distributed 1,500 copies of the black-and-white Montana Water 2011 calendar to elected officials, water resource managers and other partners and supporters. Designed to educate the public about water issues and aquatic life, photographers from all over the state contributed to the calendar.

* The Montana Watercourse, which is part of the Montana Water Center, provides comparable outreach to watershed groups, teachers, developers, realtors and landowners. The Watercourse provided the following services and trainings in 2010.

- Professional workshops and trainings for realtors and others on Montana water law – satisfied six mandatory continuing education credits for realtors
- Volunteer water monitoring training for communities and schools
- Assistance with local water education program development
- Publications and guides on water resource and watershed topics

- Teaching trunks filled with interactive water resource activities
- Educator workshops, trainings and tours using Project WET and other curricula and materials
- Direct support of landowners on such things as groundwater education, preventing nonpoint source pollution and other water quality issues

USGS Summer Intern Program

None.

Student Support					
Category	**Section 104 Base Grant**	**Section 104 NCGP Award**	**NIWR-USGS Internship**	**Supplemental Awards**	**Total**
Undergraduate	15	0	0	0	15
Masters	12	0	0	0	12
Ph.D.	10	0	0	0	10
Post-Doc.	0	0	0	0	0
Total	37	0	0	0	37

Notable Awards and Achievements

The Montana Water Center assists small drinking water operators throughout the country by providing continuing education via online download and CDs for system operators. To date, more than 50,000 water-utility workers have taken the Center's training courses nationwide.

Seth Kurt-Mason, a graduate student supported by a USGS/Montana Water Center research grant, earned second place honors at the Montana AWRA conference for student posters. Seth Kurt-Mason is a master’s student at Montana State University in Land Resources and Environmental Sciences.

Publications from Prior Years